ISSN 0975-2366
DOI:https://doi.org/10.31838/ijpr/2022.14.01.005

Research Article

Antidiabetic Activity of *Selenicereus Undatus* (Haw). Fruit Extract Against Alloxan Induced Diabetic Mice

P.SONU, M.KISHORE, N.SANDHYA, S.JITHENDER KUMAR NAIK*, ANUSHA C PAWAR, S.RAJESWARI, B.NAGESH.
Department of Zoology, Osmania University Hyderabad, Telangana, India
*Corresponding author
Email: drnaik8777@yahoo.com
Received: 11.10.21, Revised: 09.11.21, Accepted: 22.12.21

ABSTRACT

The disruption of glucose homeostasis caused by Diabetes mellitus (the most common endocrine illness) can result in severe diabetic complications such as retinal, vascular, renal disease, including neurpathy. Alloxan (ALN, 150 mg/kg body weight)-induced diabetic mice were treated with an ethanolic extract of Selenicereus undatus (45 mg /kg and 75 mg / kg body weight), a medicinal fruit that has long been utilized in traditional Chinese medicine. Diabetic mice were administered with an ethanolic crude extract of the fruit at the rate per kg body weight for 27 days, blood glucose levels significantly reduced as compared to the control animals. Furthermore, diabetic mice had significantly higher levels of hepatic and renal marker activity against the control mice, indicating the influence of the diabetes. The treatment, which included Selenicereus undatus ethanolic fruit extract and metformin, could able to normalize the tested parameters to the normal levels.

Keywords: Selenicereus undatus, Alloxan monohydrate, Antidiabetic activity, Metformin, Hyperglycemic.

1. INTRODUCTION:

Diabetes mellitus is a metabolic disease characterized by abnormal high blood sugar levels caused along with combination of hereditary and environmental factors (hyperglycemia) by impaired insulin secretion or action [1, both of which are impaired]. Hyperglycemia, lipoprotein abnormalities, an increased basal metabolic rate, enzyme deficiency, and an elevated level of oxidative stress are all signs and symptoms of diabetes mellitus, which causes damage to the pancreatic acinar cells. They are the most common type of endocrine disorder, affecting glucose homeostasis and resulting in severe diabetic outcomes such as retinal, angiogenic, and neuropathy [2], as well as neurological ailments caused by a disruption in glucose use.Type 2 diabetes affects up to 2 out of every 6 newly diagnosed cases in children and adolescents under the age of 18, with a disproportionately high prevalence among ethnic minorities and children and adolescents aged 10 to 20 in the United States. Current projections show that the number of people living with diabetes will rise from 315 million in 2015 to 386 million by 2030 [3]. Diabetes mellitus type 2 is becoming more common, with three new cases being identified every ten seconds. It is also being diagnosed at a younger age, with three new cases being diagnosed every ten seconds. Chronic stress and depression, environmental pollution and poisons, obesity, and a sedentary lifestyle are all risk factors for the disease [5].

Diabetes is a major public health concern in India, where the diabetic population is the world's largest. According to the International Journal of Diabetes in Developing Countries, diabetes prevalence in India has risen at an alarming rate in recent years. According to estimates, an estimated 3.2 million people die each year as a direct result of uncontrolled blood sugar levels.

Diabetes-related deaths are expected to triple between 2005 and 2030, according to the World Health Organization (WHO). According to the WHO, low- and middle-income countries account for 70% of all diabetes deaths [6, 7]. There are Selenicereus species all over the world, including Antarctica. According to research, it has anti-inflammatory, anti-microbial,antibacterial, anti-inflammatory, antioxidant, and anti-tumor properties, among other things. This species, one of the most extensively studied plant species, has been discovered to have a wide range of therapeutic effects on a wide range of organs, as well as a

wide range of biochemical processes and physiological activities, such as photosynthesis,that are beneficial in a variety of ways. According to the literature, the potential utility of Selenicereus extract species in the prevention of pathologies such as heart ischemia, renal ischemia, neurodegenerative disorders, and diabetes must be investigated in conditions where protein oxidative stress damage appears to play a significant role.

Selenicereus undatus

2. MATERIALS AND METHODS:

2.1. Collection and Extraction of Fruit Material: The fruit of Selenicereus undatus was donated by the Deccan exotics farm in Sangareddy, Telangana, which is close to Hyderabad. After thoroughly cleaning the fruits with water and allowing them to dry naturally, the peel, pulp, and seeds were removed. The fruit was then ground up with an electric mixer to remove any remaining skin, pulp, or seeds. Sohxelation of 500g of each dry powder takes 10-12 cycles, which is stored and circulated for a total of 500g. The ethanolic extract was extracted from the fruit material using a rotary evaporator while it was still at room temperature. It was then sealed in an airtight container and stored for later use.

2.2. Preliminary Phytochemical Screening: Secondary metabolite screening with phytochemicals was performed in the laboratory to determine whether any of the plant's therapeutic capabilities were present.

2.3. Experimental Animals:
For this study, we used 25-30 g mice obtained from the Vyas Labs animal home in Medchal, Malkajigiri District, Telangana. A constant temperature of 37 °C was maintained in the mice's housing, as well as a 12-hour light/dark cycle. The mice were also given free access to tap water and pellets to eat. The project has been approved by the Osmania University Department of Zoology's Institutional Ethical Committee. There were no deviations from the CPCSEA recommendations in terms of experimental protocols, which were strictly followed by the Indian investigators.

2.4. Acute Toxicity:
In the experiment, mice weighing between 28 and 30 grams were used. In this study, four groups of six mices were given ethanolic extracts of the plant Selenicereus undatus orally at doses of 45 mg/kg and 75 mg/kg, respectively. The third group of six mice, induced by alloxan, received metformin as well as a fruit extract supplement. They were all kept under strict guidelines and kept under 24-hour observation for any signs of mortality, such as lethality, toxic symptoms, behavioral changes, or even death

2.5. Induction of Diabetes:
An alloxan solution containing saline (150 mg/kg dosage) to induce diabetic Mellitus in mice. After 72 hours, behavioral abnormalities (excess thirst and frequent urination) confirmed the presence of hyperglycemia, as did the presence of high blood glucose levels (excess thirst and frequent urination). The mice used in the study had blood glucose levels greater than or equal to 200 milligrams per deciliter, which was the investigation's upper limit.

3. Glucose Tolerance Test:
3.1. Experimental Design for GTT of Diabetic Mice:
The glucose tolerance test was studied in the ethanolic extract of Selenicereus undatus on diabetic mice. The animals were divided into 8 groups as follows:
Group 1: Control mice;
Group 2: Diabetic mice ;
Group 3: Diabetic mice treated with metformin
Group 4: Mice treated with 45 mg/kg of epicarp of ethanolic extract of S.undatus;

Group 5: Mice treated with 75 mg/kg of epicarp of ethanolic extract of S.undatus;
Group 6: Mice treated with 45 mg/kg of mesocarp and endocarp ethanolic extract of S.undatus;
Group 7: Mice treated with 75 mg/kg of mesocarp and endocarp ethanolic extract of S.undatus;
Group 8: Mice treated with the S.undatus whole fruit.
The animals were not allowed to eat or drink for the duration of the trial. The O-Toluidine procedure and hemoglucostrips in the glucometer (Life scan, Johnson and Johnson Ltd.) were used to demonstrate that a fasting blood sample was collected from the tail. Mice in both the control and diabetes groups were only given water to drink during the GTT trial. Groups 4, 5, 6, and 7 mice were given ethanolic fruit extract of S.undatus at 45 and 75 mg/kg doses, respectively, and the results were recorded. The patient's blood sugar level was then checked again after 30 minutes.
Glycemic index was calculated by using formula:

$$\text{Gylcemic index} = \left(\frac{Intial-final}{Intial}\right) X100$$

3.2. Antidiabetic Study:
There were a total of six mice in each group, and each group was divided into eight equal sections. The control group consisted of healthy mice who were fed a pelleted diet; the group 2 mice were injected intraperitoneally with 150 mg/kg BW of alloxan; even the groups 3,4,5,6,7 were administered alloxan the group 3 diabetic mices were given Metformin (10 mg/kg BW) orally through an oral intragastric tube for 27 days; the group 4 and 6 diabetic mice were injected orally with Selenicereus undatus of 45 mg/kg of body weight over 27 days, which was divided equally among them. Groups 5, 7, received Selenicereus undatus (75 mg/kg BW) orally for a total of 27 days, except group 8 which received whole fruit extract. During the 27-day experiment, the animals were fed the extract through intragastric tubes before being euthanized. The blood and serum that had been extracted from it were used in biochemical studies that were carried out in the laboratory. Organ tissues for antidiabetic tests, such as liver, kidney, and pancreatic tissue, were preserved using formaldehyde.

3.3. Biochemical Analysis:
The kit method was used to estimate the blood glucose levels. Drabkin's method was used to calculate glycosylated and total hemoglobin levels. Using a diagnostic reagent kit from Span Diagnostics Ltd, a one-step technique [13] was used to assess serum cholesterol and HDL levels. GPO-PAP, an endpoint assay developed by Span Diagnostics Ltd, and a diagnostic kit developed by Span Diagnostics Ltd were used to measure triglycerides. A commercially available kit was used to determine the activity of serum aspartate aminotransferase (AST) and alanine aminotransferase (ALT) .Alkaline phosphatase activity was also measured. The total protein and albumin levels in the serum were determined using the previously described Biuret method [17]. We were able to calculate the urea and creatinine levels using a DAM-based diagnostic kit [18], which we used in conjunction with the DAM technique. A study was carried out to see if this kit was capable of detecting bilirubin in the blood [20].

3.4. Antioxidant Analysis in Tissues:
This study looked at the antioxidant activity of Selenicereus undatus ethanolic fruit extract in the liver, kidney, and pancreas. After 27 days, the mice were killed and their organs were preserved in formaldehyde liver to measure glycogen levels.

4. Statistical Analysis:
We used an F-test to compare the statistical differences between the groups, then computed their averages (standard deviations) and P-values. To determine their significance, all factors were subjected to independent ANOVA tests. Using Duncan's Multiple Range Test (DMRT) on the data, we were able to determine whether or not there was a statistically significant difference between the groups. Stata was used to evaluate the data obtained in the social sciences (SPSS.26 Inc, IBM). To determine whether or not a study was statistically significant, P values of 0.05 and 0.01 were used.

4.1. RESULTS AND DISCUSSION:
Fruits contain phytochemicals, which aid in interspecies defense and defense against predation, microorganisms, and stress, all of which are beneficial to the organism. The components of these fruits are effective in the treatment of breast cancer. Because phytochemical screening is a preliminary step in identifying potentially active compounds in fruits, it is an excellent starting point for further research. The phytochemicals found in S.undatus ethanolic fruit extract are listed in Table-1. Phytochemical screening of S.undatus revealed the presence of a diverse range of phytochemicals in the species (Table 1). Selenicereus undatus ethanolic extract, revealed the presence of alkaloids, tannins, phenolic compounds, flavonoids, steroids, cardiac glycosides, terpenoids, and carbohydrates, among other plant constituents. In the acute toxicity study, the experimental mice had slept several hours, after administration of Selenicereus undatus extracts to the mice when compared to normal control mice. But there were no gross behavioral changes or morphological changes like respiratory distress, hair loss, restlessness, convulsions, laxative, coma, weight loss, urination, itching, and so forth. There was no lethality and no toxic reaction was found at any of the doses selected till the end of the treatment. This indicates the safe nature of

Selenicereus undatus of the extract on mice.

Table-1 : Phytochemical screening aqueous fruit extract of *Selencereus undatus*.

Extracts	AL	SA	TP	FL	ST	CG	OF	TN	AP	CHO
Aqueous	+++	++	++	+++	+	++	++	+	++	+++

AL: alkaloids; CHO: carbohydrates; ST: steroids; CG: cardio glycosides; FL: flavanoids; SA: saponins; TP: tannin and phenolic compounds; OF: oils and fats; AP: amino acids and protein;TN: terpenoids. "+": present; "–" absent.

The results of a glucose tolerance test (GTT), which measures blood glucose levels, are shown in Table 2. The experimental animals were given an oral dose of Selenicereus undatus ethanolic fruit extract (45 and 75 mg/kg, respectively) on day 27 of their experiment. After 60 minutes, diabetic mice had a significant increase in blood glucose levels, which lasted for an additional 120 minutes. Glucose levels in diabetic mice treated with Selenicereus undatus decreased by 30.3 percent at 60-minute and 120-minute intervals, and by 33.3 percent at 12 0-minute intervals. Glucose levels decreased by 40.2 percent and 27.5 percent at the 60-minute and 120-minute intervals, respectively (Figure 2). When tested using the OGTT, the doses epi 45 mg /kg and endo 75 mg/kg.of Selenicereus undatus that showed profund effect when compared with alloxan induced diabetic mice. Glycogenolysis and gluconeogenesis may be inhibited as a result of decreased intestinal glucose absorption or an increase in glycogenic activities. Diabetic mice who were not given metformin and selenincereus undatus experienced an increase in serum glucose levels as a result of alloxan-induced tissue death. As a result, there was an insulin shortage. High blood glucose levels are eventually caused by low insulin levels [23].

Table:-2 Effects of Selenicereus undatus on Blood glucose and HbA1c

PARAMETERS	CONTROL	ALLOXAN	ALLOXAN +METFORMIN	EP45	EP75	EM45	EM75	FRUIT
BLOOD GLUCOSE	99.50±3.93	235.16±3.7	100.83±4.26	111.83±7.88	121.00±2.96	122.33±3.77	107.66±8.33	98.33±2.42
HbA1C	4.26±0.72	12.04±1.69	4.98±0.32	5.58±0.13	5.68±0.19	5.76±0.23	5.40±0.29	4.96±0.36

Values are in mean ±sd n=6; $p<0.05$

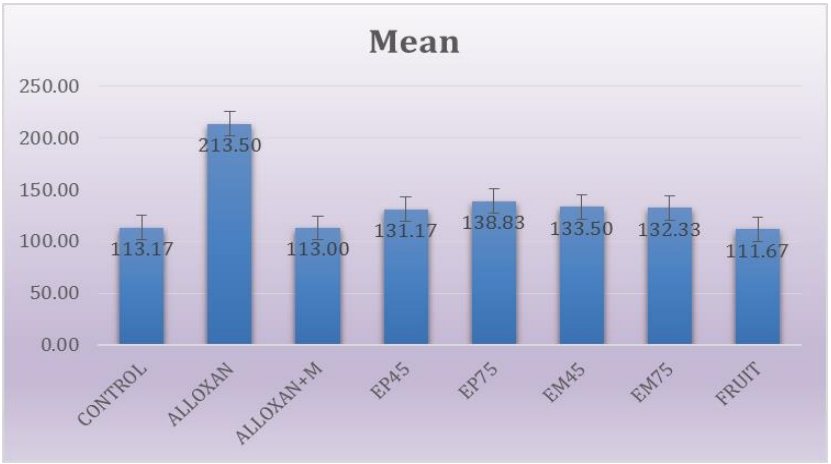

Figure-1 Oral glucose tolerance test of ethanolic extract of Selenicereus undatus in experimental mice

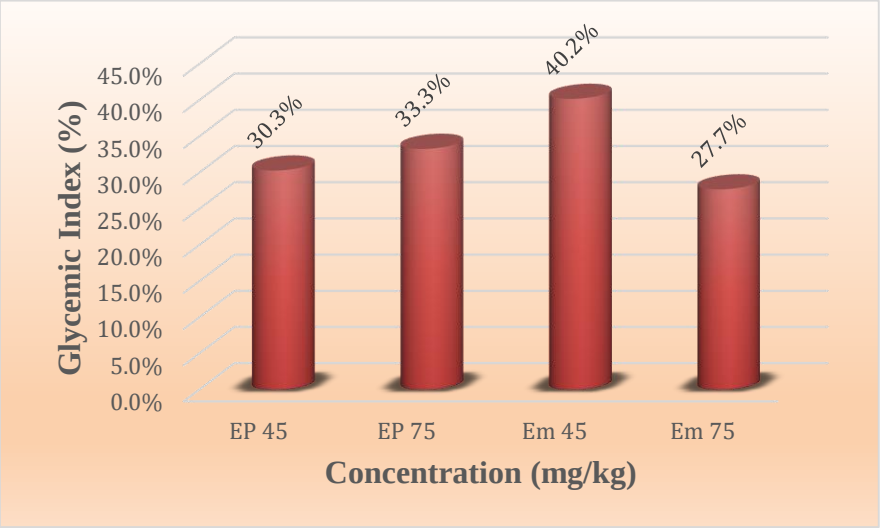

Figure 2: The glycemic index of ethanolic extract of *Selenicereus undatus*

Glucose levels are significantly higher in diabetic control mice than in non-diabetic control mice. Alloxan monohydrate (Sigma Aldrich) 982244-11-3 has been shown to cause selective cell death in the pancreatic islets of Langerhans [24]. This study's findings show that when mice are given 150 mg/kg of alloxan, they develop a significant diabetogenic response. According to the findings of this study, an ethanolic extract of S.undatus reduced blood glucose levels in a way similar to metformin (see Table 2). The combination of an ethanolic fruit extract of S.undatus and metformin reversed elevated glycosylated hemoglobin levels. In diabetic mice, high glucose levels cause low hemoglobin levels, which are caused by excess glucose interacting with hemoglobin to form glycosylated hemoglobin in the blood (Table 2). After being treated with S.undatus, ALN mice had significantly lower levels of glycosylated hemoglobin (HbA1c), with both hemoglobin and glycosylated hemoglobin remaining within normal ranges. S.undatus, as demonstrated by this discovery, plays an important role in the regulation of blood glucose levels.

LSD was also performed to compare between the groups and mean differences are presented with significant values when diabetic mice were compared to control mice, diabetic mice had a significant increase in (Table 2). Lipolysis is not blocked in diabetics due to insulin deficiency, resulting in hyperlipidemia (high cholesterol). These readings were significantly reduced and returned to near-normal levels after 27 days of oral administration of Selenicereus undatus fruit extract to diabetic mice. Selenicereus undatus increases insulin secretion, which lowers total cholesterol and triglyceride levels while increasing HDL levels. We are in charge of regulating blood glucose levels, and we play an important role in this process (Figure 3 to 9).

Table 3: Effect of S.undatus on glucose, hemoglobin, glycosylated hemoglobin, and lipid profile in serum of control and experimental mice

EXPERIMENTAL GROUPS								
	Control	**ALLOXAN**	**ALLOXAN+M**	**EP45**	**EP75**	**EM45**	**EM75**	**FRUIT**
Control		100.33*	0.16	-18.0*	-25.66*	-20.33*	-19.16*	1.5
ALLOXAN			100.5*	82.33*	74.6*	80.0*	81.16*	101.8*
ALLOXAN+M				-18.16*	-25.5**	-20.5*	-19.3*	1.3
EP45					-7.6	-2.3	-1.16	19.5*
EP75						5.33	6.5	27.1*
EM45							1.6	21.83*
EM75								20.6*
Fruit								

*significant at 1% level (2-tailed)

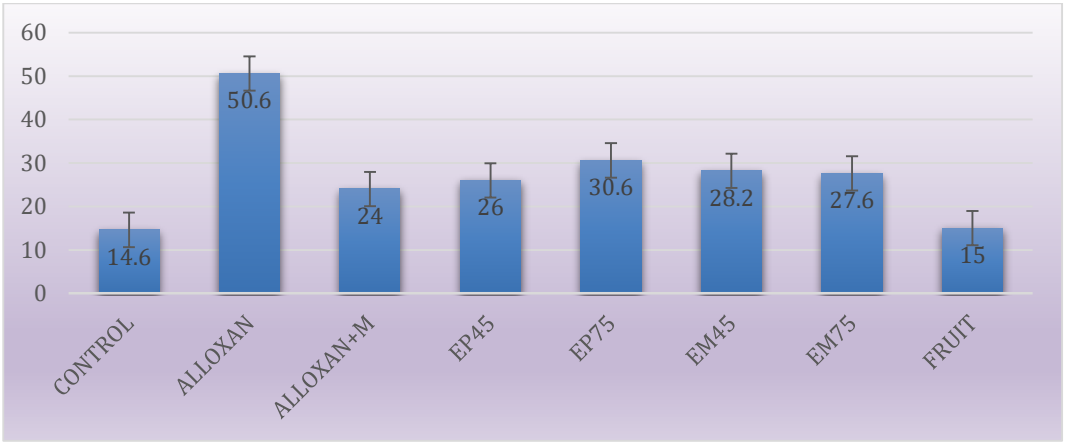

Figure 3: Different parameters Mean scores of SGOT

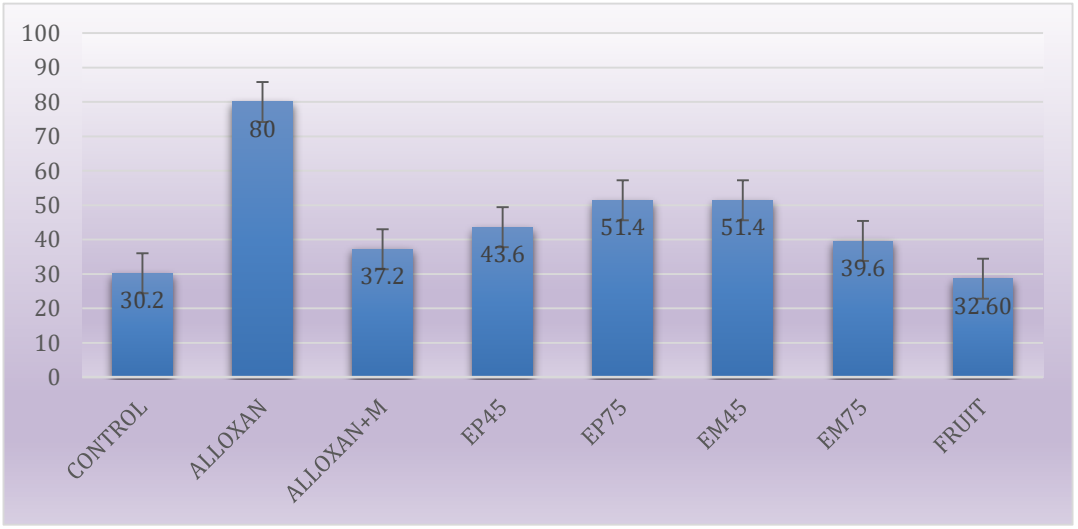

Figure 4: Different parameters Mean scores of SGPT

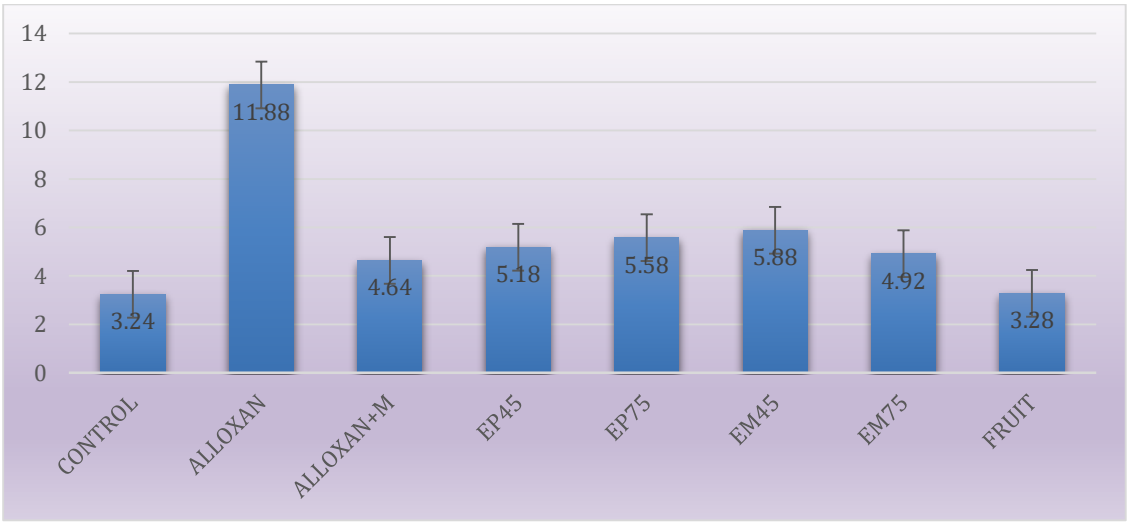

Figure 5: Different parameters Mean score of Urea

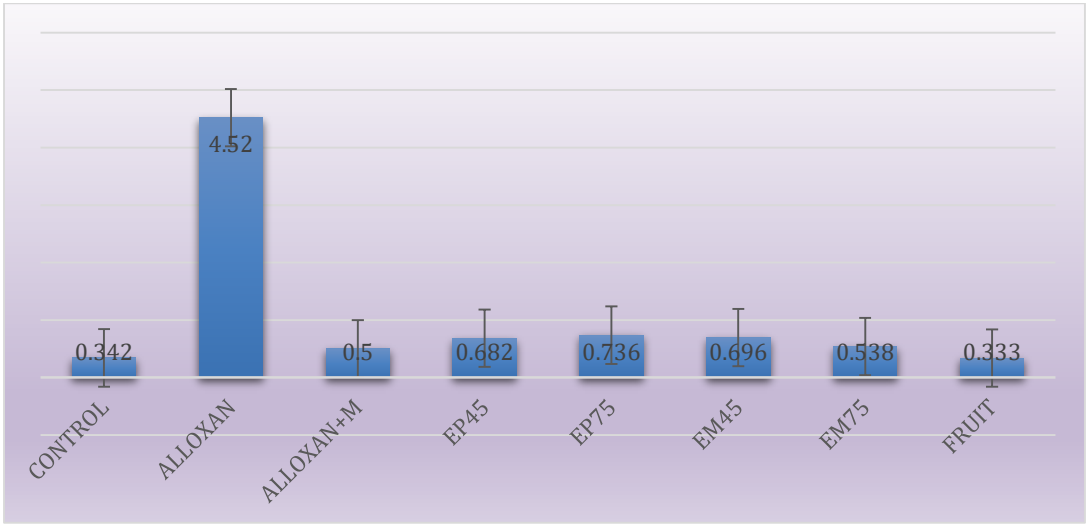

Figure 6: Different parameters Mean score of creatinine

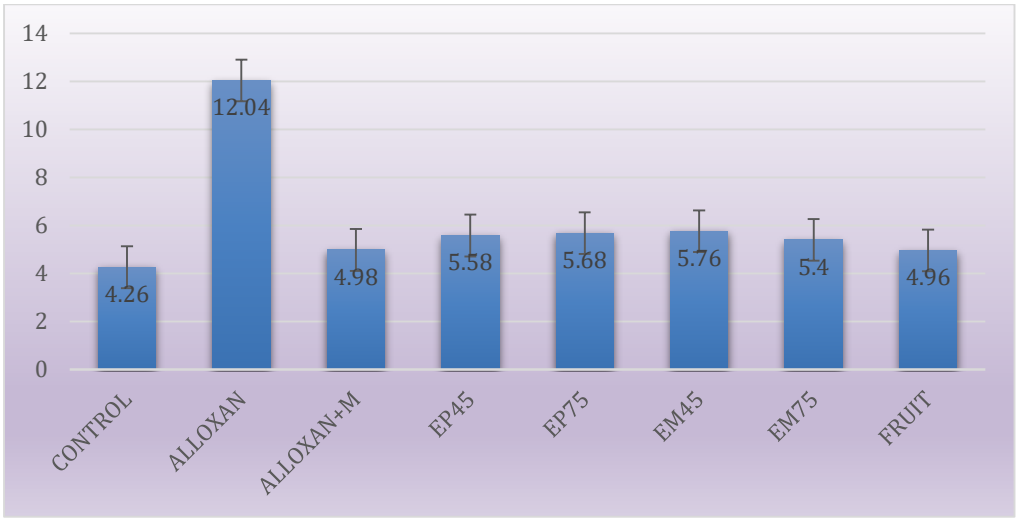

Figure 7: Different parameters Mean scores of HbA1C

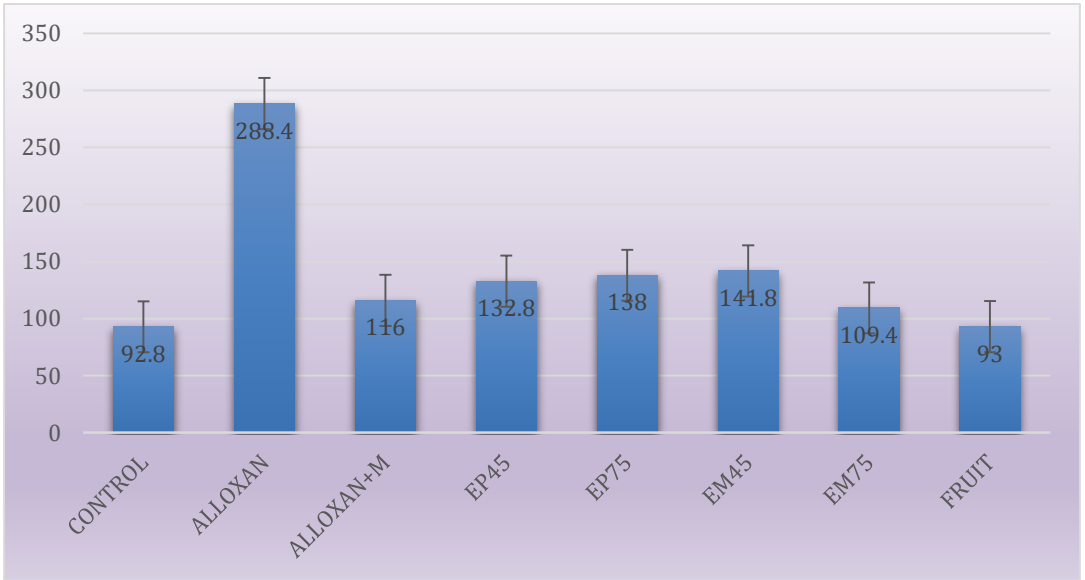

Figure 8: Different parameters Mean scores of Triglycerides

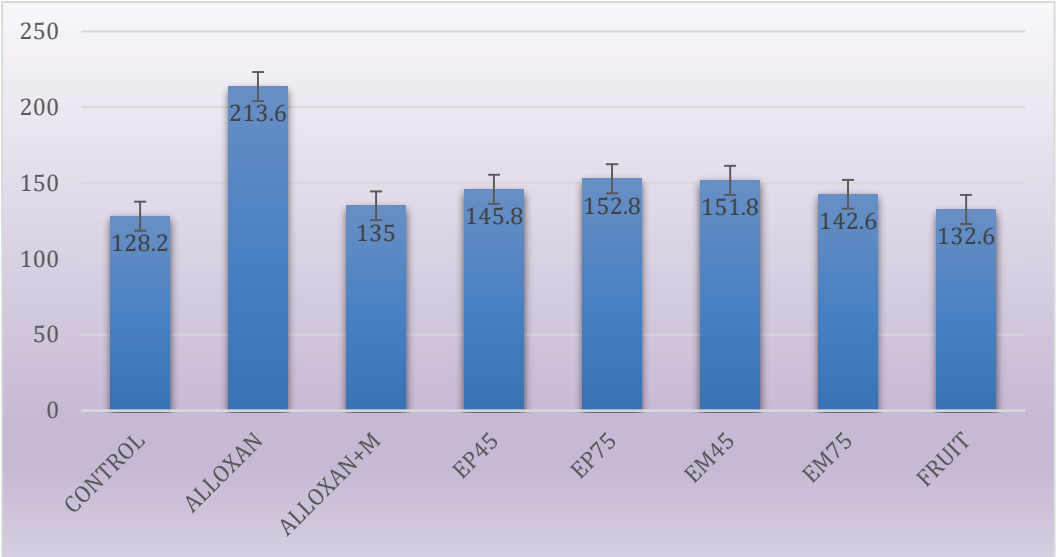

Figure 9: Different parameters Mean scores of Cholesterol

Table 4: Effect of S. undatus on kidney liver and pancreas of control and experimental mice.

PARAMETERS	CONTROL	ALLOXAN	ALN+M	ALN+EP45	ALN+EP75	ALN+EM45	ALN+EM75	FRUIT
SGOT	14.60 ± 1.14	50.60 ± 5.12	24.00 ± 3.39	26.00 ±3.80	30.60 ± 3.71	28.20 ± 3.83	27.60 ± 2.07	15.00 ± 0.70
SGPT	30.20 ± 6.90	80.00 ± 7.71	37.20 ± 5.35	43.60 ± 6.28	51.40 ± 11.50	51.40 ± 6.4	39.60 ±4.247	32.60 ± 6.98
UREA	3.24 ± 0.23	11.88 ± 2.54	4.64 ± 0.95	5.18 ± 0.73	5.58 ± 0.73	5.88 ±0. 80	4.92 ±0. 43	3.28 ±0. 19
CREATININE	0.30 ± 0.12	4.25 ± 1.84	0.50 ±0. 80	0.68 ±0 .13	0.73 ± 0.15	0. 69 ±0. 06	0.53 ± 0.04	0. 33 ±0 .14
HbA1C	4.26 ± .72	12.84 ± 1.69	4.98 ±. 32	5.58 ± .13	5.68 ± .19	5.76 ±. 23	5.40 ±. 29	4.96 ±. 36
TRIGLYCERIDES	92.80 12.63	288.40 ± 90.64	116.00 ±14.91	132.80 ± 4.65	138.00 ± 4.84	141.80 ±5.63	109.40 ± 42.03	93.00 ± 8.03
CHOLESTROL	128.20±8.19	213.60 ± 15.33	135.00 ± 9.69	145.80 ± 4.76	152.80 ± 6.14	151.80 ± 9.98	142.60 ± 4.39	132.60 ±2.40

After 27 days of treatment with Selenicereus undatus extract, diabetics saw significant reductions in their urea, and bilirubin levels when compared to the control group (Table 3). As with mice given Selenicereus undatus extract fruit, all metformin-treated mices had the same effect as control mices. One of the most sensitive indicators of liver injury is an increase in AST or ALT levels [25]. A decrease in the structural integrity of the liver has been linked to an increase in AST and ALT levels in the bloodstream. When diabetic mices were compared to non-diabetic mices, the ethanolic extract of S.undatus significantly reduced the levels of AST and ALT in the diabetic mices livers. S.undatus's liver appears to function normally and to protect the liver as a result of its hepatoprotective properties.

The liver, renal, and pancreatic damage, as well as hyperglycemia-related alterations, may persist in the tissues. This includes changes in protein levels within the tissues of the experimental animals, such as the liver, pancreas, and kidneys. Diabetics have lower levels of protein in their liver and kidneys than the control group. For 27 days, diabetic mice were given Selenicereus undatus ethanolic fruit extract in addition to the standard medication metformin, and their values increased dramatically to levels close to normal. There were no negative effects observed in the group treated solely with Selenicereus undatus ethanolic extract. Endoplasmic reticulum injury causes P450 loss, which reduces protein synthesis and, as a result, the amount of total protein in an induced mice. Protein levels increased in the treated groups, indicating endoplasmic reticulum stability and subsequent induction of protein synthesis. Selenicereus undatus administration has been shown to stabilize the endoplasmic reticulum and thus increase protein production. According to the findings of this study, the liver glycogen levels of diabetic mice in this study were significantly lower than those of diabetic mice who received metformin as a standard treatment or those of diabetic mice who received Selenicereus undatus treatment. Diabetes was found to cause ALN hepatic glycogen loss in diabetic mice (Figure 3). Because insulin stimulates intracellular glycogen deposition while inhibiting glycogen phosphorylase, there is a

direct correlation between insulin activity and glycogen levels in various tissues [27]. This is because insulin stimulates intracellular glycogen deposition while inhibiting glycogen phosphorylase. According to the findings of a study on diabetic mice treated with extract, the glycogen synthase system in their livers has been restarted. According to the findings of the trials, Selenicereus undatus ethanolic fruit extract has a high level of antidiabetic activity as well as a stable level of liver glycogen.

5. CONCLUSION:

The ethanolic extract of S. undatus has been shown to lower blood glucose levels, which could be due to an increase in insulin secretion produced by pancreatic cell regeneration. Aside from that, it is discovered that S.undatus contains alkaloid and flavonoid compounds that can help treat diabetes and other diseases. They discovered that the ethanolic extract of S.undatus has anti-diabetic properties and could be useful in the treatment of diabetes.

Conflict of Interests

No conflict of interests

Acknowledgments

The authors are thankful to their Department Head of Zoology of Osmania University for providing facilities and encouragement

References:

1. Akah, P. A., Uzodinma, S. U., & Okolo, C. E. (2011). Antidiabetic activity of aqueous and methanol extract and fractions of Gongronema latifolium (Asclepidaceae) leaves in alloxan diabetic rats. Journal of Applied Pharmaceutical Science, 1(9), 99.
2. Shetti, A. A., Sanakal, R. D., & Kaliwal, B. B. (2012). Antidiabetic effect of ethanolic leaf extract of Phyllanthus amarus in alloxan induced diabetic mice. Asian journal of plant science and research, 2(1), 11-15.
3. Copeland, K. C., Zeitler, P., Geffner, M., Guandalini, C., Higgins, J., Hirst, K., ... & TODAY Study Group. (2011). Characteristics of adolescents and youth with recent-onset type 2 diabetes: the TODAY cohort at baseline. The Journal of Clinical Endocrinology & Metabolism, 96(1), 159-167.
4. Unwin, N., Gan, D., & Whiting, D. (2010). The IDF Diabetes Atlas: providing evidence, raising awareness and promoting action. Diabetes research and clinical practice, 87(1), 2-3.
5. Ghamarian, A., Abdollahi, M., Su, X., Amiri, A., Ahadi, A., & Nowrouzi, A. (2012). Effect of chicory seed extract on glucose tolerance test (GTT) and metabolic profile in early and late stage diabetic rats. DARU Journal of Pharmaceutical Sciences, 20(1), 1-9.
6. Kumar, K. S., Bhowmik, D., Srivastava, S., Paswan, S., & Dutta, A. (2012). Diabetes epidemic in India—a comprehensive review of clinical features, management and remedies. The Pharma Innovation, 1(2), 18.
7. Moglad, E. H., Alhassan, M. S., Koko, W. S., & Saadabi, A. M. (2012). In vitro antimicrobial activity of Sudanese medicinal plants. J. Med. Sci, 12(7), 219-223.
8. Anusooriya, P., Malarvizhi, D., Gopalakrishnan, V. K., & Devaki, K. (2014). Antioxidant and antidiabetic effect of aqueous fruit extract of Passiflora ligularis Juss. on streptozotocin induced diabetic rats. International Scholarly Research Notices, 2014.
9. Robards, K., & Antolovich, M. (1997). Analytical chemistry of fruit bioflavonoidsA review. Analyst, 122(2), 11R-34R.
10. Bonner-Weir, S. (1988). Morphological evidence for pancreatic polarity of ß-cell within islets of Langerhans. Diabetes, 37(5), 616-621.
11. Sasaki, T. (1972). Effect of acetic acid concentration on the colour reaction in the O-toluidine boric acid method for blood glucose determination. Rinsho kagaku, 1, 346-350.
12. Drabkin, D. L., & Austin, J. H. (1935). Spectrophotometric studies. J. biol. Chem, 112, 51-65.
13. Wybenga, D. R., Pileggi, V. J., Dirstine, P. H., & Giorgio, J. D. (1970). Direct manual determination of serum total cholesterol with a single stable reagent. Clinical chemistry, 16(12), 980-984.
14. Bucolo, G., & David, H. (1973). Quantitative determination of serum triglycerides by the use of enzymes. Clinical chemistry, 19(5), 476-482.
15. Reitman, S., & Frankel, S. (1957). A colorimetric method for the determination of serum glutamic oxalacetic and glutamic pyruvic transaminases. American journal of clinical pathology, 28(1), 56-63.
16. Kind, P. R. N., & King, E. (1954). Estimation of plasma phosphatase by determination of hydrolysed phenol with amino-antipyrine. Journal of clinical Pathology, 7(4), 322.
17. WQ, W. (1948). A rapid procedure for the estimation of total protein, true albumin, total globulin, alpha globulin, beta globulin and gamma globulin in 1.0 ml of serum. American Journal of Clinical Pathology, 18(9), 723-730.
18. Coulambe, C. G., & Favrean, L. A. (1965). Quaternary ammonium compound toxicity in chicken. Clinical Chemistry, 11(17), 624.
19. Bonsnes, R. W., & Taussky, H. H. (1945). On the colorimetric determination of creatinine by the Jaffe reaction. Journal of biological chemistry, 158(3), 581-591.
20. Anusooriya, P., Malarvizhi, D., Gopalakrishnan, V. K., & Devaki, K. (2014).

Antioxidant and antidiabetic effect of aqueous fruit extract of Passiflora ligularis Juss. on streptozotocin induced diabetic rats. International Scholarly Research Notices, 2014.
21. Morales, M. A., Jabbagy, A. J., & Terenizi, H. R. (1973). Mutations affecting accumulation of glycogen. Neurospora News Lett, 20(1), 24-25.
22. Chew, Y. L., Chan, E. W. L., Tan, P. L., Lim, Y. Y., Stanslas, J., & Goh, J. K. (2011). Assessment of phytochemical content, polyphenolic composition, antioxidant and antibacterial activities of Leguminosae medicinal plants in Peninsular Malaysia. BMC complementary and alternative medicine, 11(1), 1-10.
23. DeFronzo, R. A., & Tripathy, D. (2009). Skeletal muscle insulin resistance is the primary defect in type 2 diabetes. Diabetes care, 32(suppl 2), S157-S163.
24. Ahmed, O. M., Abdel-Reheim, E. S., Ashour, M. B., Fahim, H. I., & Mohamed, H. H. (2016). Efficacies of Eruca sativa and Raphanus sativus seeds' oils in streptozotocin-induced diabetic rats. International Journal of Clinical Endocrinology and Metabolism, 2(1), 034-043.
25. Yadav, N. P., Pal, A., Shanker, K., Bawankule, D. U., Gupta, A. K., Darokar, M. P., & Khanuja, S. P. (2008). Synergistic effect of silymarin and standardized extract of Phyllanthus amarus against CCl4-induced hepatotoxicity in Rattus norvegicus. Phytomedicine, 15(12), 1053-1061..
26. Naskar, S., Islam, A., Mazumder, U. K., Saha, P., Haldar, P. K., & Gupta, M. (2010). In vitro and in vivo antioxidant potential of hydromethanolic extract of Phoenix dactylifera fruits. Journal of Scientific Research, 2(1), 144-157.
27. Malini, P., Kanchana, G., & Rajadurai, M. U. R. U. (2011). Antibiabetic efficacy of ellagic acid in streptozotocin-induced diabetes mellitus in albino wistar rats. Asian J Pharm Clin Res, 4(3), 124-128.

ISSN 0975-2366
DOI:https://doi.org/10.31838/ijpr.2022.14.01.014

Research Article

Antidiabetic activity of alcoholic extract of *Momordica Charantia* and *Murraya koenigii* in alloxan induced albino rat

V.MANGESH[1], M.KISHORE[1], S.JITHENDER KUMAR NAIK[1*], ANUSHA C PAWAR[1], S.VAMSHI[1], K.SIREESHA[2], N.RAMESH KUMAR[3]

[1]Toxicology Lab, Department of Zoology, University College of Science, Osmania University, Hyderabad, Telangana State-500007 India.

[2]Department of Environmental sciences, College of Science Osmania University, Hyderabad, Telangana State, Telangana State-500007 India.

[3]Department of Genetics, University College of Science Osmania University, Hyderabad, Telangana State, Telangana State-500007 India.

*Corresponding author:
Email: drnaik8777@yahoo.com

Received: 12.10.21, Revised: 05.11.21, Accepted: 22.12.21

ABSTRACT

Diabetes mellitus (DM), one of the most metabolic illnesses, has a major influence on health and quality of life. Phytotherapy has gained a significance as one of the complementary alternative and safe treatment modalities against diabetes than the synthetic medication. *Momordica charantia* (MC) and *Murraya koenegii* (MK) are extensively used as antidiabetic agent. In this study, we have examined the effect of oral administration of extracts of MC- fruits and MK leaves in comparison with standard antidiabetic drug, Metformin (120mg/kg body weight) in alloxan induced diabetic albino rat on biochemical parameters such as fasting blood glucose (FBG), hemoglobin, serum creatinine, albumin and urea, serum glutamate oxaloacetate and pyruvate transaminase (SGOT and SGPT), catalase, superoxide dismutase (SOD), and lipid peroxidase (LPO). The results show a significant decrease ($p \geq 0.05$) in serum glucose levels (range 5.39±0.11 mmol/L to 6.41±0.09 mmol/L) in MC and MK treated diabetic rats and non-diabetic rats fed with both MC and MK (400mg/kg body weight), metformin (4.41±0.07 mmol/L) compared to the alloxan induced non treated diabetic rats (8.41±0.08 mmol/L). The administration of diabetic rats with plant extracts for 14 days periods brought a remarkable alteration in returned blood glucose levels that are close to normal values reported in control group (4.44±0.14 mmol/L. For all the parameters evaluated, the results observed were significant and in close comparison with the standard antidiabetic drug, Metformin. This indicates that the extracts of MC and MK have diminishing effect on severity of diabetes.

Keywords: *Murraya Koenegii*, *Momordica charantia*, antidiabetic activity, Metformin

1. INTRODUCTION

Diabetes has become a serious worldwide health problem rising concern among nations around the world and research to address the problem. Diabetes mellitus (DM) is a multisystem illness characterized by lack of insulin secretion (Type-I) or insensitivity (Type-II) [1]. It is frequently associated with comorbidities such as hyperlipidemia, diabetic nephropathy and cardiovascular illnesses. Recent Studies on Type-I and Type-II diabetes indicates alarming situations in posing a serious health hazard across the worldwide population [2, 3]. Biguanides, glibenclamide, and Dipeptidyl peptidase-4 (DPP-4) inhibitors Provide an excellent therapeutic results for DM and are expensive with adverse effects [4-6]. Although insulin and several types of synthetic oral hypoglycemic medications are available to treat diabetes, synthetic medicines can have significant side effects and toxicity. Given the long-term need for therapy, finding effective, nontoxic, and affordable antidiabetic agents is critical. As a result, complementary and functional foods, as well as alternative pharmaceuticals, have emerged as novel therapeutic options for the management of diabetes.

The quest for safe and effective medications has been a major focus of current research. The research for safe and effective anti-diabetic agents from natural materials is gaining importance. Many studies are now being conducted to investigate plant natural products containing particular phyto components with anti-diabetic potential as an alternative treatment [2].

Murraya koenegii and *Momordica charantia* are two prominent plants that are referenced in Ayurveda for their therapeutic benefits. M. charantia, popularly known as bitter melon, belongs to the Cucurbitaceae family of cucumbers. It grows in tropical and subtropical climates across the globe. Bitterness may be found in all sections of the plant, including the fruit. Bitter melon has anti-diabetic, anti-inflammatory, anti-microbial, anti-HIV, anti-leukemic, anti-ulcer, anti-tumor effects in its fruits and seeds. It may be used as an alternate treatment for diabetic people who need to reduce their blood glucose levels [7]. This is attributable to the bitter melon extract's complex effect of several components [8]. The bioactive compounds responsible for its hypoglycemic effect include a combination of steroidal saponins known as charantins, insulin-like peptides, and alkaloids [9].

M. koenigii leaf also known as curry leaves, (L), are extensively used as a condiment and spice in India and other tropical nations. It is a member of the Rutaceae (citrus) family and has been used as a diabetes therapy in Ayurveda [10]. Several investigations on diabetic animal models have shown that MK leaves have anti-diabetic properties [11-13]. *Murraya koenigii* leaves have a phytochemical profile that includes vitamins, carbazole alkaloids, triterpenoids, minerals and phenolic compounds [14, 15]. MK's antioxidant action is primarily due to carbazole alkaloids [16]. Given the richness of natural plant products with anti-diabetic potential, research into herbal medicines as an alternative therapy and should be prioritized in its usage by reduce in synthetic drugs. As a result, the bioactive components of two plant sources, both of which are dietary constituents and high in antioxidants, were studied in the current research. In alloxan- induced diabetic rats, the effects of alcoholic extracts of *M. charantia* (karela) and *Murraya koenigii* (curry leaves) on hyperglycemia and other related markers, blood hemoglobin, liver functional tests (SGOT and SGPT as key indicators), SOD, Catalase as antioxidant defenses. the oxidative stress in terms of LPO activity, creatinine, serum albumin, and urea as renal functional test were performed. A comparison of the plant treatments with metformin, a commonly used synthetic antidiabetic drug, was also made.

2. MATERIALS AND METHODS

Induction of diabetes in rats

All the animals, except control group and group-VI were allowed to fast 12 h and were intraperitoneally injected with ice cold alloxan monohydrate, 150mg kg body weight (freshly prepared) with sterile water (2%) at a dose of

Materials and chemicals Alloxan, Metformin, bovine serum albumin and d- glucose were purchased from Sigma Chemical Co. All other chemicals used were of analytical grade.

Plant material preparation

The fresh fruits of *M. charantia* and the leaf of *M. koenegii* were collected from local farms and markets. The plants were identified and authenticated by a taxonomist from Department of Botany, Osmania University, Hyderabad and the voucher specimens were deposited as herbarium. The plant materials leaf and fruit were washed, dried under shade, then cut into pieces, and seeds were removed from the pulps, then ground to homogeneous powder (40– 60 mesh) and stored at a dry place for further use.

Extraction of plant phytochemicals

Extraction was carried out by methanol solvent using soxhlet apparatus as described by [17]. *M. charantia* fruit and *M. koenegii* were extracted using methanol (100g/1000mL) for 10 h up to 22 cycles at 40ºC until in the extractor siphon became colorless. The extract was then filtered and the residue re-extracted with 80% ethanol. The extraction process was repeated for three times. After filtration, the combined filtrates were evaporated to remove the solvent with a rotary evaporator (Make) at 40ºC. The extract was freeze-dried and then preserved at 4 ºC for further experimentation.

Acclimatization of animals

Thirty six male albino rats roughly weighing (200 - 250g) were purchased from jeeva life sciences (Hyderabad, India). All animals were kept in clean, sanitized PVC coated stainless steel cages in an air-conditioned animal house with typical climatic conditions such as a constant temperature of 20–25˚C, relative humidity of 45– 55%, and a 12 hour light–dark cycle. Animals were fed with a regular pelletized feed and free access to water before and throughout the experiment. Animals were fasted for 12 hours before administering experimental treatments, but were allowed proper access to water. All of the trials were carried out during the day. Before the commencement of the experiment, the procured rats were acclimatized to the laboratory conditions for 7-days. This work is carried out in accordance with the animal ethics as also approved by the intuitional animal ethics committee of the department.

150mg/kg body weight. Fasting blood glucose levels (FBG) were measured after a week when the condition of diabetes was stabilized. Animals with marked hyperglycemia (fasting blood glucose concentration level above 11.1mmol/L) were considered to be diabetic and used for further the experimentation.

.

Experimental design

The experiment was conducted for a period of 21 days. The first 7 days were for the induction of diabetes in rats and the following 14 days were the investigational period with crude alcoholic extracts of MC and MK administered, separately. The plant extracts were dissolved in and administered orally on daily basis for a period of 14 days.

The experiment was conducted in six groups of six rats each.

Group-1: Normal saline treated rats (Normal control-NC)

Group-2: Normal saline treated alloxan induced diabetic rats (Diabetic Control-DC) (AID)

Group-3: Alloxan induced diabetic rats treated with metformine synthetic drug, (120 mg/kg. of body weight) (AIM)

Group-4: Alloxan induced Diabetic rats treated with *M.charntia* Fruit crude extract (400mg/kg of body weight (DMC)

Group-5: Alloxan induced Diabetic rats treated with *M.Koengii* leaves crude extract. (500mg/kg of body weight (DMK)

Group-6: Non-diabetic rats treated with crude extract of M.charantia Fruit + *M.Koengii* leaves, 400mg/kg of body weight (CMM)

At the end of the experimental period, the animals were fasted overnight and then sacrificed by cervical decapitation. Blood was collected in tubes containing EDTA for the estimation of glucose as described by [18], hemoglobin as described by [19]. Estimation of creatinine, albumin [20-21] and urea as biochemical markers of kidney functioning was performed by method similar [22].

Measurement of antioxidant parameters in the liver

The liver tissue was homogenized in 0.9% NaCl solution, and then centrifuged at 3000 rpm for 10 minutes. The above procedures were performed at 4°C. The supernatant obtained was used for determination of SGOT and SGPT as biochemical markers of liver functioning by Reitman and Frankel method [23] and antioxidant enzymes (Superoxide dismutase (SOD), Catalase, lipid peroxidase (LPO) according to the procedure described by [24]. Total protein content was determined by Lowry *et al.*,(1951)

STATISTICAL ANALYSIS

The analysis data was subject to statistical analysis by a one-way analysis of variance was (ANOVA) using SPSS -22 version software performed. The POST-Hoc test was run at a 5% level of significance. All the values are represented as Mean ± SD results are shown as bar graphs. When the p-value was less than 0.05, the results were deemed statistically different.

RESULTS

The blood glucose and haemoglobin levels of the control and experimental groups of rats (Table 1 and 2). Blood glucose and hemoglobin levels were relatively same in experimental rats given plant extracts and Metformin medication, with small variations, however in the AID-group, there was a considerable increase in blood glucose (2- fold rise) and a drop in hemoglobin content (13.25 mg/dL). These levels were found to be equivalent to those of normal rats after oral treatment of plant extracts of MC and MK, as well as the synthetic antidiabetic medication Metformin, and the MC extract has shown more pronounced significant antidiabetic activity as compared to M. Koingeii extract. The extracts, as well as the Metformin therapy, significantly reduced blood sugar levels in diabetic rats.

Table 1: Effect of MC and MK plant extracts on blood glucose levels and Hemoglobin levels

Group	**Mean±SD (m.mol/L)** blood glucose levels	**Mean±SD (m.mol/L) Hemoglbin** levels
CONTROL	4.44 ± 0.36	14.98 ± 0.29
AID	8.41 ± 0.21	13.25 ± 0.51
AIM	4.41 ± 0.17	14.75 ± 0.50
DMM	5.39 ± 0.26	14.78 ± 0.11
DMK	5.51 ± 0.29	14.75 ± 0.60
CMM	6.41 ± 0.23	14.26 ± 0.74

Values are Mean ± SD; significance P<0.05

There was a substantial difference in mean blood glucose levels between the alloxan-induced diabetes groups and the normal control group ($p<0.05$), as shown in Table-1. The blood glucose

level of the normal control group was 4.44 0.14 mmol/L, but the blood glucose level of the MC and MK extract treated diabetic rats varied from 5.390.11 mmol/L to 6.410.09 mmol/L. Thus, it was clear that intraperitoneal administration of metformin at a dose of 120 mg/kg body weight generated a strong diabetogenic reaction in rats, as shown by elevated blood glucose (8.410.08 mmol/L). In diabetic rats, administration of *M. charantia* extract resulted in a statistically significant decrease in mean blood glucose levels (p 0.05). The blood glucose level of untreated diabetic rats was considerably greater than that of treated diabetic rats (p0.05). The diabetics' blood glucose levels were reduced to 5.390.11 mmol/L and 6.410.09 mmol/L, respectively, after administration of plant extracts, with no significant difference between the two dose groups and the normal control group.

Effects of Plant extracts on Renal functioning

There were significantly high levels of serum creatinine (1.58±0.06 mg/dL), albumin (6.5±0.21 mg/dL) and urea (66.33±2.04 mg/dL) levels were observed in alloxan induced diabetic rats (Table-2). Compared with the non-treated alloxan induced diabetic rats, diabetic rats treated with plant extracts exhibited considerable decreased levels (Figure-1, 2 and 3). 14 days treatment with plant extracts significantly reduced creatinine (AIM-1.25±0.03 mg/dL, DMC-1.4±0.11 mg/dL, DMK-1.48±0.12 mg/dL and CMM-1.56±0.27 mg/dL) levels compared to control group (0.68±0.09 mg/dL). The albumin levels ranged from (AIM-4.47±0.28 mg/dL, DMC-5.45±0.27 mg/dL, DMK-5.39±0.17 mg/dL and CMM-5.49±0.15 mg/dL) levels compared to control group (4.50±0.15 mg/dL). The urea levels ranged from (AIM-31.67±0.55 mg/dL, DMC-35.23±1.2 mg/dL, DMK-38.66±0.97 mg/dL and CMM-41.23±0.64 mg/dL) levels compared to control group (29.85±1.44 mg/dL). The creatinine, urea and albumin levels in diabetic rats treated with plant extracts were comparable with metformin treated diabetic rats (AIM). Whereas, in non-diabetic rats treated with mixed crude extract exhibited a faint response for all the parameters studied.

Table: 2. Effect of *Momordica charantia* and *Murraya Koenigii*, crude extract on creatinine, albumin and urea

S. No	Parameter	Control n=6	Alloxan Induced Daibetic Mice (AID)	Alloxan Induced Diabetic Metformine (AIM)	Alloxan Induced Diabetic Mice + *M.Charntia* (DMM)	Alloxon Induced Diabetic Mice + M.Koengii (DMK)	Crude extract of M.Charanti + M.Koengii (CMM)
1	Creatinin mg/dl	0.68 ± 0.91	1.58 ± 0.06	1.25 ± 0.03	1.40 ± 0.11	1.48 ± 0.12	1.56 ± 0.27
2	Albumin mg/dl	4.50 ± 0.15	6.50 ± 0.21	4.47 ± 0.28	5.45 ± 0.27	5.39 ± 0.17	5.49 ± 0.15
3	Urea mg/dl	29.85 ± 1.44	66.33 ± 2.04	31.67± 0.55	35.23 ±1.2	38.66± 0.97	41.23 ±0.64

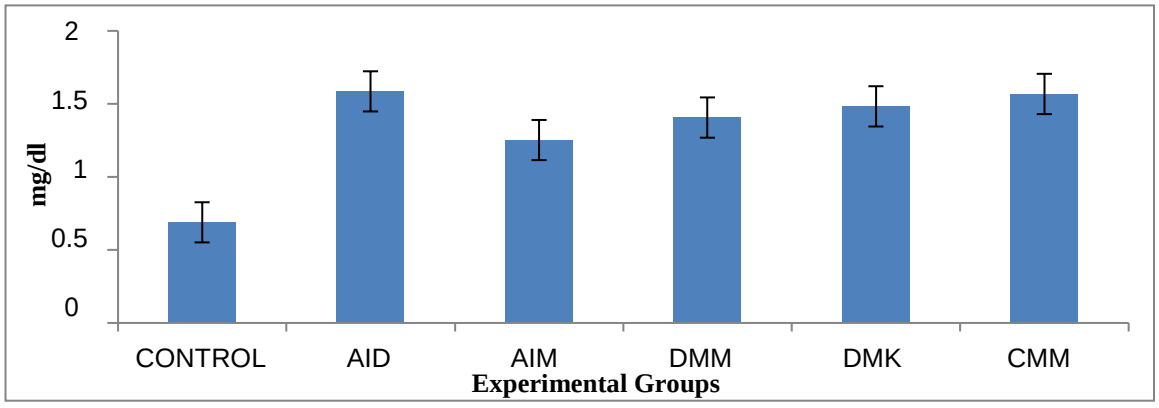

Fig.1: Effect of *Momordica charantia* and *Murraya Koenigii*, crude extract on creatinine

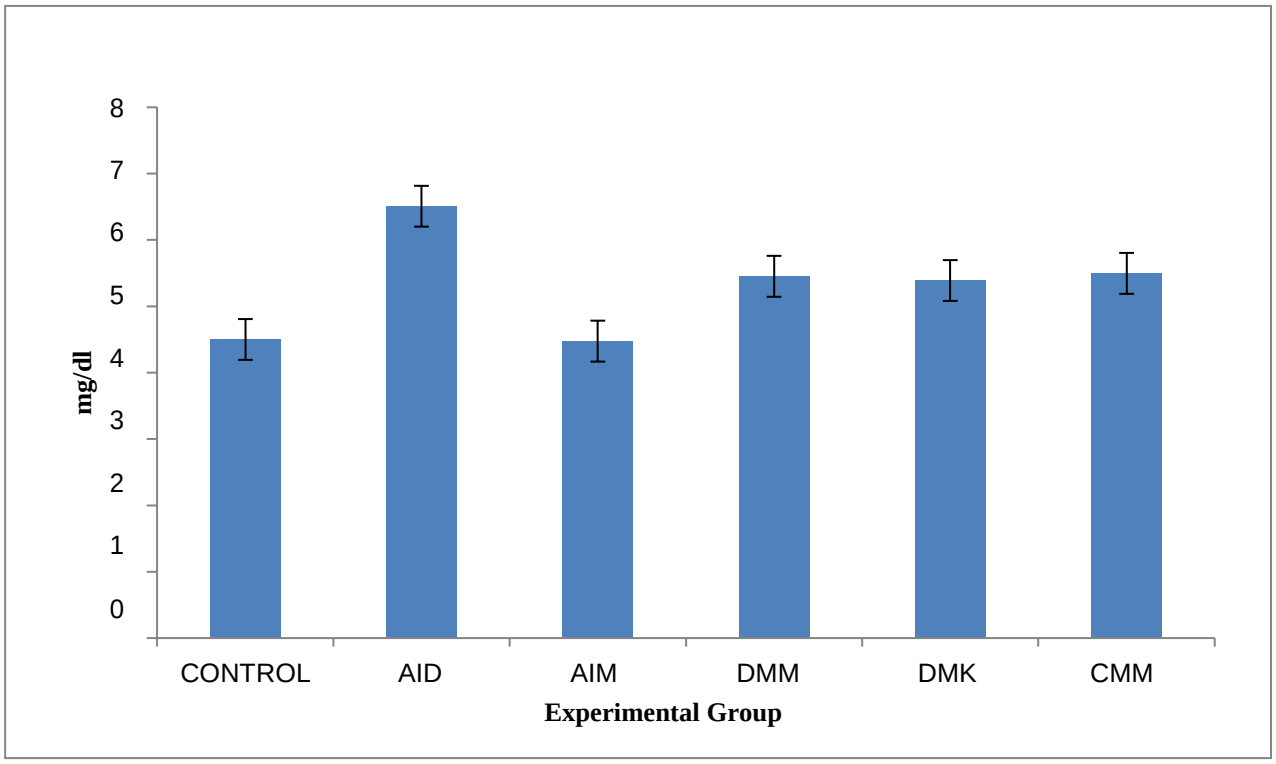

Fig.2: Effect of *Momordica charantia* and *Murraya Koenigii*, crude extract on albumin

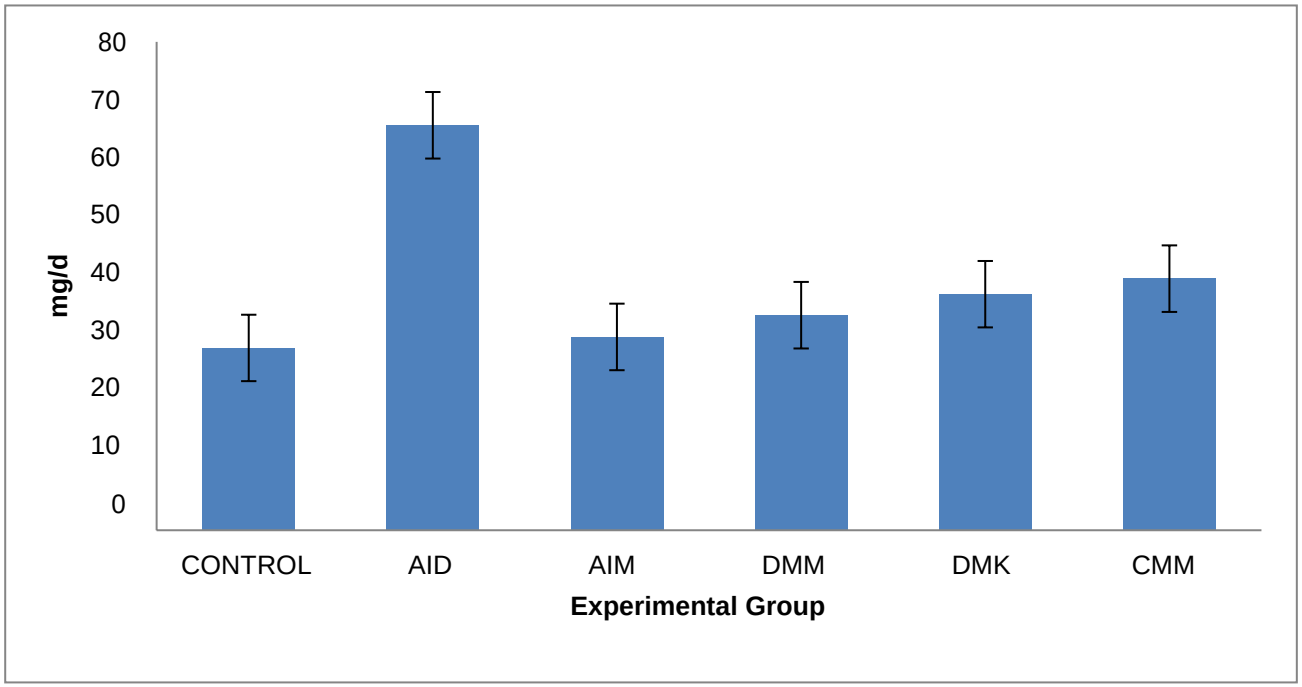

Fig.3: Effect of *Momordica charantia* and *Murraya Koenigii*, crude extract on urea

Effects of Plant extracts on liver functioning

A significant increase in SGOT (122.5±0.11 mg/dL) and SGPT (123.3±1.24 mg/dL) levels were observed in alloxan induced diabetic rats (Table-4). Compared with the non-treated alloxan induced diabetic rats, diabetic rats treated with plant extracts exhibited considerable decreased levels (Figure-4 and 5).14 days treatment with plant extracts significantly reduced SGOT (AIM-62.3±1.4 mg/dL, DMC-64.4±1.08 mg/dL, DMK 67.7±1.41 mg/dL and CMM-75.05±1.68mg/dL) levels compared to control group 61.47±1.17 mg/dL). The SGPT levels ranged from (AIM-54.9±0.96 mg/dL, DMC-57.9±2.07mg/dL, DMK-64.92±2.39 mg/dL and CMM- 69.87±1.99 mg/dL)

levels compared to control group (53.9±1.2 mg/dL).

The SGOT and SGPT levels in diabetic rats treated with plant extracts were comparable with metformin treated diabetic rats (AIM). Whereas, in non-diabetic rats treated with mixed crude extract exhibited a faint response for all the parameters studied. The values are significant at P<0.01/0.05 leads. The antioxidant enzymes such as SOD-CAT along with LPO activity was analyzed as a key parameters for oxidative stress. Significant and nearly equivalent results were observed among the metformin treated diabetic group and plant extract treated groups (Figures 6-8). Comparatively, no significant on tested parameters was observed with mixed crude extract treated non-diabetic rats.

Table: 3 Effect of *Momordica charantia* and *Murraya koenigii*, ethanol extract on Liver function

S.No	Parameters	Control	Alloxan Induced Daibetic Mice (AID)	Alloxan Induced Mice+ Metformi ne (AIM)	Diabetic Mice + *M.Charntia* (DMM)	Diabetic Mice + *M. koengii* (DMK)	Crude extract of *M.Charantia* + *M.Koengii* (CMM)
1	SGOT (mg/d l)	61.47 ± 1.17	122.5 ± 0.11	62.3 ± 1.40	64.4 ± 1.08	67.7 ± 1.41	75.05 ±1.68
2	SGPT (mg/d l)	53.9 ± 1.20	123.3 ± 1.24	54.9 ± 0.96	57.9 ± 2.07	64.92 ± 2.39	69.87 ±1.99

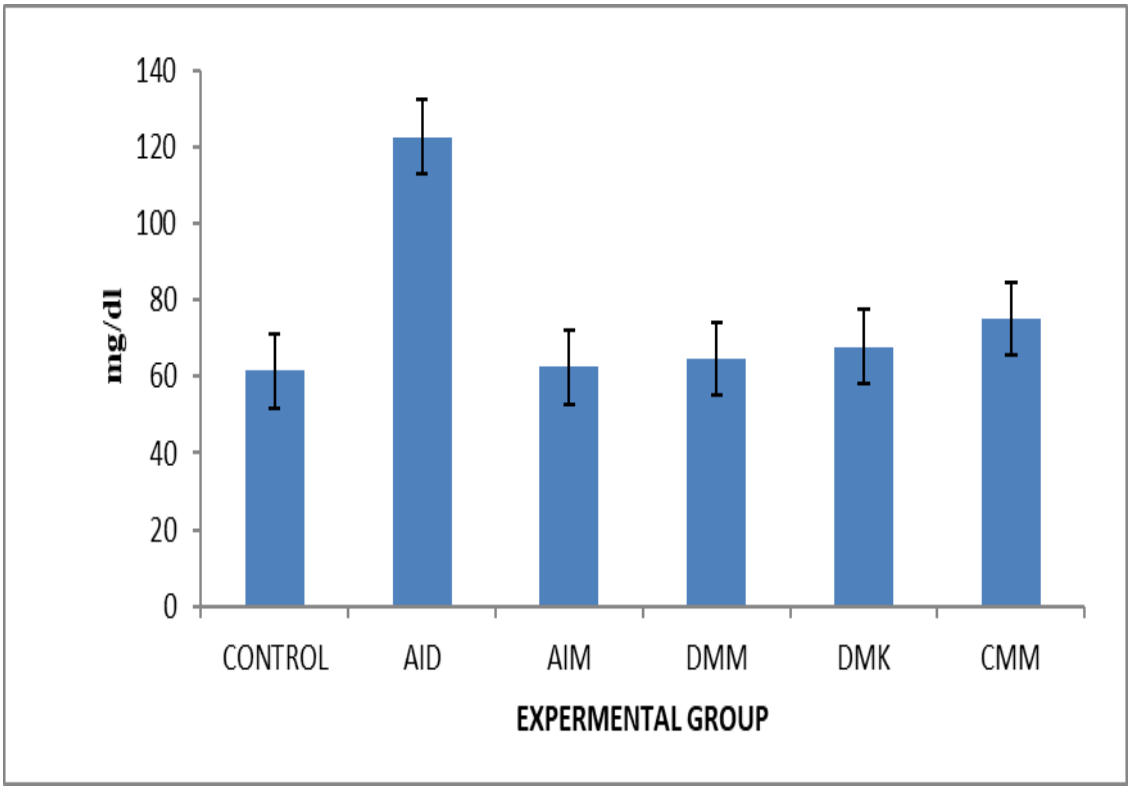

Fig.4: Effect of *Momordica charantia* and *Murraya Koenigii*, crude extract on SGOT

Table: 4 Effect of Momordica charantia and Murraya koenigii, Ethanolic extract on plasma antioxidant profiles

S.No	Parameters	Control Group - I	Alloxan Induced Daibetic Mice Group - II	Alloxan Induced Mice + Metformine Group - III	Diabetic Mice + M.Charntia Group-IV	Diabetic Mice + M. Koengii Group - V	Crude extract of M.Charantia + M. Koengii Group - VI
1	LPO (g/dl)	0.13 ± 0.01	0.36 ± 0.02	0.13 ± 0.02	0.24 ± 0.23	0.25 ± 0.03	0.24 ± 0.02
2	Antioxidant enzymes SOD (U/mg protein)	80.6 ± 0.53	185.5 ± 0.29	87.5 ± 1.4	95.7 ± 3.9	104.05 ± 1.16	110.2 ± 1.8
3	CAT (U/mg protein)	33.45 ± 3.3	9.87 ± 1.45	29.9 ± 1.6	29.6 ± 1.12	28.02 ± 2.29	27.2 ± 1.43
4	Total Protein (g/dl)	8.11 ± 0.43	9.91 ± 0.77	10.0 ± 0.70	10.8 ± 0.58	12.2 ± 0.62	14.85 ± 0.53

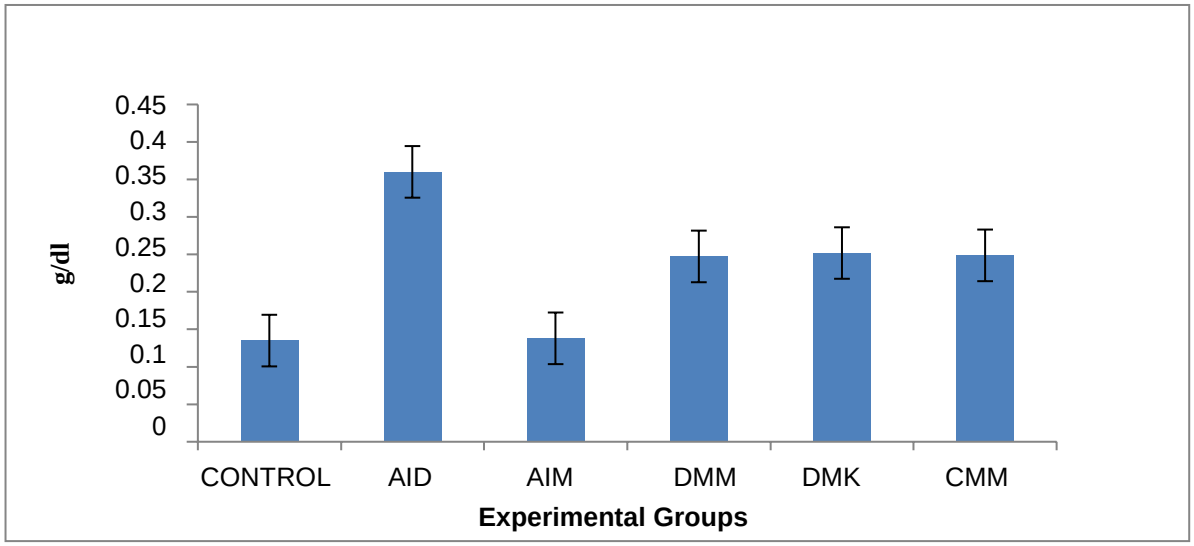

Fig.5: Effect of *Momordica charantia* and *Murraya koenigii* ethanolic extract on LPO

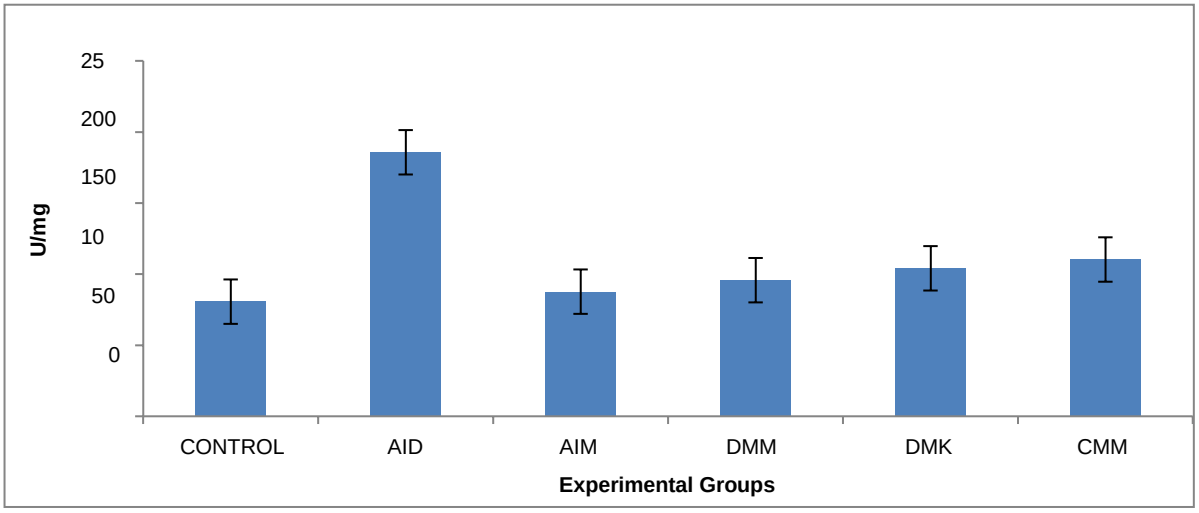

Fig.6: Effect of *Momordica charantia* and *Murraya koenigii* ethanolic extract on SOD

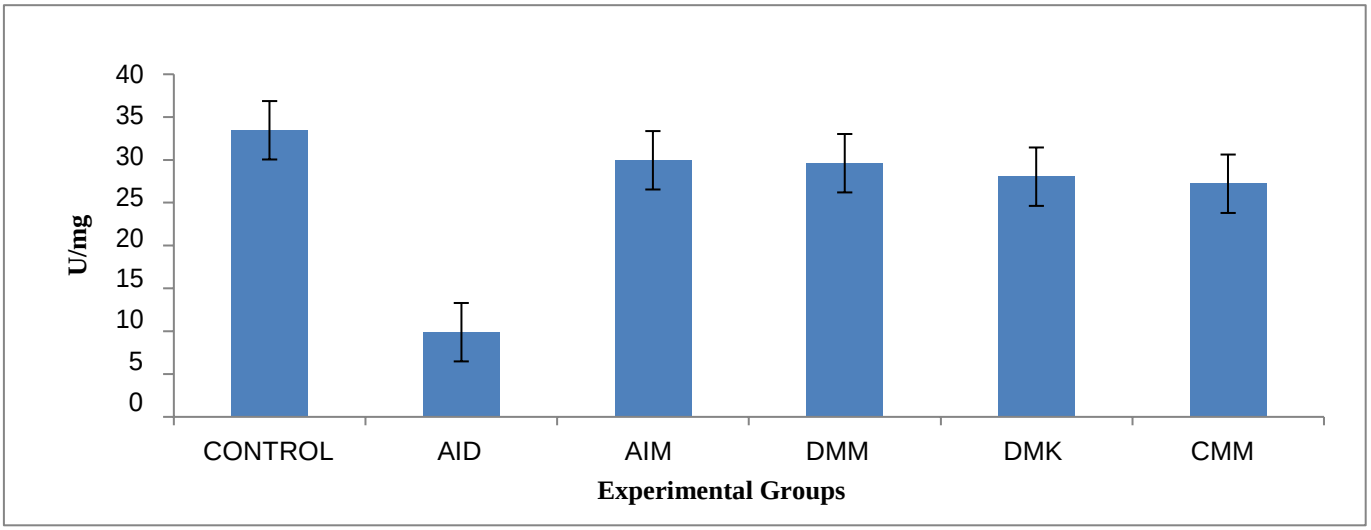

Fig.7: Effect of *Momordica charantia* and *Murraya koenigii*, ethanolic extract on catalase

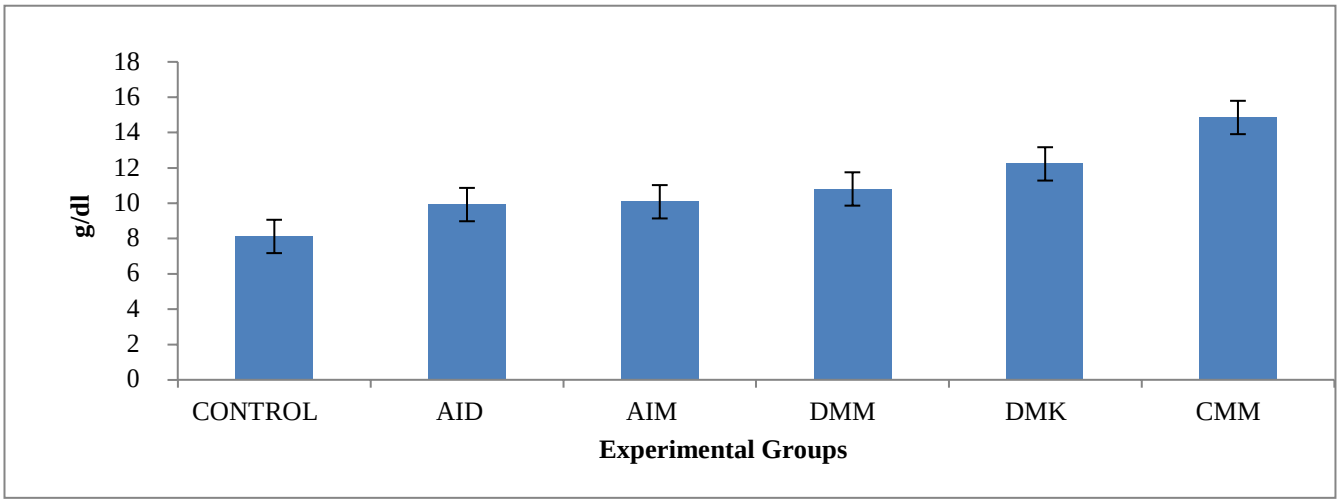

Fig.8: Effect of *Momordica charantia* and *Murraya koenigii*, ethanolic extract on serum protein

DISCUSSION

A wide range of foods, including cereals, vegetables, and spices, have been studied for their anti-hypoglycemic properties. MC and MK are well-known for its medicinal properties and used to treat the diabetes by the traditional practitioners. Alloxan has been proven to destroy pancreatic beta cells, resulting in hyperglycemia. Hyperglycemia was the hallmark of diabetes in our studies. Treatment with alcoholic extracts of MC and MK reduced plasma glucose in diabetic rats considerably ($P < 0.05$). Many researchers have reported the hypoglycemic impact of MC and MK [27-29]. This may be due to enhanced glycogenesis, reduced glycogenolysis, or gluconeogenesis [29], and/or the increased glucose uptake and use by cells, might be the mechanisms of action [30]. When the serum glucose concentrations of diabetic MC and diabetic MK treated groups were evaluated, it was shown that both plant extracts are similarly effective as hypoglycemic agents when compared to the conventional antidiabetic medicine metformin. This might be related to the fact that the test groups had comparable insulin responses. This indicated that both plant extracts work as insulin secretagogues in the same way.

Glaciation of proteins such as haemoglobin occurs when blood glucose levels are high [31], resulting in the generation of reactive oxygen species (ROS), which leads to increased lipid peroxidation and cytotoxicity [32]. Diabetic patients' total haemoglobin levels are often substantially lower than usual [33]. In the current investigation, there was no significant difference in haemoglobin levels between diabetic rats treated with plant extract and non-diabetic control rats. The preventive effect of MC and MK plant extracts is supported by these findings. By measuring blood creatine, albumin, and urea, the impact of MC

and MK extracts on kidney function was determined.

SOD and catalase play an important role in protection against oxidative damage, which are the hallmark of toxicity. Increased SOD activity would result in the creation of hydrogen peroxide, which, unless quenched by catalase and LPO, would result in the development of reactive oxygen species (ROS) that cause damage. Hepatotoxicity is linked to high levels of these enzymes. In the present study, nearly close results were observed for SOD and catalase among metformin treated diabetic rats and plant extract treated rats. The plant extracts have shown decreased levels of SOD, LPO and catalase as comparable to protection offered by standard drug metformin. The incidence of heart and liver illnesses will rise as SGOT and SGPT levels rise. Their elevated levels are often linked to heart attacks and liver problems. Administration of plant extracts in diabetic rats has significantly decreased the SGPT, SGOT and catalase levels, which is an indication of hepatoprotective effect.

CONCLUSION

In diabetes adequate care, and optimal glycemic Index control is critical. In the present study both *M. charantia* and *M. koenigii* crude extracts exerts it's beneficial in controlling the blood glucose levels, limits the lipid peroxidation by antioxidant activity by quenching the overproduction of free radicals which in terms supported by an increased SOD and CAT antioxidant enzymatic defenses and decreased creatinine, albumin and urea in experimental alloxan-induced diabetic rats. Diabetic management is a mix of antihyperglycemic medication therapy and monitoring of liver and kidney function. Thus, both leaf extracts studied in our investigation demonstrated powerful antidiabetic effects equivalent to the synthetic medication metformin, with *M. charntia*-treated rats exhibiting a stronger impact. Finally, our investigation demonstrates that extracts of *M. charantia* and *M. koenigii* leaves have a modulatory effect in the treatment of diabetes mellitus and may be used as part of diabetes management therapy. Because these plants have long been used as stable food in day to day life, they may be safe to use as dietary supplements and medications. However, a long-term research is required since plant compounds are slower to work than synthetic medications, and greater dosages may cause a plateau effect, which would be detrimental to diabetes treatment. Further studies are to be carried out to isolate, and identify specific active compounds responsible for antidiabetic activity in the tested plant materials.

ACKNOWLEDGMENT:

This work is supported by the financial assistance under BSR-JRF, UGC. We are thankful to the Head Department, Dean, and UGC for their support and suggestions. We also thankful to members of IAEC, Osmania University.

Conflict of Interest:

The authors declare that they don't have any conflict of interest.

REFERENCES

1. Yousef, F., Mansour, O., & Herbali,. (2018). Sulfonamides: Historical discovery development (structure-activity relationship notes). vitro In-vivo In-silico Journal, 1(1), 1-15.
2. Wild, S., Roglic, G., Green, A., Sicree, R., & King, H. (2004). Global prevalence of diabetes: estimates for the year 2000 and projections for 2030. Diabetes care, 27(5), 1047-1053.
3. Noor, A., Gunasekaran, S., Manickam, A. S., & Vijayalakshmi, M. A. (2008). Antidiabetic activity of Aloe vera and histology of organs in streptozotocin-induced diabetic rats. Current science, 1070-1076.
4. Noor, A., Gunasekaran, S., Manickam, A. S., & Vijayalakshmi, M. A. (2008). Antidiabetic activity of Aloe vera and histology of organs in streptozotocin-induced diabetic rats. Current science, 1070-1076.
5. Kesari, A. N., Gupta, R. K., & Watal, G. (2005). Hypoglycemic effects of Murraya koenigii on normal and alloxan-diabetic rabbits. Journal of Ethnopharmacology, 97(2), 247-251.
6. Larmer, J., & Gilman, A. G. (1985). Insulin and oral hypoglycemic drugs, glucogan. The pharmacological basis of therapeutics. 7th Edition New York: Macmillan Publishing, 1490.
7. Joseph, B., & Jini, D. (2013). Antidiabetic effects of Momordica charantia (bitter melon) and its medicinal potency. Asian pacific journal of tropical disease, 3(2), 93-102.
8. Basch, E., Gabardi, S., & Ulbricht, C. (2003). Bitter melon (Momordica charantia): a review of efficacy and safety. American Journal of Health- System Pharmacy, 60(4), 356-359.
9. Raman, A., & Lau, C. (1996). Anti-diabetic properties and phytochemistry of Momordica charantia L. (Cucurbitaceae). Phytomedicine, 2(4), 349-362.
10. Satyavati, G. V., Raina, M. K., & Sharma,M. (1976). Medicinal plants of India ICMR. New Delhi, 1, 278-281.
11. Vinuthan, M. K., Girish Kumar, V., Ravindra, J. P., & Narayana, K. (2004). Effect of extracts of Murraya koenigii leaves on the levels of blood glucose and plasma insulin in alloxan-induced diabetic rats. Indian journal of physiology and pharmacology, 48(3), 348-352.

12. Kesari, A. N., Gupta, R. K., & Watal, G. (2005). Hypoglycemic effects of Murraya koenigii on normal and alloxan-diabetic rabbits. Journal of Ethnopharmacology, 97(2), 247-251.
13. Murraya koenigii on normal and alloxan-diabetic rabbits. Journal of Ethnopharmacology, 97(2), 247-251.
14. Tembhurne, S. V., & Sakarkar, D. M. (2010). Protective effect of Murraya koenigii (L) leaves extract in streptozotocin induced diabetics rats involving possible antioxidant mechanism. Journal of Medicinal Plants Research, 4(22), 2418-2423. Chakrabarty, M., Nath, A. C., Khasnobis, S., Chakrabarty, M., Konda, Y., Harigaya, Y., & Komiyama, K. (1997). Carbazole alkaloids from Murraya koenigii. Phytochemistry, 46(4),751-755.
15. Narendhirakannan, R. T., Subramanian, S., & Kandaswamy, M. (2005). Mineral content of some medicinal plants used in the treatment of diabetes mellitus. Biological trace element research, 103(2), 109-115.
16. Tachibana, Y., Kikuzaki, H., Lajis, N. H., & Nakatani, N. (2003). Comparison of antioxidative properties of carbazole alkaloids from Murraya koenigii leaves. Journal of agricultural and food chemistry, 51(22), 6461-6467.
17. Igbinosa, O. O., Igbinosa, E. O., & Aiyegoro, O. A.(2009). Antimicrobial activity and hytochemical screening of stem bark extracts from Jatropha curcas (Linn). African journal of pharmacy and pharmacology, 3(2), 058-062.
18. Wang, Q., Lu, G., & Yang, B. (2004). Direct electrochemistry and electro catalysis of hemoglobin immobilizedon carbon paste electrode by silica sol–gel film. Biosensors and Bioelectronics, 19(10), 1269-1275.
19. Khan, R. A., Khan, M. R., & Sahreen, S. (2010). Evaluation of Launaea procumbens use in renal disorders: A rat model. Journal of ethnopharmacology, 128(2), 452-461.
20. Kelner, M. J., & Bagnell, R. (1991). Alteration of growth rate and fibronectin by imbalances in superoxide dismutase and glutathione peroxidase activity. In Biological ReactiveIntermediates IV (pp. 305-309). Springer, Boston, MA.
21. Osswaldi, W. F., Kraus, R., Hippeli, S., Benz, B., Volpert, R., & Elstner, E. F. (1992). Comparison of the Enzymatic Activities of Dehydroascorbic acid Reductase, Glutathione Reductase, Catalase, Peroxidase and Superoxide Dismutaseof Healthy and Damaged Spruce Needles (Picea abies (L.)Karst.)'. Journal of Plant Physiology, 139(6), 742-748.
22. Babizhayev, M. A. (1989). Accumulation of lipid peroxidation products in human cataracts. Acta Ophthalmologica, 67(3), 281-287.
23. Reitman, S., & Frankel, S. (1957). A colorimetric method for the determination of serum glutamic oxalacetic and glutamic pyruvic transaminases. American journal of clinical pathology, 28(1), 56-63.
24. Levey, A. S., Perrone, R. D., & Madias, N. E. (1988). Serum creatinine and renal function. Annual review of medicine, 39(1), 465-490.
25. Khan, B. A., Abraham, A., & Leelamma, S. (1995). Hypoglycemic action of Murraya koenigii (curry leaf) and Brassica juncea (mustard): mechanism of action. Indian journal of biochemistry & biophysics, 32(2), 106-108.
26. Yadav, S., Vats, V., Dhunnoo, Y., & Grover, J. K. (2002). Hypoglycemic and antihyperglycemic activity of Murraya koenigii leaves in diabetic rats. Journal of ethnopharmacology, 82(2-3), 111-116.
27. Perumal, V., Khoo, W. C., Abdul-Hamid, A., Ismail, A., Saari, K., Murugesu, S. & Khatib, A. (2015). Evaluation of antidiabetic properties of Momordica charantia in streptozotocin induced diabetic rats using metabolomics approach. International Food Research Journal, 22(3).
28. El-Amin, M., Virk, P., Elobeid, M. A., Almarhoon, Z. M., Hassan, Z. K., Omer, S. A.,& Al-Olayan, E. M. (2013). Anti-diabetic effect of Murraya koenigii (L) and Olea europaea (L) leaf extracts on streptozotocin induced diabetic rats. Pak J Pharm Sci, 26(2), 359-65.
29. Hakhoe, T. S., Hakhoe, T. Y., & National Institutes of Health. (1997). The Korean journal of physiology & pharmacology: official journal of the Korean Physiological Society and the Korean Society of Pharmacology.
30. Arulselvan, P., Senthilkumar, G. P., Sathish Kumar, D., & Subramanian, S. (2006). Anti-diabetic effect of Murraya koenigii leaves on streptozotocin induced diabetic rats. Die Pharmazie-An International Journal of Pharmaceutical Sciences, 61(10), 874-877.
31. Gayathri, M., & Kannabiran, K. (2008). Ameliorative potential of aqueous extract of Pterocarpus marsupium Roxb bark on diabetes associated metabolic alterations. Current Trends in Biotechnology and Pharmacy, 2(2), 327-333.

Xi'an ShiyouDaxueXuebao (ZiranKexue Ban)/
Journal of Xi'an Shiyou University, Natural Sciences Edition
ISSN:1673-064X
E-Publication:Online Open Access
Vol: 65 Issue 03 | 2022
DOI 10.17605/OSF.IO/P4Y6E

BIOREMEDIATION OF HEXAVALENT CHROMIUM BY USING CYANOBACTERIA AND ITS APPLICATION OF THE BEST ISOTHERMS

Kishore Mendam[1], Yerkala Kumar[1], Niharika Burgula[2], Vineela Sai Megavath[2], Usha Sree Anandas[3], A. Rajani[3], A. Kavitha[3], Thirupathi Padala[4] and Shanthi Kuthadi[5]*

[1]Department of Zoology & Botany, Dr.B.R. Ambedkar Open University, Hyderabad, Telangana, India
[2]R&D division, Sri Yuva Biotech Pvt Ltd, Hyderabad, Telangana, India
[3]Department of Botany & Applied Nutrition, Raja Bahadur Venkat Rama Reddy Women's College, Narayanaguda, Hyderabad, Telangana, India
[4]Department of Botany, Govt. Degree College for Women, Jagtial, Telangana, India
[5]Dept of Microbiology, Osmania University, Hyderabad, Telangana, India
* Corresponding Author

ABSTRACT

The present study aimed to evaluate the efficiency of hexavalent chromium Cr(VI) removal from synthetic waters using locally available Cyanobacteria is also called blue-green algae are commonly found in lakes, rivers, and ponds. Various sorption factors like optimum pH, period of exposure, biomass dose, and primary chromium concentrations were investigated to originate their impacts on the sorption of Cr(VI). FTIR (Fourier-transform infrared spectroscopy) and SEM (Scanning electron microscopy) were used to examine the biosorption mechanisms of Cr(VI) ions onto blue-green algal biomass. The Langmuir and Freundlich isotherm models accurately illustrate the equilibrium experimental results. The Results indicated that the biosorption of blue-green algal biomass was shown to be biomass and pH-dependent. The hexavalent chromium removal efficiency was found to be 97.6% for an initial chromium concentration of 500 mg/L within 60 minutes at pH 2, 250 rpm, and a 10g/L blue-green algal biomass dose. According to the Langmuir isotherm, the highest biosorption ability was about 396 mg/g of dry biomass, and the Freundlich constants Kf and n were 0.514 [mg/g (1/mg) n] and 32.73, respectively. At the outset, the study of “blue-green algae” can be well-advised as a propitious and precious universal adsorbent to treat the waters contaminated with toxic Cr(VI) ions.

Keywords: Biosorption, Blue-green algae, Hexavalent chromium, Heavy metal pollution, Isotherm models, Water pollution.

Introduction

Water contamination is the world's most vulnerable issue. Major research and the state of art technologies are coming to treat the wastewater and to remove the pollutants from the wastewater. Pollution of the water mainly due to toxic heavy metals containing effluents from textile, paint, leather tanning, etc. is discharging the wastewater into the water bodies. Currently, this is one of all the major environmental concerns within the world.

In heavy metals Chromium, being one of the most hazardous and carcinogenic metals has drawn a lot of interest from researchers. Only two of the chemical forms of chromium (Cr (III) and Cr(VI)), are stable and found in nature. Electroplating, chromate production, alloy manufacturing companies, metal purification and handling, leather processing, and

Xi'an ShiyouDaxueXuebao (ZiranKexue Ban)/
Journal of Xi'an Shiyou University, Natural Sciences Edition
ISSN:1673-064X
E-Publication:Online Open Access
Vol: 65 Issue 03 | 2022
DOI 10.17605/OSF.IO/P4Y6E

wood maintenance are just a few of the industrial sources that employ this metal and its derivatives. Because of its significant adverse health properties, Cr (VI) should be effectively removed before disposal. Ramsenthil (2018).

Many researchers reported that the different treatment technologies for removal of chromium like membrane separation, ion exchange, chemical reduction/precipitation, and adsorption. However, these methods are not economically facing able, which, need a very huge amount of chemical reagents and a lot of energy, to overcome these problems researchers proposed biosorption to adsorb pollutants through biological sources as a potential alternative.

Innovative ways of using various biological sources, rockweed, amphibious plants, and plant-based sorbents as economical and effective absorbents are being developed. Because of its environmentally benign character, even wastewaters with metal pollution may be remedied with this high-performance, low-cost domestic approach, biosorption has become an essential and state-of-the-art technology in recent years. M. Costa (2003), G. Donmez (2002), Chi-ChuanKan (2017), WC Leung, (2001), R Majumder (2017), S.K Das (2007), D. Park (2005), Parul Sharma (2007), S Basha (2008), P Suksabye (2007), H Gao et al (2008).

Studies have shown that, the short-term accumulation of chromium (VI) by contacts with Cyanobacteria using their capability to seize chromium. D Shukla (2002). Aksu & Balibek (2007) studied the impact of salt addition on the adsorption of Cr (VI) by dried *Rhizopusarrhizus*. Arica et al. (2005) investigated the kinetics of Cr (VI) adsorption from synthetic waters expending free and restrained biomass produced from *Lentinussajorcaju*. Arica (2015). As a result, fungal species may remove chromium ions as well. The biosorption of Cr (VI) ions on the cell surface of trichoderma fungus under aerobic conditions at pH 5.5 was found to be 97.39 percent Vankar et al (2008). *Chlamydomonas reinhardtii*, natural, heat-treated, and acid-treated microalgae, was used for chromium (VI) ion biosorption.

The purpose of this research is to study the effect of several factors on the removal efficiency of chromium ions, such as adsorbent dosage, initial pH, time duration, and optimum Cr (VI) levels, on the adsorption of hexavalent chromium from synthetic chromium solutions using blue-green algae as an absorbent. To describe the experimental data, adsorption isotherms were used.

Materials and methods:

Biomass preparations:

A blue-green alga sample was taken from a small water body near Rajendra Nagar in Hyderabad, India. To eliminate contaminants and other undesirable components like sand and soil particles, the biomass was thoroughly washed in running tap water, then three to four times in Millipore water. The collected biomass was allowed to air dry before

Xi'an ShiyouDaxueXuebao (ZiranKexue Ban)/
Journal of Xi'an Shiyou University, Natural Sciences Edition
ISSN:1673-064X
E-Publication:Online Open Access
Vol: 65 Issue 03 | 2022
DOI 10.17605/OSF.IO/P4Y6E

being dried in a 60°C oven. Dry biomass was mashed in a marble crusher blender and mesh sieve to achieve the desired particle size (0.5mm).

Preparation and analysis of metal solution

The Chromium primary solution was made by dissolving 2.827g potassium dichromate ($K_2Cr_2O_7$) in Milli-Q water. It was then diluted with ultra-pure ultra-distilled water to make solutions with concentrations of 500 to 1500 mg/L. The complete study was conducted in batches at 28±2°C. The hexavalent chromium concentration was determined by a UV-Spectrophotometer method based on red-violet colored complex production of chromate ions by the interaction of DPC (1,5-diphenylcarbazide) in an acidic solution. Gilcreas et al (1965). The Systronic-2205UV-Vis spectrophotometer was used to detect absorbance across a wavelength of 540 nm after 15 minutes. The pH was adjusted using Systronic pH system-361, well-calibrated with NIST traceable pH buffers. Remi manufactured a mechanical shaker used for adsorption and kinetic studies.

Hexavalent chromium adsorption studies:

250 ml conical flasks were swirled at 250 rpm on a stirrer at ambient temperature (28±2°C) for batch biosorption studies. The impact of pH solutions ranging from 1.0 to 10.0, exposure time (060 minutes), and optimal Cr(VI) ions concentration (500 to 1500 ppm with 10g biomass dosage) on the biosorption rate and efficiency were investigated To explore the adsorption efficiency of Cr(VI) and blue-green algal biomass, 10g/L biomass was soaked in Cr (VI) synthetic water of various concentrations ranging from 500 - 1500 ppm to evaluate biosorption isotherms. The samples were obtained at various periods (0 to 60 mins). The supernatant was tested for residual chromium metal ion concentration after centrifugation at 4500 rpm for 15 minutes. The following equation was used to calculate the quantity of Cr (VI) ions adsorption efficiency per unit biomass of the adsorbent under equilibrium conditions Qe (mg/g).

$$\mathrm{Qe} = (\mathrm{C_o} - \mathrm{C_e})\mathrm{V} \div \mathrm{m} \qquad \text{Equation-1}$$

Where, C0 and Ce (mg/L) are initial & equilibrium concentrations of chromium solution respectively, V is the volume of solution (L), and m is Blue-green algal biomass (g).

The efficiency of biosorption (%) was determined using the following equation:

$$\mathrm{R\%} = \frac{\mathrm{C_o} - \mathrm{C_e}}{\mathrm{C_o}} \mathrm{X}\ 100 \qquad \text{Equation-2}$$

Characterization of adsorbent

The studies were conducted using a Perkin Elmer Model Spectrum BXI FTIR spectrophotometer (FTIR) on KBr discs with a finely powdered 1% sample. In the

Xi'an ShiyouDaxueXuebao (ZiranKexue Ban)/
Journal of Xi'an Shiyou University, Natural Sciences Edition
ISSN:1673-064X
E-Publication:Online Open Access
Vol: 65 Issue 03 | 2022
DOI 10.17605/OSF.IO/P4Y6E

wavenumber varies from 650-4000cm^{-1}, spectral data with a resolution of 4 cm^{-1} was analyzed using spectrum software. The biomass was evaluated after and before the chromium ion interaction. The surface structure and metal adsorption on biosorbent were studied using a scanning electron microscope (SEM).

Equilibrium Isotherms analysis:

The biosorption data were applied to several sorption isotherms, notably the Freundlich and Langmuir, to quantitatively explain chromium metal sorption by the blue-green algal biomass. The nonlinear regression method was used to determine qe and b in this investigation. The findings of the correlation coefficient (R2) were used to determine which of the two models described above was the most well-fitting.

The Freundlich isotherm is an empirical equation that defines adsorption on a heterogeneous surface with non-uniform energy distribution. The biosorption studies were conducted out with a predetermined initial adsorbent dosage (10g) and various initial adsorbate levels (500, 750, 1000, 1250, and 1500 mg/L) solutions, with the data's relevance to the Langmuir adsorption isotherm being evaluated. The tests were performed for sufficient time to achieve equilibrium at the original pH of 2. The Langmuir model was used to deal with uncertainties.

Results and Discussion:

Cr (VI) adsorption by blue-green algae is optimum when the pH is 2 and the biomass dose is 10g. According to the findings of this study, the highest adsorption capacity of blue-green algal biomass is 396 mg/g, and the optimum agitation rate of 250 rpm is continued during the 60-minute preset time. The current results of blue-green algae's maximal adsorption capacity are compared to similar research on Cr (VI) adsorption utilizing various sorbents. The highest adsorption rate using activated charcoal (made from wood apple shell) employed to absorb chromium from water with a concentration of 1250 mg/g was reported to be 151.51 mg/g at a pH of 1.8. Their substance is shown to be more effective at low pH, and their qmax was lower than this research Doke & Khan(2017).

At pH 2 and 0.2g of dosage, a magnetic natural zeolite Chitosan composite was used as an absorber to absorb Cr (VI) from a 200 mg/L aqueous solution, with a removal efficiency of 98% Gaffer et al (2017). The chemically-treated banana peels were used as an adsorbent in 400 mg/L chromium synthetic water and revealed that the maximum removal efficiency was 6.178 mg/g within 120 minutes of contact time with 4 g/L dosages at pH 3 Ali et al (2016).

pH Impact on adsorption:

The objective of this study was to determine the ideal pH for removing chromium ions from aqueous solutions. Experiments were performed in batches with various concentrations of chromium solution by ranging the pH levels from 1 to 10 and results

Xi'an ShiyouDaxueXuebao (ZiranKexue Ban)/
Journal of Xi'an Shiyou University, Natural Sciences Edition
ISSN:1673-064X
E-Publication:Online Open Access
Vol: 65 Issue 03 | 2022
DOI 10.17605/OSF.IO/P4Y6E

were evaluated (Figure 1). In aqueous solutions, chromium is known to have pH-dependent equilibria. When the pH varies, the equilibrium shifts. The $HCrO^{4-}$ and $Cr_2O_7^{2-}$ ions were in equilibrium in the pH range of 1 to 10. On the other hand, at pH 2.0, Cr_3O^{10-} and $Cr_4O_{13}^{2-}$ species are released. The optimal initial pH for Cr (VI) bioremediation using this biosorbent was found to be pH 2.0, suggesting that lower pH causes more polymerized chromium oxide molecules to be produced. The decreased chromium removal effectiveness at higher pH is thought to be owing to ions being repelled by anions on the surface of the adsorbent. The removal efficiency rose as the pH was reduced, reaching 97.6% at 500 mg/L Cr (VI) concentrations, according to the findings. Some of the organic carbons in the biomass were transformed to inorganic carbon during Cr (VI) reduction (HCO3- and CO2). Protons were consumed during absorption when pH decreased.

Effect of Contact Time

The amount of Cr (VI) absorbed varies depending on the starting concentration, which ranges from 500 to 1500 mg/L at pH 2. (Table 1). Since the pH affects the system's sorbent equilibrium, the combination of chromium levels and adsorbent is an important factor to consider for successful biosorption. The time it took for the system to reach equilibrium was less than 60 minutes. Metal uptake was affected by variables disrupting mass flow from the bulk solution to binding sites Mohanty et al (2018).

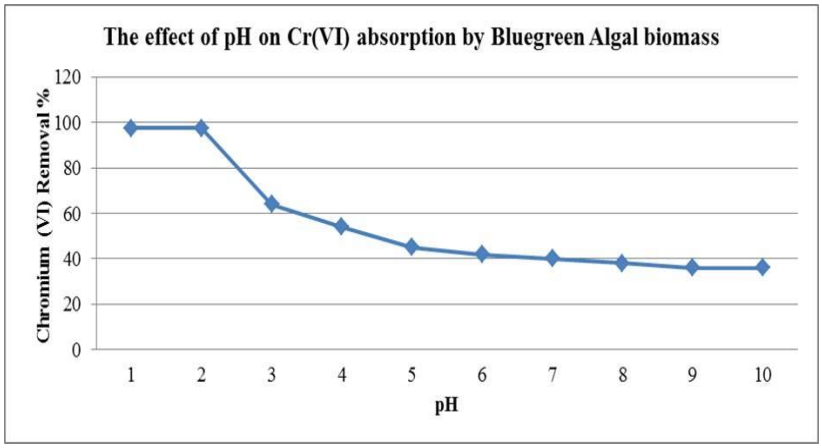

Figure 1. The effect of pH on the removal efficiency of hexavalent chromium.

However, even though sorption equilibrium was achieved at the same time, chromium ion biosorption declined with time. It is explained as a result of a rise in the number of ions vying for accessible binding sites in biomass, as well as a scarcity of binding sites. Because binding sites are saturated at greater concentrations, more Chromium ions are left in the solution.

Xi'an ShiyouDaxueXuebao (ZiranKexue Ban)/
Journal of Xi'an Shiyou University, Natural Sciences Edition
ISSN:1673-064X
E-Publication:Online Open Access
Vol: 65 Issue 03 | 2022
DOI 10.17605/OSF.IO/P4Y6E

Table 1: Chromium (VI) removal percentage at a different contacting time using blue-green algae

Removal Percentage of chromium VI by using blue-green algal biomass						
Concentration (ppm)	**10 min**	**20 min**	**30 min**	**40 min**	**50 min**	**60 min**
500	40	56	68	74	89	98
750	36	48	52	68	72	96
1000	32	54	58	76	84	92
1250	28	59	66	80	88	88
1500	16	28	43	56	66	72

FTIR Spectra Analysis:

An unreacted, chromium-treated blue-green algae sample was prepared and scanned using FTIR, with percentage transmission for various wavenumbers shown. The attribution of corresponding functional groups to absorption bands identified using acquired spectra is explained.

The existence of OH groups on the biosorbent surface was indicated by wavenumbers of 3,000 and 3,399 cm^{-1} for blue-green algae. The existence of C-H groups is indicated by the dip seen at 2,927 cm^{-1} and 893 cm^{-1}. The presence of an amide band is shown by the 1,649 cm^{-1} band, which is the consequence of CO stretching mode coupled to NH deformation mode. The dip at 1,154cm^{-1} is caused by CO or CN groups, which proves the existence of numerous efficient ions on the surface of blue-green algae that bind Cr(VI) ions. (Figure 2).

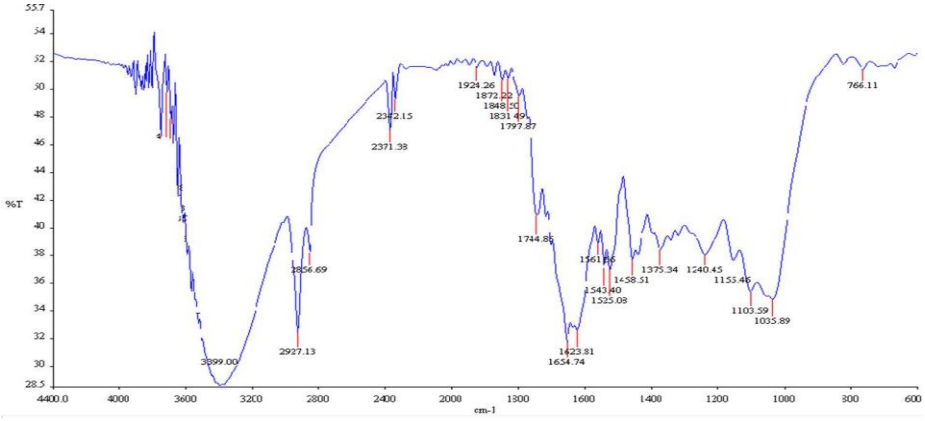

Figure 2. FTIR Spectrum for blur green algae biomass.

Xi'an ShiyouDaxueXuebao (ZiranKexue Ban)/
Journal of Xi'an Shiyou University, Natural Sciences Edition
ISSN:1673-064X
E-Publication:Online Open Access
Vol: 65 Issue 03 | 2022
DOI 10.17605/OSF.IO/P4Y6E

Scanning Electron Microscope (SEM) combined with Energy Dispersive X-ray (EDX) spectroscopy was used to explore the Cr (VI) adsorption and surface structure of the blue-green algal biomass sample. EDX spectroscopic experiment found the percent quantity of Cr (VI) in the biomass after biosorption, which was used to determine the percentage of elements.

The blue-green algal biomass sample was tested against 500 mg/L hexavalent chromium, and the biomass removed 97.6% of the Cr (VI) ion using 10 g of biomass at pH 2. This indicates that the biomass's surface area is acting as a biosorption agent. The morphology of biomass was explained by SEM micrographs, as illustrated in Figs. 3 and 4, respectively.

Biosorption equilibrium studies:

Experiments were conducted through adsorbent doses of 10 g/L and various adsorbate contents (500-1500 mg/L) solutions, the results were examined by Langmuir adsorption isotherm. The tests were performed for sufficient time to achieve equilibrium at the original pH of 2. The findings were familiar to the Langmuir model that can be articulated by using the equation.

$$q_e = \frac{bq_{max}C_e}{1+bC_e} \qquad \text{Equation – 3}$$

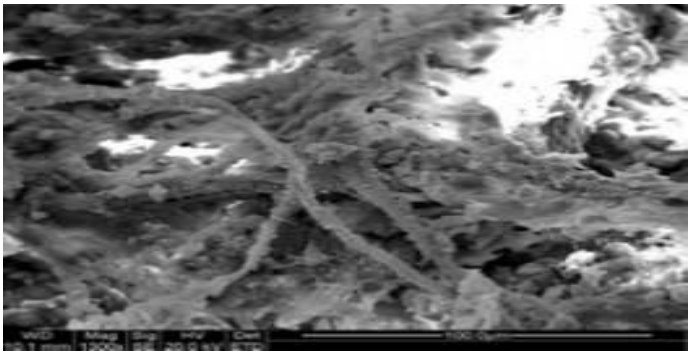

Fig. 3. SEM of blue-green algae biomass before biosorption.

Xi'an ShiyouDaxueXuebao (ZiranKexue Ban)/
Journal of Xi'an Shiyou University, Natural Sciences Edition
ISSN:1673-064X
E-Publication:Online Open Access
Vol: 65 Issue 03 | 2022
DOI 10.17605/OSF.IO/P4Y6E

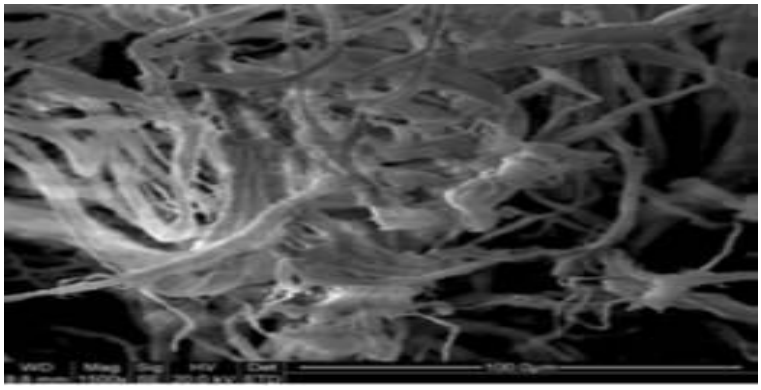

Fig. 4. SEM of Bluegreen algae biomass after biosorption

Where q_e is the metal uptake (mg/g) at equilibrium; q_{max} is the maximum Langmuir uptake (mg/g); C_e is the final metal concentration at equilibrium (mg/L); b is the Langmuir affinity constant (L/mg of the metal). The Langmuir affinity constant was found to be highly linked with the similarity between biomass and Cr (VI), with a higher value indicating a high affinity. Using a linear representation of the Langmuir model (Ce/qe vs Ce), these adsorption variables may be derived from the isotherm:

$$\frac{C_e}{q_e} = \frac{C_2}{q_{max}} + \frac{1}{bq_{max}} \qquad \text{Equation –4}$$

These assumptions underpin the Langmuir isotherm. Langmuir (1916). Metal ions are adsorbed chemically at a finite number of well-defined sites, each of which can only hold one ion at a time. The ions do not interact, and all sites are energetically equivalent.

The linear plot of C_{eq}/q vs C_{eq} shows the adsorption follows the Langmuir adsorption model (Figure 5). 0.99 was the correlation coefficient. The slope and intercept of the figure were used to determine b and qmax, which were 0.06 L/mg and 396 mg/g, respectively.

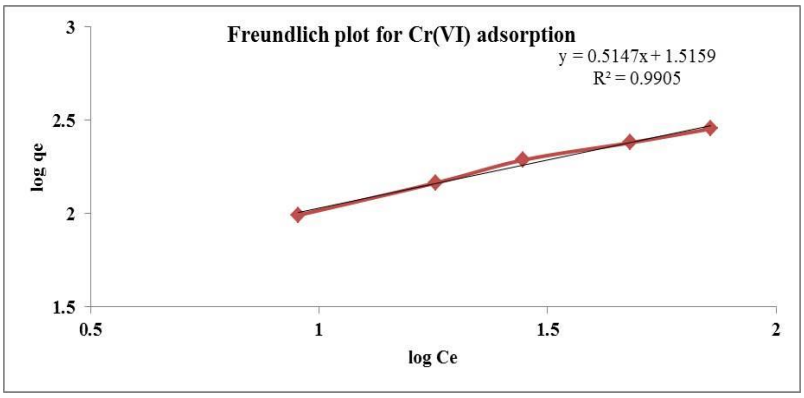

Figure 5. Freundlich plot for hexavalent chromium adsorption efficiency.

Xi'an ShiyouDaxueXuebao (ZiranKexue Ban)/
Journal of Xi'an Shiyou University, Natural Sciences Edition
ISSN:1673-064X
E-Publication:Online Open Access
Vol: 65 Issue 03 | 2022
DOI 10.17605/OSF.IO/P4Y6E

Separation factor - R_L

The main characteristics of the Langmuir isotherms may be represented as dimensionless constant separation factors or equilibrium parameters. R_L, which is well-defined as:

$$R_L = \frac{1}{1+bC_o} \qquad \text{Equation -5}$$

Where C_o=initial concentration in mg/L; b=Langmuir constant

R_L values define the isotherm categories; if the R_L value is greater than one, the isotherm is unfavorable and linear; if the R_L value is less than one, the isotherm is favorable; For Cr (VI) adsorption, the R_L values obtained are smaller than one (Table 2). R_L values between 0 and 1 recommend good adsorption Mcka et al (1982).

Table 2.The values of Separation factor

C_o	R_L
500	0.032209
750	0.021705
1000	0.016368
1250	0.013137
1500	0.010972

The adsorption of chromium (VI) on a blue-green algal biomass was also investigated using the Freundlich isotherm, which was assessed using the equation below Freundlich (1906).

$$\log q_e = \log K_F + \frac{1}{n}\log C_e \qquad \text{Equation-6}$$

Where Kf is a constant proportional to the Freundlich biosorption capability (L/mg), and the log is an experimental measure indicating sorption efficiency, which differs with substance variability. Freundlich isotherms derived by applying equilibrium data to equation 6 are shown in Figure 6.

Xi'an ShiyouDaxueXuebao (ZiranKexue Ban)/
Journal of Xi'an Shiyou University, Natural Sciences Edition
ISSN:1673-064X
E-Publication:Online Open Access
Vol: 65 Issue 03 | 2022
DOI 10.17605/OSF.IO/P4Y6E

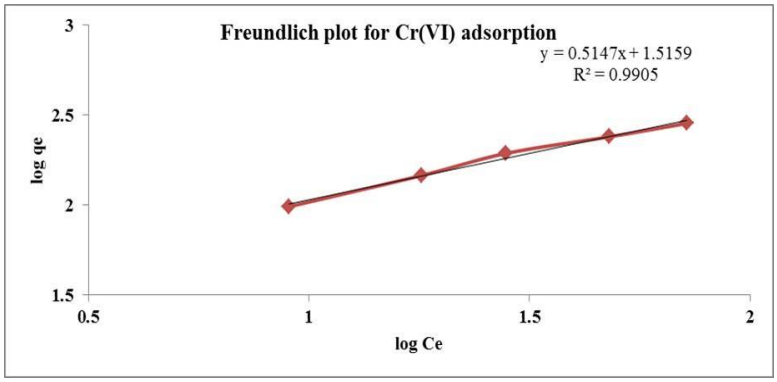

Figure 6. Freundlich plot for hexavalent chromium adsorption efficiency.

Kf and 1/n were found to have values of 32.74 and 0.541, respectively. The1/n results falling well under the specified values (0- 1), which denotes chromium ion adsorption was satisfactory under these conditions. Magnitudes of Kf and n reveal a strong adsorption capability and removal efficiency of hexavalent chromium from contaminated waters. Ozel Ucun et al (2002).

Conclusion

According to the results of this study, blue-green algae is a viable substitute for absorbing Cr (VI) from the waters. In biosorption, the results of FTIR bands related to its functional groups made a crucial impact. The optimum hexavalent chromium removal percentage was optimum at pH.2, and raising the pH from acidic to alkaline resulted in a decrease in chromium removal percentage. The maximal chromium VI ion removal was determined to be 97.6% in 60 minutes at pH 2 with 250 rpm agitation and 10 g/L blue-green algae biomass. Studies of equilibrium isotherms indicated that they were significant and fit well within the allowable limits. Cr(VI) ion biosorption on blue-green algae eventually reached a maximum capacity of 396 mg/g biomass. Blue-green algae is an inexpensive and easily available biosorbent, making it a viable choice for removing chromium ions from contaminated wastewaters.

Funding & Acknowledgments: The authors would like to express deep gratitude to the Sri Yuva Biotech Pvt Ltd, and Department of Botany & Applied Nutrition, Raja Bahadur Venkat Rama Reddy Women's College, Hyderabad, Telangana, India for providing financial assistance for the study.

Declaration of Competing Interest

All the authors confidently declare that there is no conflict of interest, and all authors for publication approve the paper.

ISSN:1673-064X
E-Publication:Online Open Access
Vol: 65 Issue 03 | 2022
DOI 10.17605/OSF.IO/P4Y6E

References:

A Gaffer, Kahlawy, A.Al. and Aman, D.: Magnetic zeolite-natural polymer composite for adsorption of chromium(VI).Egypt.J.Petrol., 26:995-999 (2017). https://doi.org/10.1016/j.ejpe.2016.12.001

Aksu, Z. Balibek, E.: Chromium(VI) biosorption by dried Rhizopusarrhizus: Effect of salt (NaCl) concentration on equilibrium and kinetic parameters, Journal of Hazardous Materials, Volume 145, Issues 1–2, 2007, Pages 210-220, ISSN 0304-3894,(2007). https://doi.org/10.1016/j.jhazmat.2006.11.011.

Ali, A. Saeed, K. and Mabood, F.: Removal of chromium (VI) from aqueous medium using chemically modified banana peels as efficient low-cost adsorbent. AlexandriaEng.J., 55:2933-2942. (2016). https://doi.org/10.1016/j.aej.2016.05.011

APHA: Standard Methods for the Examination of Water and Wastewater.12th ed. American Public Health Association, New York. (2018).

Arica, Yakup & Bayramoglu, Gulay.: Cr(VI) biosorption from aqueous solutions using free and immobilized biomass of Lentinussajor-caju: preparation and kinetic characterization. Colloids and Surfaces A: Physicochemical and Engineering Aspects. 2015. 253. 203-211.(2015). doi:10.1016/j.colsurfa.2004.11.012.

Basha, S. Murthy, Z.V.P. Jha, B.: (2008). Biosorption of hexavalent chromium by chemically modified seaweed, Cystoseiraindica. Chemical Engineering Journal. 137. 480-488. 10.1016/j.cej.2007.04.038. https://doi.org/10.1016/j.cej.2007.04.038

Chi-ChuanKan, Aldwin, Ibe. Kim Katrina Rivera, P. Renato Arazo, O. Mark Daniel, G. Luna, de.: Hexavalent chromium removal from aqueous solution by adsorbents synthesized from groundwater treatment residuals, Sustainable Environment Research, Volume 27, Issue 4, Pages 163-171,ISSN 2468-2039,(2017) https://doi.org/10.1016/j.serj.2017.04.001.

Costa, M. Potential: hazards of hexavalent chromate in our drinking water. ToxicolApplPharmacol. Apr 1;188(1):1-5.(2003). doi: 10.1016/s0041-008x(03)00011-5. https://pubmed.ncbi.nlm.nih.gov/12668116/

Das, S.K. Guha. A.K.: Biosorption of chromium by Termitomycesclypeatus. Colloids and surfaces. B, Biointerfaces, 60(1), 46–54. (2007). https://doi.org/10.1016/j.colsurfb.2007.05.021

Doke, K.M. and Khan E.M.: Equilibrium, kinetic and diffusion mechanism of Cr(VI) adsorption onto activated carbon derived from wood apple shell. Arabian J. Chem., 10:S252-S260 (2017). http://dx.doi.org/10.1016/j.arabjc.2017.07.031 1

Donmez, G. Aksu, Z.: Selective adsorption of Cr(VI) in industrial waste water using low-cost abundantly available adsorbents, Process Bioc hem. 38 751–762. (2002). https://doi.org/10.1016/j.serj.2017.04.001.

Freundlich, H. Ueber.: die Adsorption in Loesungen, *Zeitschrift fur PhysikalischeChemie (Leipzig)*1906,**57**,385-470 https://www.scirp.org/(S(oyulxb452alnt1aej1nfow45))/reference/ReferencesPapers.aspx?ReferenceID=1467146.

Gao, H. Liu, Y. Zeng, G. Xu, W. Li, T. Xia, W.: Characterization of Cr(VI) removal from aqueous solutions by a surplus agricultural waste--rice straw. Journal of hazardous materials, 150(2), 446–452.(2008). https://doi.org/10.1016/j.jhazmat.2007.04.126

Langmuir, I.: The adsorption of gases on plane surfaces of glass, mica and platinum, *Journal of the American Chemical Society*, 1918. 40, 1361-1403. (1918). https://pubs.acs.org/doi/10.1021/ja02242a004

Leung, W.C. chua, H & Lo, W.: Biosorption of heavy metals by bacteria isolated from activated sludge. ApplBiochemBiotechnol 91, 171–184 (2001). https://doi.org/10.1385/ABAB:91-93:1-9:171

ISSN:1673-064X
E-Publication:Online Open Access
Vol: 65 Issue 03 | 2022
DOI 10.17605/OSF.IO/P4Y6E

Majumder, R. Sheikh, L. Naskar, A.: Depletion of Cr(VI) from aqueous solution by heat dried biomass of a newly isolated fungus Arthriniummalaysianum: A mechanisticapproach. SciRep **7,** 11254(2017). https://doi.org/10.1038/s41598-017-10160-0.

Mcka, G. Blair, H.S. Gardener, J.R.: Adsorption of dyes on chitin I. Equilibrium studies, *Journal of Applied Polymer Science*, 27, 1982. 3043-3057. (1982). https://doi.org/10.1002/app.1982.070270827

Mohanty, K. Das, D. and Biswas, M.N.: "Treatment of Phenolic Wastewater ina Novel Multistage External Loop Airlift Reactor Using Activated Carbon", *SeparationandPurificationTechnology,* Vol.58,No.3,pp.311-319.(2008).. http://www.bioline.org.br/request?er10031

Ozel, Ucun. Handan & Bayhan, Kemal, Y. & Kaya, Yusuf & Cakici, Avni & O Algur.: Biosorption of chromium (VI) from aqueous solution by cone biomass of Pinus sylvestris. Bioresource technology.85. 155-8. 10.1016/S0960-8524(02)00086 (2002). http://www.bioline.org.br/pdf?ej05029.

Park, D. Yun, Y.S. Park, J.M.: Studies on hexavalent chromium biosorption by chemically-treated biomass of Ecklonia sp. Chemosphere, 60(10), 1356–1364. (2005). https://doi.org/10.1016/j.chemosphere.2005.02.020

Parul Sharma, Pritee Goyal &Shalini Srivastava.: Biosorption of trivalent and hexavalent chromium from aqueous systems using shelled Moringaoleifera seeds, Chemical Speciation & Bioavailability, 19:4, 175-182, (2007). https://doi.org/10.3184/095422907X255938

Ramsenthil Ramadoss and Dhanasekaran Subramaniam: Adsorption of chromium using blue green algae-modeling and application of various isotherms. Int. J. Chem. Technol., 10: 1-22. (2018). https://scialert.net/abstract/?doi=ijct.2018.1.22

Shukla, D. Vankar, P.S. Srivastava S.K.: Bioremediation of hexavalent chromium by a cyanobacterial mat. Appl Water Sci 2**,** 245–251 (2012).https://doi.org/10.1007/s13201-012-0044-3

Suksabye, P. Thiravetyan, P. Nakbanpote, W. Chayabutra. S.: Chromium removal from electro plating wastewater by coir pith. Journalofhazardousmaterials, 141(3),637–644.(2007). https://doi.org/10.1016/j.jhazmat.2006.07.018.

Vankar, Padma S & Srivastava, Jyoti.: Comparative Study of Total Phenol, Flavonoid Contents and Antioxidant Activity in Canna indica and Hibiscus rosasinensis: Prospective Natural Food Dyes. International journal of food engineering. 2008. 4. 10.2202/1556-3758.1232. (2008). https://doi.org/10.2202/1556-3758.1232

frontiers | Frontiers in Molecular Biosciences

TYPE Original Research
PUBLISHED 23 September 2022
DOI 10.3389/fmolb.2022.1010603

OPEN ACCESS

EDITED BY
Chandrabose Selvaraj,
Alagappa University, India

REVIEWED BY
Ramar Vanajothi,
Bharathidasan University, India
Teng Fu,
Kangwon National University, South Korea
Althaf Shaik,
King Saud University, Saudi Arabia

*CORRESPONDENCE
Natthiya Buensanteai,
natthiya@sut.ac.th

SPECIALTY SECTION
This article was submitted to Biophysics, a section of the journal Frontiers in Molecular Biosciences

RECEIVED 03 August 2022
ACCEPTED 30 August 2022
PUBLISHED 23 September 2022

CITATION
Papathoti NK, Mendam K, Sriram Kanduri BH, Thepbandit W, Sangpueak R, Saengchan C, Hoang NH, Megavath VS, Kurakula M, Le Thanh T and Buensanteai N (2022), Investigation of bioactive compounds from Bacillus sp. against protein homologs CDC42 of Colletotrichum gloeosporioides causing anthracnose disease in cassava by using molecular docking and dynamics studies.
Front. Mol. Biosci. 9:1010603.
doi: 10.3389/fmolb.2022.1010603

Investigation of bioactive compounds from *Bacillus* sp. against protein homologs CDC42 of *Colletotrichum gloeosporioides* causing anthracnose disease in cassava by using molecular docking and dynamics studies

Narendra Kumar Papathoti[1], Kishore Mendam[2], Bala Hanumath Sriram Kanduri[3], Wannaporn Thepbandit[1], Rungthip Sangpueak[1], Chanon Saengchan[1], Nguyen Huy Hoang[1], Vineela Sai Megavath[4], Madhuri Kurakula[4], Toan Le Thanh[5] and Natthiya Buensanteai[1]*

[1]School of Crop Production Technology, Suranaree University of Technology, Nakhon Ratchasima, Thailand, [2]Department of Zoology, Dr. B.R. Ambedkar Open University, Hyderabad, Telangana, India, [3]R&D Division, Sri Yuva Biotech Pvt Ltd., Hyderabad, Telangana, India, [4]Department of Biotechnology, Mahatma Gandhi University, Nalgonda, Telangana, India, [5]Department of Plant Protection, Can Tho University, Can Tho City, Viet Nam

Manihot esculenta, commonly called cassava, is an economically valuable crop and important staple food, grown in tropical and subtropical regions of the world. Demand for cassava in the food and fuel industry is growing worldwide. However, anthracnose disease caused by *Colletotrichum gloeosporioides* severely affects cassava yield and production. The bioactive molecules from *Bacillus* are widely used to control fungal diseases in several plants. Therefore, in this study, bioactive compounds (erucamide, behenic acid, palmitic acid, phenylacetic acid, and β-sitosterol) from *Bacillus megaterium* were assessed against CDC42, a key protein for virulence, from *C. gloeosporioides*. Structure of the CDC42 protein was generated through the comparative homology modeling method. The binding site of the ligands and the stability of the complex were analyzed through docking and molecular dynamics simulation studies, respectively. Furthermore, a protein interaction network was envisaged through the STRING database, followed by enrichment analysis in the WebGestalt tool. From the enrichment analysis, it is apparent that bioactive from *B. megaterium* chiefly targets the MAP kinase pathway that is essential for filamentous growth and virulence. Further exploration through experimental studies could be advantageous for cassava improvement as well as to combat against *C. gloeosporioides* pathogen.

KEYWORDS

Colletotrichum gloeosporioides, Cdc42, Manihot esculenta, docking, molecular dynamics simulation

Introduction

Plants are an important source for humans, animals, birds, and other living organisms. Plants protect themselves from a variety of biotic and abiotic stresses (Gong et al., 2020). Biotic stress occurs due to bacterial and fungal pathogens (Peck and Mittler, 2020). One of the important plants on which more than 800 million people worldwide are depending for major food sources is *Manihot esculenta* Crantz (Atwijukire et al., 2019). The crop, commonly known as cassava, is enriched with several nutrients such as starch, carotenoids, vitamins, and minerals. Cassava is consumed as the primary food source mainly in the regions of tropical and sub-tropical countries. Later, due to increased industrial importance such as the production of animal feed, biomedicine, and cosmetics, the production of cassava has been highly increased (Li et al., 2017). In addition, the raw materials from *M. esculenta* were used for biopolymer, starch, and bioethanol production (El-Sharkawy 2004). Apart, the by-products from the cassava industries are rich with organic residues essential for the production of value-based products (Ayling et al., 2012). Hence, the crop with human value and with the immense industrial application was cultivated by both low-scale and high-scale cultivators. However, the plant is restricted at an economical level due to several factors such as the presence of cyanogen compounds (Balyejusa Kizito et al., 2007), a low level of proteins, and infectious disease.

Anthracnose disease (AD) damages the healthy planting materials of cassava, leading to low yield and total economic loss for the planters. AD occurs in cassava due to the fungal pathogen *Colletotrichum gloeosporioides* f. sp. *manihotis* (Machado et al., 2020). The fungal strain infects the shoot tips of the healthy plants; develops cancerous growth on the stem and leaves. AD is notorious to cause shoot tip-die-back disease because the pathogen infects the stem region, weakens the parts and leads to major destruction during strong wind and rain (Pinweha et al., 2015). The primary interaction of the pathogen with the cassava plant was established by producing an infection cell known as appressorium. The melanized cell surrounding the aspersorium supports the internal solute concentration and rigidity of the cells (Wang et al., 2021). After the interaction with the host, the pathogen develops infection vesicles and primary hyphae. Later, the fungi develop secondary hyphae structures that spread the infection and kill the plants. Generally, after the successful infection into the host, the fungi adapt to the biotrophic mode of nutrition for their survival (Li et al., 2021). The pathogen produces lesions on leaves, stems, and other parts of the plant. Sequentially, switches to the necrotrophic mode of nutrition in which the pathogen absorbs nutrition from the dead cells of the infected region. This nutrition adaptation by the pathogen is known as the hemibiotrophic mode of infection (Jacobs et al., 2019). Thus, it is very challenging to impair the growth and spread of infection by *C. gloeosporioides*. This pathogen also infects humans but knowledge about the type of disease and mode of infection is not clear so far.

To prevent fungal infection, chemical fungicides were widely used to control the disease (Ons et al., 2020). The use of several fungicides has resulted in impacts on human health and environmental issues. Hence, as an alternative approach to overcome AD-mediated damage in the cassava, different novel approaches were promoted for the development of fungal resistant-cassava crops (Koehorst-van Putten et al., 2012). The genetic engineering approach was one of the conventional strategies known to be the most economical, safe, and effective method to generate anthracnose disease-resistance cassava plants (Hormhuan et al., 2020). The use of a conventional breeding strategy with cassava crops leads to high heterozygosity, low fertility, delayed flowering, and prolonged vegetative stage. Hence, the approach of *Agrobacterium*-mediated transformation is considered to improve the acquired resistance in plants. One of the important plant-pathogen resistance genes, transferred into cassava has been reported to show improved resistance against a wide variety of plant pathogens. Thus, alternative strategies were required to incredulous the current scenario of anthracnose disease in cassava plants. The cell division cycle (CDC42) protein present in the fungi performs the function of the molecular switch by regulating signal transduction pathways and cytoskeleton-mediated cellular process. The protein belongs to the Rho-family of the GTP-binding protein, which plays a pivotal role in the transduction of polarity signals for morphogenetic development (Wang et al., 2018). The CDC42 protein also plays an important role in cell differentiation and appressoria development. CDC42 protein reported with plants is highly diverse, however, the protein is conserved in other eukaryotic species. The protein CDC42 from different fungal species (*Magnaporthe grisea*, *Claviceps purpurea,* and *Ustilago maydis*) has a key role in plant-pathogen interaction (Oeser et al., 2017; Zheng et al., 2009). Thus, the deletion of CDC42 from pathogens has significantly reduced the virulence mechanism during infection. Therefore, in the present study, CDC42 of *C. gloeosporioides* was selected as the therapeutic target to screen for inhibitors against the protein. Also, the detailed investigation using a protein-protein interaction network will pave the way to study the characteristic properties of CDC42 involved in the different biological processes of host-pathogen interaction.

Materials and methods

Generation of homology model and structure validation

The three-dimensional structure of Cell division control protein 42 homologs (CDC42) from *C. gloeosporioides* was determined through the comparative homology modeling method. The structure of CDC42 was built through the SWISS-MODEL server (https://swissmodel.expasy.org/). The accuracy of the model was assessed by QMEAN4 score analysis (Benkert et al., 2011). Later, energy minimization was performed using the steepest descent algorithm using GROMACS (Van Der Spoel et al., 2005). The structure of the predicted model was assessed through the structure validation tool SAVES v6.0 program - VERIFY 3D (Agarwal et al., 2021; Hasan et al., 2021), ERRAT (Adewole and Ishola, 2021), WHAT CHECK (Sekhar Pagadala et al., 2009), and PROCHECK analysis (Laskowski et al., 1996). The geometry and stereochemistry of the modeled structure were analyzed through the Ramachandran plot analysis method (Agarwal et al., 2021). In addition, structural validation of the generated model was performed through ProSA score analysis (Wiederstein and Sippl., 2007). Then, the overall quality score of the homology model was compared with the score of the template structure.

Binding site prediction

Prediction of druggable cavities is a crucial step for structure-based drug designing. The active site as predicted for CDC42 model protein using sitemap. The prediction of the active site reveals the shape, size and chemical interaction of the ligands with the receptor protein.

Molecular docking

Five monomeric bioactive compounds identified from the ethyl acetate extract of *Bacillus megaterium* erucamide, behenic acid, palmitic acid, phenylacetic acid, and β-sitosterol, were examined against CDC42 protein of *C. gloeosporioides*. The structure of the bioactive compounds was obtained from the PubChem database. The selected ligands were prepared and the three-dimensional (3D) coordinates were generated. For molecular docking, the proteins used for the study were prepared using protein preparation wizard. The proteins were subjected for H-bond optimization. The entire protein structure were relaxed using Uff force field. Energy minimization for protein and ligand was performed before docking using default parameters. Autodock tools were utilized for the addition of hydrogen, Kollman charges, and solvation parameters (Azam and Abbasi, 2013). Molecular docking was performed through the Autodock Vina program (Trott and Olson, 2010). The grid size of 3 Å for the coordinates X, Y, and Z centered at X: 12.20; Y: 5.95; Z: 7.22 with a grid spacing of 0.375 Å was used for the docking program. The pose with the lowest binding energy was selected as the best conformation. The modeled structures were visualized through the BIOVIA Discovery Studio visualizer (Studio, 2015). Molecular mechanics of combined generalized born surface area and surface area continuum solvation (MM/PBSA and MM/GBSA) methods were performed for studying the effectiveness of interaction. The calculation for average binding free energy ΔGbind was represented for estimating the free energy of ligands binding to the macromolecules. During molecular dynamics simulation of the receptor-ligand complex, the molecular mechanics is applied with empirical scoring and perturbation methods for predicting the accuracy during their simulation run. The formula for average binding free energy ΔGbind was calculated as; ΔGbind = ΔEMM+ ΔGSolv+ ΔGSA.

ΔEMM: denotes minimized energies of protein and ligand.

ΔGSolv: solvation-free energy.

ΔGSA: surface area energy.

ADMET properties of the ligands

SMILE structure of the lead molecules used for the present study were downloaded from Pubchem database. The pharmacokinetic properties of molecules were predicted using ADMETSAR2.0. The properties such as acute oral toxicity, BBB, fish aquatic toxicity and carcinogenicity of the molecules were analysis.

Molecular dynamics simulation

For each protein-ligand system, their pose with the lowest binding energy was assessed. The system was minimized and equilibrated under the number of particles, volume, and temperature (NVT) and the number of particles, pressure, and temperature (NPT) conditions. The molecular dynamics simulation was performed for 50 ns in DESMOND with GPU support. The Optimized Potential for Liquid Simulations (OPLS) force field was used. The system was solvated in a dodecahedron box using a simple point charge (SPC) model with a periodic boundary condition. The system was neutralized by adding sodium chloride ions. Energy minimization was performed through the steepest descent algorithm. Harmonic position restraints were applied during the NVT ensemble simulation. The molecular dynamics production runs were carried out at a 2 fs time step. Temperature and pressure were controlled by setting the Langevin dynamics and Berendsen barostat at 300 K and 1 bar, respectively. Standard periodic boundary conditions and cut-off distance (1 nm) were updated. The particle-mesh Ewald (PME) method was used to assess the interactions. The bonds were constrained with a linear constraint solver (LINCS) and the water molecules were constrained with SETTLE (Hess 2008; Tripathi et al., 2022). Molecular dynamics simulation was

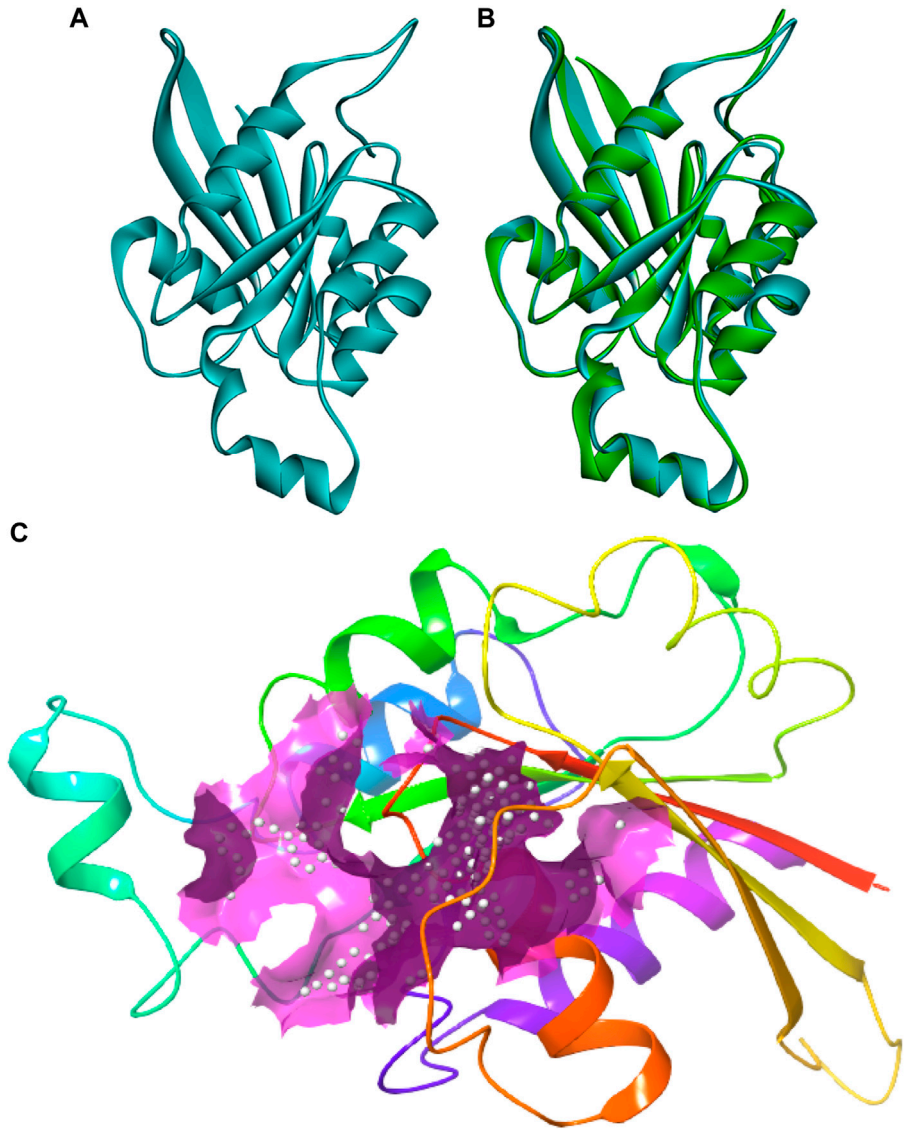

FIGURE 1
Three-dimensional structure of CDC42 predicted through homology modeling **(B)** The structure of CDC42 protein superimposed with the template (2NGR) structure. **(C)** Binding site prediction representing the active site region (pink).

evaluated using root mean square deviation (RMSD) and hydrogen bond analysis.

STRING analysis

The interacting proteins of CDC42 were predicted through the STRING database (http://string-db.org) and the network is built by providing the CDC42 protein sequence in the input box. The search was performed against *C. gloeosporioides*. The confidence score was set to high (0.7). The interactions were based on the experiments, co-expression, databases, gene fusion, neighborhood, and co-occurrence. The maximum number of interactions was set to no more than ten in the first and second shells.

Identification of clusters from the protein-protein interaction network

Clustering of interactions from large protein-protein interaction networks is essential to define the molecular complexes and topological modules. It is difficult to comprehend and interpret the network properties as such in

TABLE 1 Docking score of different ligands from *B. megaterium* with CDC42 protein.

S. No	PubChem ID	Compound name	Dock score (kJ mol $^{-1}$)	ΔGbind (Kcal/mol)
1	222284	beta-Sitosterol	−10	-42.35
2	999	Phenylacetic acid	−10	-39.26
3	985	palmitic acid	−9.4	-41.51
4	8,215	Behenic acid	−9.2	-37.90
5	5365371	Eurcamide	−9.2	-39.49

TABLE 2 GO Slim summary is based on Entrez gene IDs.

S. No	Gene symbol	Gene name	Entrez gene
1	BMH1	14-3-3 family protein BMH1	856924
2	BUD6	Bud6p	851029
3	CLA4	serine/threonine protein kinase CLA4	855418
4	SHO1	osmosensor SHO1	856854
5	SPA2	Spa2p	850639
6	STE50	Ste50p	850325

large protein-protein interaction networks. Therefore, clustering of networks is significant in unraveling the pure network properties as well as finding the network connections in the dense regions. The network obtained from the STRING database is a network based interaction evidence for data support. The obtained network was reconstructed in Cytoscape 3.8.0. The constructed network was evaluated further using Molecular Complex Detection (MCODE) plug-in to visualize the central network. The cut off parmaters were set as MCODE score >3 and node number >4. The subclusters generated were further visualzed and group to study the clossness and degree of interaction in their group.

Gene ontology (GO) analysis and protein interaction analysis

The gene ontology (GO) analysis was performed in which the functional annotation was achieved through DAVID (database for annotation, visualization, and integrated discovery) database. GOView, a web-based WebGestalt (WEB-based GEne SeT AnaLysis Toolkit) application, is used to visualize and compare the interactional relationship in the network (Zhang et al., 2005; Zhang et al., 2004). Furthermore, the central gene sets were annotated and the hierarchical associations were defined. The protein SHO1 involved in the MAPK signaling pathway was modelled using modeler. SHO1 from yeast was used as the template (2vkn. Pdb) with 61.02% with target sequence. The model of SHO1 and CDC42 was loaded into Patchdock server and protein-protein docking was performed (Yousafi et al., 2021). The protein complex was analysed and results were represented.

Results

Generation of homology model and structure validation

The protein sequence of the CDC42 homolog of *C. gloeosporioides* (O94103) was retrieved from the NCBI database (https://www.ncbi.nlm.nih.gov/protein/O94103). The sequence contains 190 amino acids and belongs to the small GTPase superfamily, the Rho family. The sequence was predicted to contain three nucleotides (GTP) binding regions: 12–19 (GDGAVGKT), 59–63 (DTAGQ), and 117–120 (TERG). Based on sequence homology, the molecular function involves GTPase activity and the biological process involves cell cycle and cell division. The sequence contains a propeptide region from amino acid 188 to 190 (LVL), which is predicted to be cleaved during protein maturation or activation. The detail for the propeptide region was revealed through the prediction evidence sequence similarity search tool ECO: 0000250 mentioned in the NCBI protein sequence database. The structure of this CDC42 protein was predicted through comparative homology modeling. It showed 70.83% sequence

10.3389/fmolb.2022.1010603

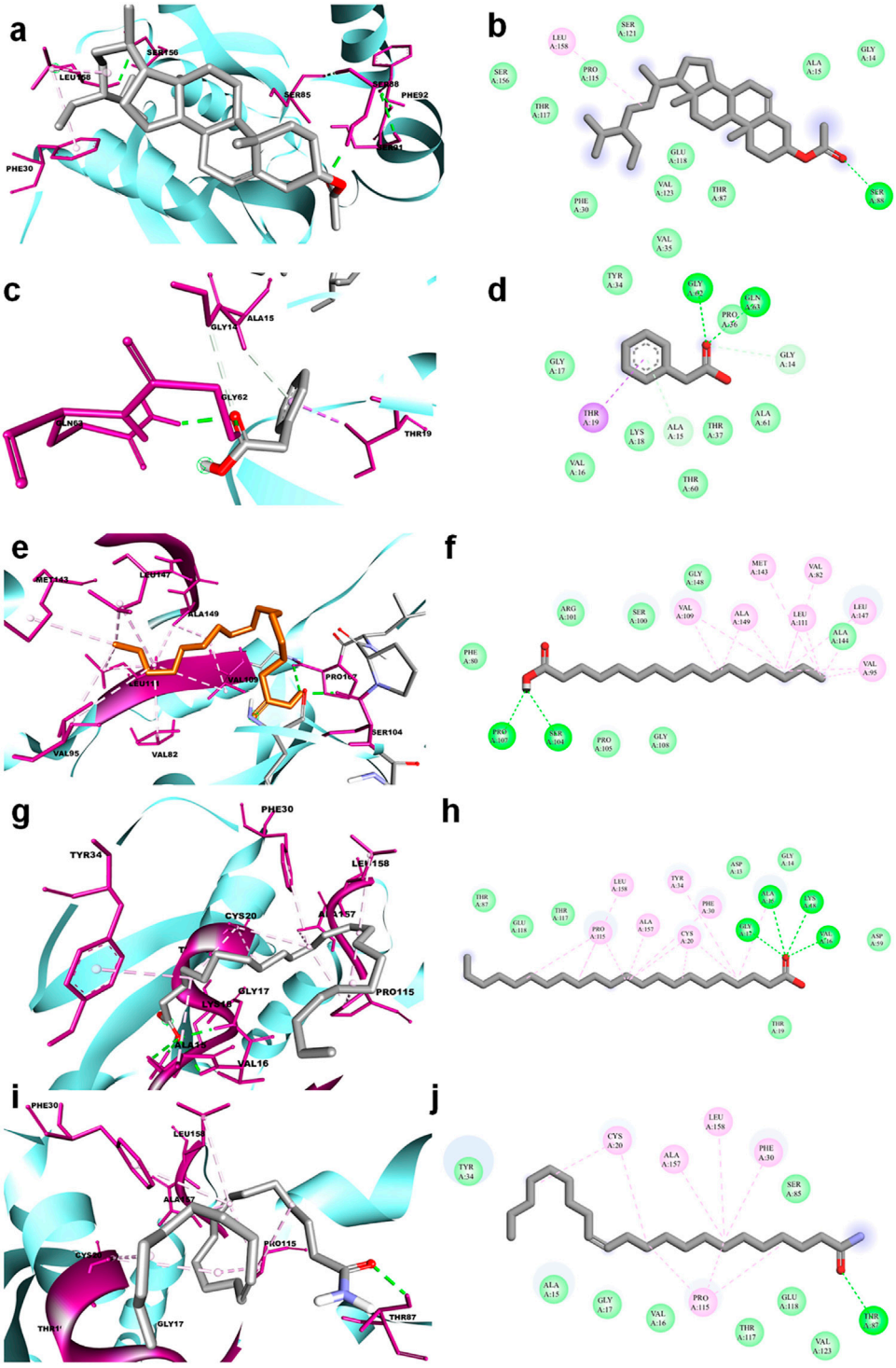

FIGURE 2
3D and 2D representation of molecular docking of CDC42 with ligands from *B. megaterium*. The ligands and their interaction are shown with the line diagram. The color code green color represents the hydrogen bond. Purple color represents pi-sigma interaction. Light pink color represents, pi-alkyl and alkyl interaction. **(A,B)** = beta sitosterol, **(C,D)** = Phenylacetic acid, **(E,F)** = palmitic acid, **(G,H)** = Behenic acid and **(I,J)** = Eurcamide.

TABLE 3 Predicted ADME physio-chemical properties of the docked compounds, all the tables cited correctly.

Compound name	Human intestinal absorption	BBB	Acute oral toxicity (log (1/(mol/kg))	Fish aquatic toxicity	Carcinogenicity (binary)
Beta sitosterol	0.9930	0.9247	1.989	0.9917	0.9714
Phenylacetic acid	0.9490	0.9659	1.697	0.4220	0.7286
palmitic acid	0.8417	0.9725	1.16	0.9178	0.6571
Behenic acid	0.8417	0.9725	0.6378	0.9178	0.6571
Eurcamide	0.9186	0.9969	0.6537	0.7699	0.6429

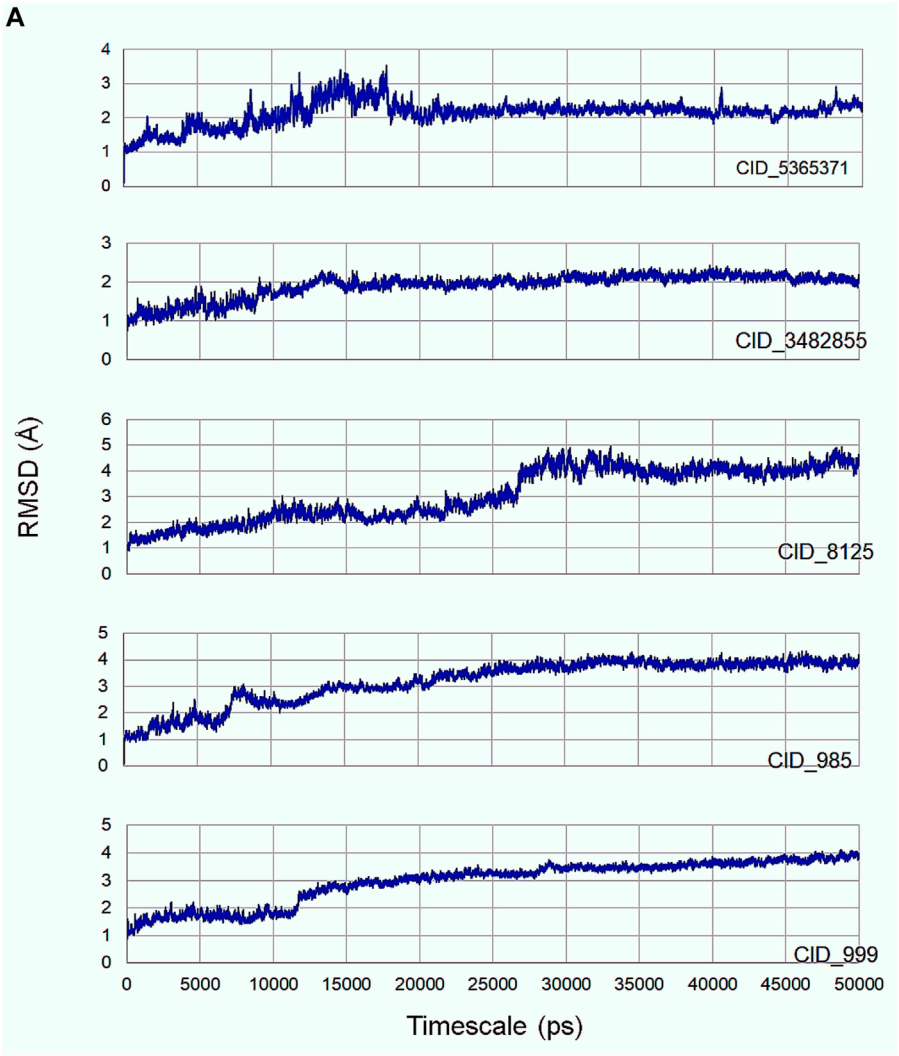

FIGURE 3
(continued).

similarity with 98% query coverage with human cell division control protein 42 homolog. The modeled structure was superimposed with the template structure and it is shown in Figure 1. The overall quality factor obtained during ERRAT analysis is 77.5281. In Verify3D, around 80.65% of the amino acid residues have scored≥0.2 in the 3D/1D profile.

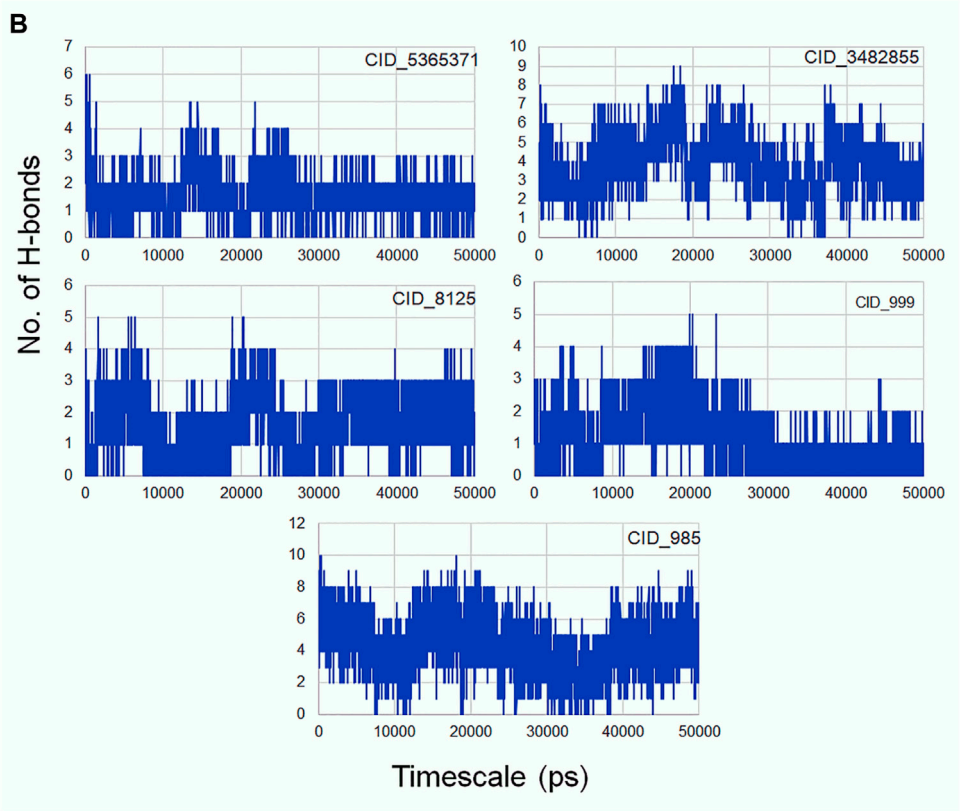

FIGURE 3
(A) Molecular dynamics simulation of CDC42 with ligands (β-sitosterol, phenylacetic acid, palmitic acid, behenic acid, and erucamide); **(B)** H-bond interaction of CDC42 and ligand molecules.

Ramachandran's Z-score was found to be −2.077 in the WHAT CHECK analysis. In Ramachandran plot analysis 88.7% amino acid residues were found in the most allowed regions. Around 10.7% residues were present in additionally allowed regions and 0.6% amino acid residues were found in generously allowed regions. The overall quality analyzed through ProSA Z-score displayed a −6.62 value for target CDC42 homology while the template displayed a Z-score value of -7.59. This Z-score comparison between the target and the template suggests the resemblance in the geometry of the conformations between the target and template. Structural validation was shown in (Supplementary Figure S1). Altogether the structural verification suggested the consistency of the generated model.

Molecular docking

The molecular docking results for active compounds identified from *B. megaterium* were shown in Table 1. Inconsistent with previous reports from Xie et al. (2021), the results from the present study also showed β-sitosterol and phenylacetic acid as the top hits in molecular docking. Through binding site prediction, it was observed that Leu158, Ser121, Thr117, Glu118, Ser88, Thr87, Ala15, Glu18, and Gly14 are the active residues of CDC42. Active site region is distributed with polar (Ser and Thr), hydrophobic residues (Leu and Ala) and negatively charged (Glu) residues. The presence of Ser residues in the active region are responsible for the interaction with the lead molecules. Presence of single Ser residues are responsible for enzymatic reaction. The binding site region consist of two Ser residues responsible for interaction of the lead molecules. Both the ligand, β-sitosterol and phenylacetic acid, presented the highest dock score of −10 kJ mol $^{-1}$. The next top hit obtained was palmitic acid (−9.4 kJ mol $^{-1}$) followed by behenic acid (−9.2 kJ mol $^{-1}$) and erucamide (−9.2 kJ mol $^{-1}$). The representative 2D and 3D images were presented in Figure 2. The CDC42 homolog protein with phenylacetic acid displayed van der Waals interactions with Gly17, Val16, Lys18, Thr37, Thr60, Ala61, Pro36, Val35, Tyr34; conventional hydrogen bond interactions with Gly62, Gln63; carbon-hydrogen bond and pi-donor hydrogen bond interactions with Ala15, Gly14; and pi-sigma bond interaction with Thr19. The CDC42 protein with β-

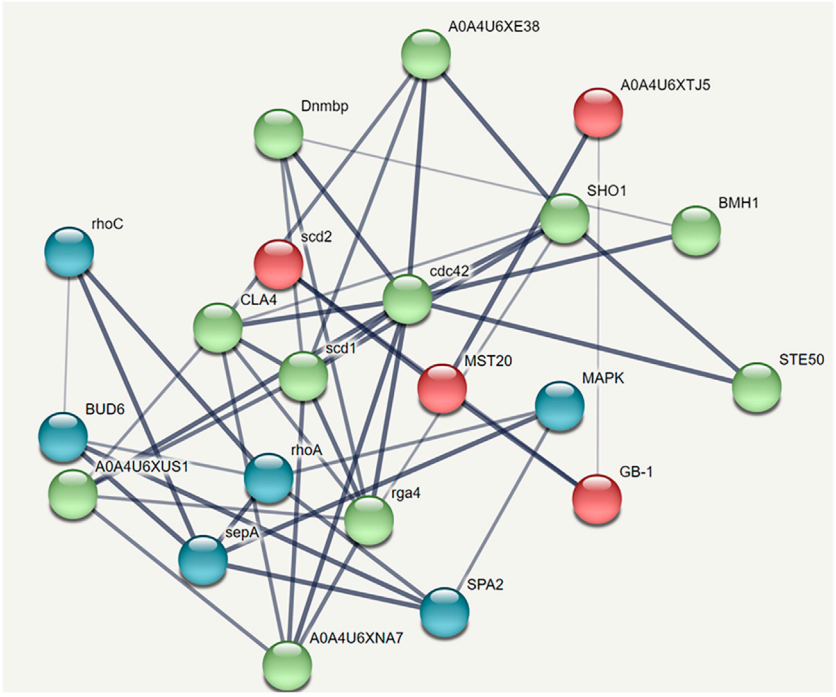

FIGURE 4
STRING network analysis displaying protein-protein interactions. Color nodes represents query proteins and first shell of interactions. Red color node represents cluster 1, green color represents cluster 2 and blue color represents cluster 3.

sitosterol displayed van der Waals interactions with Pro115, Ser121, Ser156, Thr117, Phe30, Val123, Glu118, Thr87, Ala15, and Gly14; conventional hydrogen bond interaction with Ser88; and alkyl bond interaction with Leu158. Palmitic acid displayed van der Waals interactions with Phe80, Pro105, Gly108, Arg101, Ser100, Gly148, Ala144; conventional hydrogen bond interactions with Ser104, Pro107; and alkyl bond interactions with Val109, Ala149, Met143, Leu111, Val82, Leu147, Val95. The CDC42 homolog with behenic acid displayed van der Waals interactions with Thr87, Glu118, Thr117, Asp13, Gly14, Asp59, Thr19; conventional hydrogen bond interactions with Ala15, Val16, Gly17, Lys18; alkyl and pi-alkyl bond interactions with Pro115, Ala157, Leu158, Tyr34, Phe30, Cys20. Erucamide showed van der Waals interactions with Tyr34, Ala15, Gly17, Val16, Thr117, Glu118, Val123, Ser85; (Table 2) conventional hydrogen bond interaction with Thr87; alkyl and pi-alkyl bond interactions with Cys20, Phe30, Pro115, Ala157, Leu158. From the free energy calculation, it was observed that β-sitosterol obtained the highest binding energy of -42.35 (Kcal/mol) compared to the other molecules used for docking. Palmitic acid with an energy of -41.51(Kcal/mol) was observed as second highest compound showing highest binding affinity. The other compounds such as phenylacetic acid, Eurcamide, and Behenic acid was observed with -39.26, -39.49 and -37.90 was observed with binding energy respectively.

ADMET

All the compounds were predicted positive for intestinal absorption and blood brain barrier. Also, from the predicted results it was observed that the compounds were non AMES toxic and non-carcinogenic. Hence the predicted compounds were determined non-toxic and can be used extensively for further studies. Also, β-sitosterol was previously predicted as FDA approved drug with no side-effects (Babu and Jayaraman, 2020). Based on the pharmacokinetic properties, the molecules were predicted to be lead molecules (Table 3).

Molecular dynamics simulation

Molecular dynamics simulation is an efficacious method for validating the stability of the ligands (β-sitosterol, phenylacetic acid, palmitic acid, behenic acid, and erucamide) docked into the binding pocket of CDC42. For this, all-atom molecular dynamics (MD) simulation study was applied which is regarded as a valuable approach to study the dynamic behavior of the ligands and proteins along with their key interacting residues. Thus, the obtained protein-ligand complexes through molecular docking were enrolled for 50 ns of all-atom MD simulation. MD simulation results revealed the protein-ligands exhibited

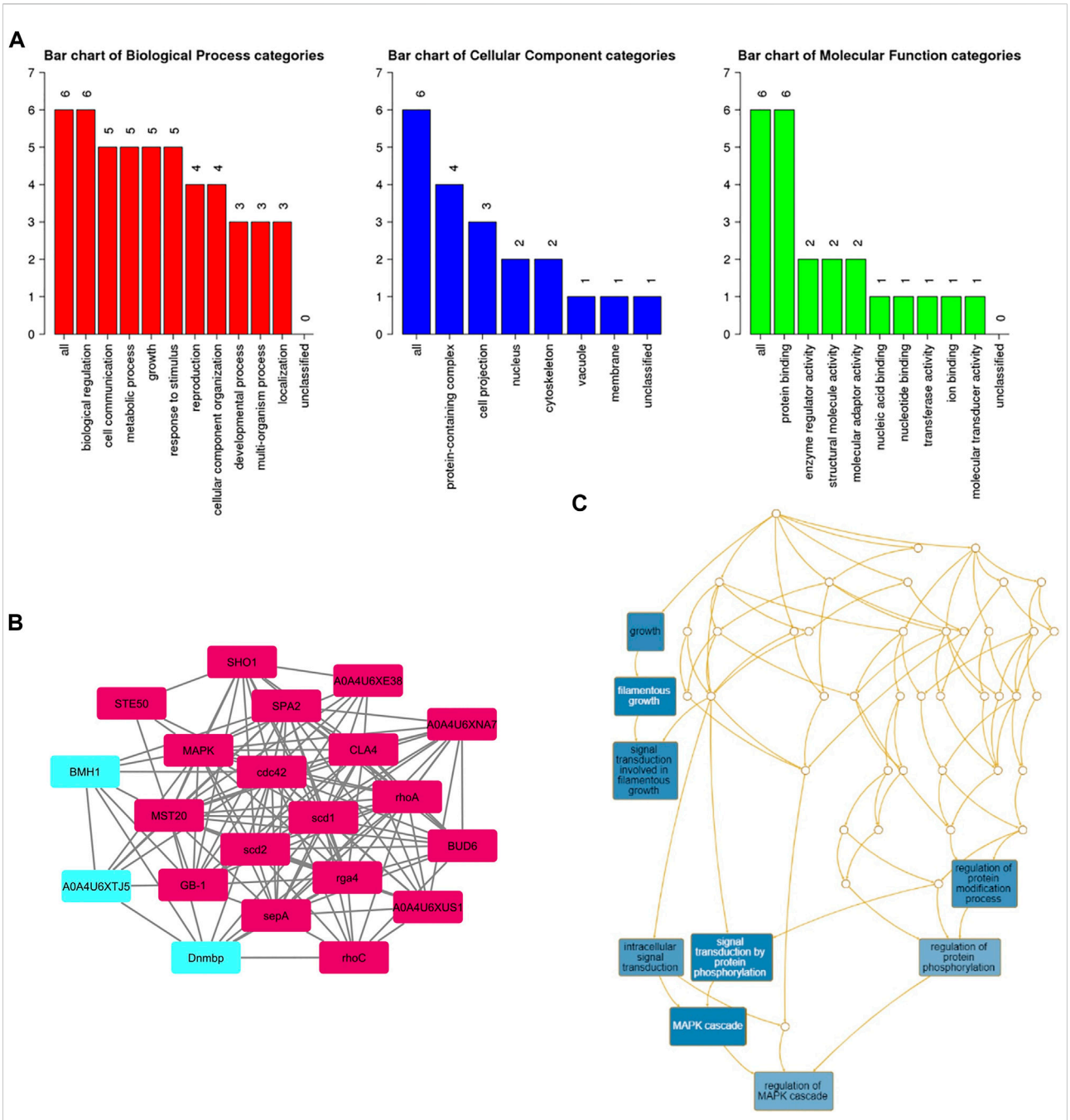

FIGURE 5
(A) Gene ontology analysisrepresents role of proteins in different process such as biological process, cellular and molecular function. The number of proteins involved in different process were represented above each bar. **(B)** node attribute enumerator analysis using MCODE available with Cytoscape (Maroon color subnetwork- 1; Cyan subnetwork-2); The subnetwork 1 is occupied with maximum numbers of proteins and subnetwork 2 is occupied with 3 proteins**(C)** Subnetworks - three clusters are highlighted in blue and the functional involvement of three clusters are represented in white font.

successful conversion of the initial start of run from 15 ns (Figure 3). The trajectories analysis of the MD run has shown the rise of initial frames at an average of 15 ns. However, the RMSD level of the trajectories proceeded with the average values with minimal fluctuation until 20 ns. The ligand β-sitosterol showing interaction with CDC42 during MD simulation has exhibited an initial rise of the frames from 10 to 15 ns. The standard plateau throughout the MD simulation interval was

TABLE 4 KEGG enrichment analysis for enriched gene set.

GeneSet	Description	Size	Overlap	Expect	Enrichment ratio	pValue	FDR	Gene symbol
sce04011	MAPK signaling pathway	114	5	0.109986	45.46053	1.12E-08	4.02E-05	BMH1; CLA4; SHO1; SPA2; STE50
GO: 0030447	filamentous growth	135	5	0.130246	38.38889	2.64E-08	4.02E-05	BMH1; BUD6; SHO1; SPA2; STE50
GO: 0000165	MAPK cascade	42	4	0.040521	98.71429	2.67E-08	4.02E-05	CLA4; SHO1; SPA2; STE50
GO: 0023014	signal transduction by protein phosphorylation	47	4	0.045345	88.21277	4.25E-08	4.80E-05	CLA4; SHO1; SPA2; STE50
GO: 0040007	growth	177	5	0.170767	29.27966	1.04E-07	9.36E-05	BMH1; BUD6; SHO1; SPA2; STE50
GO: 0001402	signal transduction involved in filamentous growth	13	3	0.012542	239.1923	1.42E-07	1.07E-04	BMH1; SHO1; STE50
GO: 0031399	regulation of protein modification process	212	5	0.204534	24.44575	2.56E-07	1.66E-04	BMH1; CLA4; SHO1; SPA2; STE50
GO: 0035556	intracellular signal transduction	252	5	0.243126	20.56548	6.10E-07	3.45E-04	BMH1; CLA4; SHO1; SPA2; STE50
GO: 0043408	regulation of MAPK cascade	32	3	0.030873	97.17188	2.45E-06	0.00123	CLA4; SHO1; SPA2
GO: 0001932	regulation of protein phosphorylation	133	4	0.128316	31.17293	2.90E-06	0.001312	CLA4; SHO1; SPA2; STE50

observed from 20 to 50 ns. The average RMSD for β-sitosterol was observed as 2.10 ± 0.20 Å. This dynamic behavior confers a more stabilized accommodation of β-sitosterol into the binding pocket of the CDC42 throughout the MD simulation. The average RMSD values for phenylacetic acid, throughout the plateau MD simulation interval (12–28 ns) was 3.1 ± 0.50 Å. However, the plateau showed a rise in level after 30 ns and remained stable until 50 ns with an average RMSD of 3.5 ± 0.30 Å. Palmitic acid showed a higher shift in trajectory frames with an RMSD value rise from 3.1 ± 0.50 Å to 4.3 ± 0.10 Å after 25 ns. However, both the ligands phenylacetic acid and palmitic acid have converged around the comparable trajectory frames with an average RMSD value of approximately above 3.5 Å. This dynamic difference between palmitic and phenylacetic acid has shown that the ligands might have deviated from the original interaction compared to the β-sitosterol ligand complex. The other ligands such as behenic acid and eurcamide have shown differential dynamic behavior, which confers the ligands shift from the binding pocket. Eurcamide initial rise in the trajectory level at 15–20 ns was about 3.1 ± 0.10 Å. Later, the plateau was depicted as steady until the end of the simulation around 50 ns. Similarly, behenic acid has shown a rise in the level of the plateau after 28 ns, which confirms the significant ligand, shifts out of the CDC2 pocket, and remained stable till the end of the MD run. Thus, the overall analysis of the MD simulation run suggests the ligand β-sitosterol has stable conformation into the binding pocket of CDC42. Comparatively, phenylacetic acid and palmitic acid have also been found to be stable. Euracamide and behenic acid ligands were observed to alter their position in their binding pocket of CDC42. The hydrogen bond formation plays a significant role during molecular interaction between the ligand and protein (CDC42). The term hydrogen bond donor and acceptor during hydrogen bonding indicate hydrogen atom from the donor and the acceptor with lone pair of electrons. From the MD simulation run, it was observed that β-sitosterol and palmitic acid shared a maximum of eight hydrogen atoms throughout the run. Phenylacetic acid has shared a maximum of four hydrogen bonds throughout the simulation run. Overall, the number of hydrogen bond donors, as well as acceptors, are within the range for β-sitosterol and palmitic acid (Figure 3B).

STRING analysis

The protein-protein interaction network predicted through STRING analysis is shown in Figure 4. The network comprises 21 nodes; 133 edges; 12.7 average degree nodes; 0.812 average local clustering coefficient; 31 expected edges with protein-protein interaction enrichment values less than $1.0e^{-16}$. In Figure 4, color nodes represent the query protein and first shell of interactors while the white nodes represent the second shell of interactors. The empty nodes indicate proteins with an unknown 3D structure. The network edges represent the confidence mode in which the thickness of the line indicates the strength of the data support. From Figure 4, it is clear that there is no 3D structure available for the first and second shell interactors. Hence, further studies are required to understand the complex mechanism and detailed functions of the

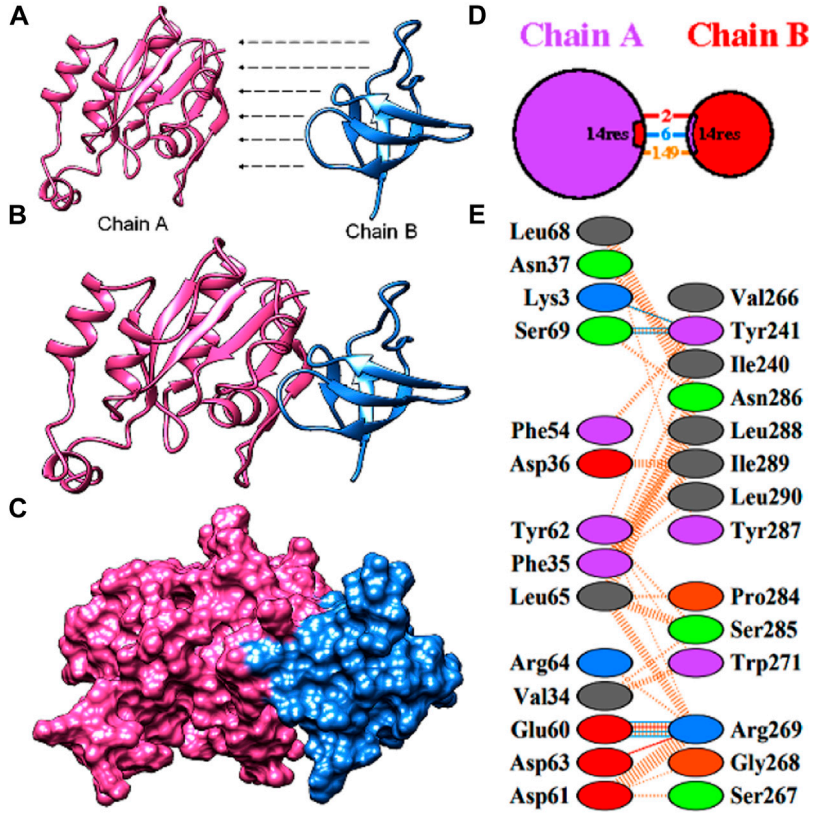

FIGURE 6
Protein-protein docking of the CDC42 with SHO1 from *C. gloeosporioides* **(A)** model proteins of CDC42 (pink) and SHO1 (blue). **(B)**and **(C)** interaction of the model proteins **(D)** pictorial representation of the interaction model and number of interactions **(E)** residues involved in interaction.

CDC42 homolog in establishing pathogenicity and diseases in plants.

Clusters identification through MCODE analysis and GO classification

A subnetwork was constructed and the result was visualized through Cytoscape. CDC42 has shown interaction with SHO1, STE50, SPEA2, A0A4U6XE38, MAPK, CLA4, A0A4U6XNA7, MST20, SCD2, SCD1, RHOA, GB-1, SEPA, RHOC, A0A4U6XUS1, BUD6, RGA4, BMH1, A0A4U6XTJ5, and DNMBP. Further functional enrichment and Gene ontology analysis performed through the WEB-based GEneSeT AnaLysis Toolkit depicting three fundamental categories were presented in Figure 5A. The three main categories are biological process, cellular components, and molecular function. MCODE provides a real-time cluster assessment quality. The node attribute enumerator provides a numerical summary of node attribute values as shown in Figure 5B. Node attribute that is available for the loaded network is shown in box-1 which contains 15 nodes and 94 edges. The members of the clusters are represented in red. Exploration of clusters is shown in box-2 which contains 3 nodes and 3 edges. The members of the clusters are represented in red. The node scoring the highest value in the cluster is referred to as the seed. It is the node from which the cluster was derived, and it is represented in squares, and other cluster members are represented in circles. Edges indicating the interactions are represented in blue while the edge directionality is represented by arrows. New sub-clusters formed from the main cluster is shown in Figures 5C,D. The GO Slim summary is based on 6 unique Entrez gene IDs including BMH1, CLA4, SHO1, SPA2, STE50, and CDC42. Among 6 unique Entrez gene IDs, 6 IDs are annotated to the selected functional categories and also in the reference list, which are used for the enrichment analysis. All the genes mentioned above are predicted to play an important role in the MAP kinase pathway. The enrichment analysis revealed that the gene is mainly involved in filamentous growth, signal transduction (by protein phosphorylation), and MAPK cascade. Altogether, the KEGG enrichment analysis revealed the association of the MAPK signaling pathway. The enriched gene set for the MAPK signaling pathway was found to

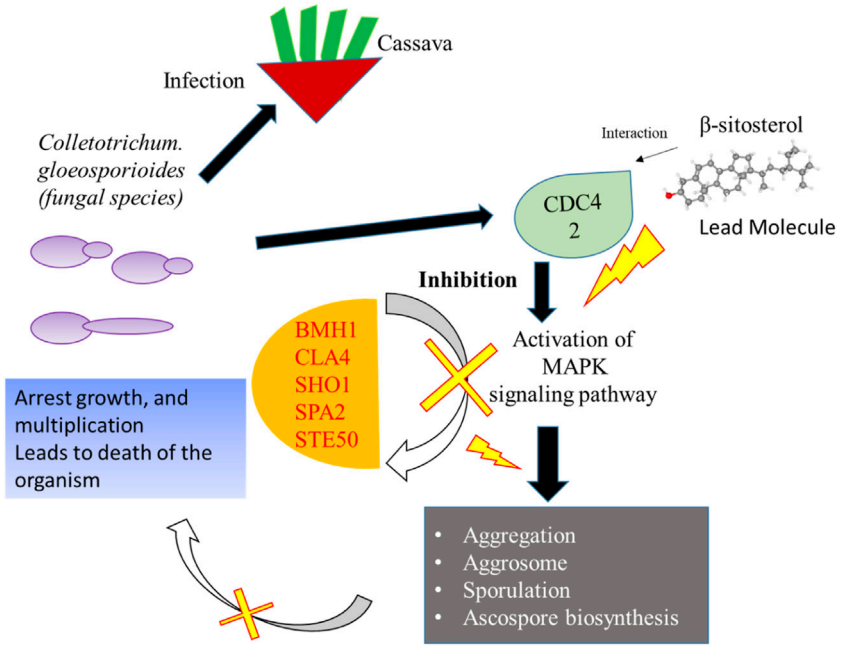

FIGURE 7
Details of the overall mechanism representing CDC42 from *C. gloeosporioides* involved infection and inhibition of the signaling pathway using lead molecules.

have a *p*-value of 1.1214^{e-8}; an enrichment ratio of 45.46 The false discovery rate for the network was predicted as 0.00004 for a gene set size of 114 (Table 4). The protein sequence of SHO1 of *C. gloeosporioides* with the accession id A0A1B2LQ50 was obtained from Uniprot database. The sequence alignment of target and template sequence (yeast SHO1) with the sequence coverage of 61.02% was used for modelling the protein. Interaction analysis of CDC42 and SHO protein has shown 14 residues from each protein have good binding affinity. H-bond (6), non-bonded 149) and 2 salt bridges were established between the drug target (CDC42) and SHO1 (Figure 6).

Discussion

Anthracnose disease occurrence in cassava can lead to total economic loss for the cultivators by damaging the total harvest into the rotting waste. Anthracnose disease occurs in plants due to fungal species of the genus Colletotrichum. The species such as *C. fructicola*, *C. gloeosporioides*, *C. tropicale*, *C. theobromicola*, *C. siamense*, *C. brevisporum*, and *C. plurivorum* are the most common group of plant pathogens that are responsible for diseases on many plant species. Infected plants with fungal strains develop dark patches and lesions on stems, leaves, or any parts of the plant. The lesions occurring on the infected region (leaves, stem) appear to be the gelatinous masses of spores. The fungi during infection come in close contact with the adherence of the spores. The germination starts after several hours with favorable conditions such as temperature. During the suitable temperature, the fungi germinate the conidia and produce the germ tubes. Fungi develop appressorium and arrest the elongation of the germ tube. The penetration of appressorium promotes turgor pressure and fungi colonize the plant tissues, which appear like a canker.

The role of genes in the penetration and development of infection has not been revealed so far in cassava. However, mitogen activator (PMK1, MPS1), ATPase (PDE1), Tetraspanins (PLS1), and fungal effector genes were reported as important genes for infection in rice blast fungus. CDC42, an important protein essential for cell division and cell cycle from cassava, was investigated as the molecular target for the present study. From the sequence analysis, CDC42 was revealed with 190 amino acids and belongs to the small GTPase family. In fungi, the presence of the small GTPase is essential for both beneficial and pathogenic interaction with the plant system. The small GTPases of cassava are characterized as Rho family, essential for the formation of virulence, a fusion of pathogen with plant cell, and production of reactive oxygen species (ROS). Thus, the protein with three motifs is structurally essential for the GTPase activity. In absence of the three-dimensional structure, the protein was modeled based on sequence similarity. The CDC42 protein from *C. gloeosporioides* has shown 70.83% homology with CDC42 of humans with query

coverage of 98%. The modeled structure was validated and used for further docking studies. Generally, *Bacillus* sp. is considered a promising source for bioactive secondary metabolites. Therefore, in the present study molecular docking was carried out with the bioactive compounds (erucamide, behenic acid, palmitic acid, phenylacetic acid, and β-sitosterol) of *B. megaterium*. There are several pieces of evidence for the compounds identified from *B. megaterium* as lead molecules. Erucamide identified from radish leaf has shown preventive effects against memory deficits related to Alzheimer's disease by modulation of cholinergic function. *In vivo* experiments have shown that erucamide has biological activity such as stimulation of angiogenesis, augmentation of neovascularization in regenerating skeletal muscle, and anti-depressive effects (Kim et al., 2018). Similarly, behenic acid-based nano micelles were prepared with dextran as the combination to deliver itraconazole as a drug. The nano micelles were used as anti-leishmaniasis for targeting the parasite (Shahriyar et al., 2021). The saturated fatty acid (C:16), the palmitic acid, selected as the lead molecule in the present study has been deeply investigated previously (Lee et al., 2009) as an antiviral agent. Palmitic acid specifically binds to the CD4 and prevents the entry of the HIV-1 virus. Moreover, beta-sitosterol has been reported from plants and is known for anticancer effects against several cancers such as breast and ovary, prostate, lung, stomach, and liver. In addition, the compound can significantly inhibit several pathways, cell signaling, apoptosis, angiogenesis, and inflammation (Bin Sayeed and Ameen, 2015). Phenylacetic acid and its derivatives were extensively used in the preparation of drugs that can be used for several ailments. Diclofenac is used as a medication for the treatment of pain and inflammation (Gan 2010). Apart, the previous report indicated that the purified components possess significant antimicrobial activity against plant pathogens such as *A. tumefaciens* (T-37), *Erwinia carotovora* (EC-1), and *Ralstonia solanacearum* (RS-2) (Xie et al., 2021). Among the five components investigated against plant pathogens, β-sitosterol, behenic acid, and phenylacetic acid displayed significant antimicrobial activity. B-sitosterol showed a very low minimum inhibitory concentration (15.6 μg/ml) against *R. solanacearum* RS-2 (Xie et al., 2021). Thus, the five compounds of choice used for the present study have already been investigated for several alignments. Mostly, these compounds were reported from different plant species; however, in the present study, the compounds identified from *B. megaterium* were used for investigation. The compounds were docked into the binding pocket of the CDC42 of *C. gloeosporioides.* β-sitosterol and phenylacetic acid showed the highest dock score of −10 kJ mol $^{-1}$. The next top hit obtained was palmitic acid (−9.4 kJ mol $^{-1}$) followed by behenic acid (−9.2 kJ mol $^{-1}$) and erucamide (−9.2 kJ mol $^{-1}$). From the binding energy analysis, it was observed that β-sitosterol obtained the highest binding affinity of −41.51(Kcal/mol).

To study the stability during their interaction, molecular simulation was performed and the results showed that the compounds were stable throughout the simulation. For a comprehensive analysis of the docked protein-ligand complex, a molecular dynamics simulation was carried out. It is the most powerful technique to study the conformational changes taking place at the atom level. Therefore, molecular dynamics simulation was performed for some time of 50 ns for all atom-docked protein-ligand complexes. The result showed b-sitosterol with stable conformation compared to the other docked complexes. The results are evidence that the docked protein- β-sitosterol complexes are highly stable for the entire period of 20–50 ns. Furthermore, RMSD plot analysis showed slight modification in the position, indicating the stable association and interactions between the ligand and the protein molecule. Also, the ligand has maintained a maximum of eight hydrogen bond interactions throughout the MD run. Thus, the stability of the ligand with CDC42 shows the ligands can be extended further as a biological agent to treat pathogenesis against *C. gloeosporioides*. Additionally, studies have shown that β-sitosterol has already been used for the treatment of various diseases due to its potent properties such as antinociceptive, anxiolytic and sedative effect, anticancer, antimicrobial, immunomodulatory, hepatoprotective, and wound healing effects. The chemical has already been approved by FDA and is a safe nutraceutical with no deleterious effects (Babu and Jayaraman, 2020).

Network-based approaches provide a deep insight to understand the biological process during the pathogenesis of *C. gloeosporioides*. The interacting partner revealed through the PPI network will pave the way to investigate the cellular activity, protein localization, and complex biological function of the protein. Besides, 20 genes have shown interaction with CDC42 and from the MCODE statistical analysis, two clusters were identified one with 15 nodes and 94 edges and the second cluster with 3 nodes and 3 edges. Furthermore, the functional enrichment analysis has revealed the BMH1, CLA4, SHO1, SPA2, and STE50 as the important genes involved in the MAPK signaling pathway. The protein BMH1 has shown to play important role in aggregation, and arrangement to form aggresomes. Additionally, BMH1 is involved in spore formation, sporulation, and ascospore biosynthesis. The CLA4 is very essential for imparting *Cladosporium* resistance in the organism. SHO1 protein, the osmosensor present in the plasma membrane of *C. gloeosporioides* activates the high osmolality glycerol (HOG) of the MAPK signaling pathway in response to high osmolality. SHO1 protein is found in bud and bud neck region of the fungal pathogen. Protein docking interaction reveals SHO1 and CDC42 has established binding affinity. Hence it is envisaged that inhibition of CDC42 can significantly prevent the signalling and inhibit the growth and development of the fungal pathogen. SPA2 perhaps a cytoskeletal protein is involved in pheromone-induced morphogenesis, budding, invasive filamentation growth, regulation of hyphal growth, cellular shape, and reproduction of *C. gloeosporioides*. STE50 protein has shown to play a significant role in signal transduction during filamentous growth, osmosensory signaling MAPK cascade thereby arrest the growth during conjugation.

Thus, the identified interacting partners of CDC42 are involved in the MAPK signaling pathway essential for growth, and virulence regulation in *C. gloeosporioides*. Therefore, from the present study, it is revealed that targeting CDC42 can impart the interaction network, prevent filament production, and arrest the reproduction in *C. gloeosporioides* (Figure 7).

Conclusion

Infections caused by *C. gloeosporioides* in cassava are very serious to impair, leading to economic damage to the cultivators. To date, there are no clear details about the type of infection and mode of transmission, and pathogenesis of the fungal pathogen. Hence, in the present study, CDC42 protein involved in cell division and cell cycle of the pathogen was selected as the target. Modeling of the protein revealed the key residues playing the functional role of the protein. The protein was targeted with five active compounds from *B. megaterium*. Interaction of β-sitosterol and phenylacetic acid with the key residue of CDC42 revealed that ligands could have a potential role in the inhibition of functional proteins that are involved in growth. Further PPI network constructed for CDC42 revealed that targeting the protein could impart MAPK signaling pathway. Additionally, targeting the interacting partner could also prevent the growth, filamentation, and hyphal growth which is essential for virulence regulation. However, further experimental insight can pave a way for preventing *C. gloeosporioides* mediated infection in cassava.

Data availability statement

The original contributions presented in the study are included in the article/Supplementary Material, further inquiries can be directed to the corresponding author.

Author contributions

NP and NB, designed the experiment. NP, KM, and BK implemented and analyzed the data. WT, RS, CS, and NH, analysis the results, discussion, VM, TL, and MK, prepared the manuscript. NP, TL, and NB revised the manuscript.

Acknowledgments

The authors are thankful to Suranaree University of Technology, Thailand for providing financial support. This research received research funding support from the SUT research and development fund (Project code: IRD 3-302-65-12-20). The authors are also thankful to Dr. B.R. Ambedkar Open University (Hyderabad), Sri Yuva Biotech Pvt. Ltd (Hyderabad), and Mahatma Gandhi University (Nalgonda), India for their help and support in this work.

Conflict of interest

BK was employed by the company Sri Yuva Biotech Pvt Ltd.

The remaining authors declare that the research was conducted in the absence of any commercial or financial relationships that could be construed as a potential conflict of interest.

Publisher's note

All claims expressed in this article are solely those of the authors and do not necessarily represent those of their affiliated organizations, or those of the publisher, the editors and the reviewers. Any product that may be evaluated in this article, or claim that may be made by its manufacturer, is not guaranteed or endorsed by the publisher.

Supplementary material

The Supplementary Material for this article can be found online at: https://www.frontiersin.org/articles/10.3389/fmolb.2022.1010603/full#supplementary-material

SUPPLEMENTARY FIGURE 1
Structural validation through Saves and ProSA program (A) Verify3D (B) Ramachandran plot for model obtained from swiss model server and modeller (C) ProSA score for the template, 2NGR (D) ProSA score for target, CDC42.

SUPPLEMENTARY FIGURE 2
superimposition of model from Swissmodel (blue) and modeler (pink).

References

Adewole, K. E., and Ishola, A. A. (2021). A computational approach to investigate the HDAC6 and HDAC10 binding propensity of psidium guajava-derived compounds as potential anticancer agents. *Curr. Drug Discov. Technol.* 18, 423–436. doi:10.2174/1568009620666200502013657

Agrawal, S., Jana, U. K., and Kango, N. (2021). Heterologous expression and molecular modelling of L-asparaginase from Bacillus subtilis ETMC-2. *Int. J. Biol. Macromol.* 1 (192), 28–37. doi:10.1016/j.ijbiomac.2021.09.186

Atwijukire, E., Hawumba, J. F., Baguma, Y., Wembabazi, E., Esuma, W., Kawuki, R. S., et al. (2019). Starch quality traits of improved provitamin A cassava (*Manihot esculenta* Crantz). *Heliyon* 5, e01215. doi:10.1016/j.heliyon.2019.e01215

Ayling, S., Ferguson, M., Rounsley, S., and Kulakow, P. (2012). Information resources for cassava research and breeding. *Trop. Plant Biol.* 5, 140–151. doi:10.1007/s12042-012-9093-x

Azam, S. S., and Abbasi, S. W. (2013). Molecular docking studies for the identification of novel melatoninergic inhibitors for acetylserotonin-O-methyltransferase using different docking routines. *Theor. Biol. Med. Model.* 10, 63. doi:10.1186/1742-4682-10-63

Babu, S., and Jayaraman, S. (2020). An update on β-sitosterol: A potential herbal nutraceutical for diabetic management. *Biomed. Pharmacother.* 131, 110702. doi:10.1016/j.biopha.2020.110702

Balyejusa Kizito, E., Rönnberg-Wästljung, A. C., Egwang, T., Gullberg, U., Fregene, M., and Westerbergh, A. (2007). Quantitative trait loci controlling cyanogenic glucoside and dry matter content in cassava (*Manihot esculenta* Crantz) roots. *Hereditas* 144, 129–136. doi:10.1111/j.2007.0018-0661.01975.x

Benkert, P., Biasini, M., and Schwede, T. (2011). Toward the estimation of the absolute quality of individual protein structure models. *Bioinformatics* 27, 343–350. doi:10.1093/bioinformatics/btq662

Bin Sayeed, M. S., and Ameen, S. S. (2015). Beta-sitosterol: A promising but orphan nutraceutical to fight against cancer. *Nutr. Cancer* 67, 1214–1220. doi:10.1080/01635581.2015.1087042

El-Sharkawy, M. A. (2004). Cassava biology and physiology. *Plant Mol. Biol.* 56, 481–501. doi:10.1007/s11103-005-2270-7

Gan, T. J. (2010). Diclofenac: An update on its mechanism of action and safety profile. *Curr. Med. Res. Opin.* 26, 1715–1731. doi:10.1185/03007995.2010.486301

Gong, Z., Xiong, L., Shi, H., Yang, S., Herrera-Estrella, L. R., Xu, G., et al. (2020). Plant abiotic stress response and nutrient use efficiency. *Sci. China. Life Sci.* 63, 635–674. doi:10.1007/s11427-020-1683-x

Hasan, R., Rony, M. N. H., and Ahmed, R. (2021). *In silico* characterization and structural modeling of bacterial metalloprotease of family M4. *Plant Mol. Biol.* 2 (191), 25. doi:10.1186/s43141-020-00105-y

Hess, B. (2008). P-LINCS: A parallel linear constraint solver for molecular simulation. *J. Chem. Theory Comput.* 4, 116–122. doi:10.1021/ct700200b

Hormhuan, P., Viboonjun, U., Sojikul, P., and Narangajavana, J. (2020). Enhancing of anthracnose disease resistance indicates a potential role of antimicrobial peptide genes in cassava. *Genetica* 148, 135–148. doi:10.1007/s10709-020-00097-0https://swissmodel.expasy.org/ https://string-db.org/cgi/input?sessionId = b7c9uFOprzGmandinput_page_active_form = single_sequence

Jacobs, R. L., Adhikari, T. B., Pattison, J., Yencho, G. C., Fernandez, G. E., and Louws, F. J. (2019). Inheritance of resistance to *Colletotrichum gloeosporioides* and *C. acutatum* in strawberry. *Phytopathology* 109, 428–435. doi:10.1094/PHYTO-08-18-0283-R

Kim, C. R., Kim, H. S., Choi, S. J., Kim, J. K., Gim, M. C., Kim, Y. J., et al. (2018). Erucamide from radish leaves has an inhibitory effect against acetylcholinesterase and prevents memory deficit induced by trimethyltin. *J. Med. Food* 21, 769–776. doi:10.1089/jmf.2017.4117

Koehorst-van Putten, H. J., Sudarmonowati, E., Herman, M., Pereira-Bertram, I. J., Wolters, A. M., Meima, H., et al. (2012). Field testing and exploitation of genetically modified cassava with low-amylose or amylose-free starch in Indonesia. *Transgenic Res.* 21, 39–50. doi:10.1007/s11248-011-9507-9

Laskowski, R. A., Rullmannn, J. A., MacArthur, M. W., Kaptein, R., and Thornton, J. M. (1996). AQUA and PROCHECK-NMR: Programs for checking the quality of protein structures solved by NMR. *J. Biomol. NMR* 8, 477–486. doi:10.1007/BF00228148

Lee, D. Y., Lin, X., Paskaleva, E. E., Liu, Y., Puttamadappa, S. S., Thornber, C., et al. (2009). Palmitic acid is a novel CD4 fusion inhibitor that blocks HIV entry and infection. *AIDS Res. Hum. Retroviruses* 25, 1231–1241. doi:10.1089/aid.2009.0019

Li, M., Liu, J., and Zhou, G. (2021). Histopathological and ultrastructural observations of *Camellia oleifera* infected with *Colletotrichum fructicola*. *Australas. Plant Pathol.* 50, 523–531. doi:10.1007/s13313-021-00811-2

Li, S., Cui, Y., Zhou, Y., Luo, Z., Liu, J., and Zhao, M. (2017). The industrial applications of cassava: Current status, opportunities and prospects. *J. Sci. Food Agric.* 97, 2282–2290. doi:10.1002/jsfa.8287

Machado, S., Silva Veloso, J., Camara, M., Campos, F. S., Sarmento, R. A., Giongo, M. V., et al. (2020). First report of *Colletotrichum chrysophillum* causing cassava anthracnose in Brazil *Plant. Dis.* 8, 1–8. doi:10.1094/PDIS-09-20-1925-PDN10.1094/PDIS-09-20-1925-PDN

Miyamoto, S., and Kollman, P. A. (1992). Settle: An analytical version of the SHAKE and RATTLE algorithm for rigid water models. *J. Comput. Chem.* 13, 952–962. doi:10.1002/jcc.540130805

Oeser, B., Kind, S., Schurack, S., Schmutzer, T., Tudzynski, P., and Hinsch, J. (2017). Cross-talk of the biotrophic pathogen *Claviceps purpurea* and its host *Secale cereale*. *BMC Genomics* 18, 273. doi:10.1186/s12864-017-3619-4

Ons, L., Bylemans, D., Thevissen, K., and Cammue, B. (2020). Combining biocontrol agents with chemical fungicides for integrated plant fungal disease control. *Microorganisms* 8, 1930. doi:10.3390/microorganisms8121930

Peck, S., and Mittler, R. (2020). Plant signaling in biotic and abiotic stress. *J. Exp. Bot.* 71, 1649–1651. doi:10.1093/jxb/eraa051

Pinweha, N., Asvarak, T., Viboonjun, U., and Narangajavana, J. (2015). Involvement of miR160/miR393 and their targets in cassava responses to anthracnose disease. *J. Plant Physiol.* 174, 26–35. doi:10.1016/j.jplph.2014.09.006

Sekhar Pagadala, N., Arha, M., Reddy, P. S., Kumar, R., Sirisha, V. L., Prashant, S., et al. (2009). Phylogenetic analysis, homology modelling, molecular dynamics and docking studies of caffeoyl-CoA-O-methyl transferase (CCoAOMT 1 and 2) isoforms isolated from subabul (*Leucaena leucocephala*). *J. Mol. Model.* 15, 203–221. doi:10.1007/s00894-008-0395-8

Shahriyar, S., Taymouri, S., Saberi, S., Asadi, P., and Tabbakhian, M. (2021). Preparation and characterization of itraconazole loaded nanomicelles based on dextran-behenic acid for cutaneous leishmaniasis treatment. *Drug Dev. Ind. Pharm.* 47, 416–428. doi:10.1080/03639045.2021.1890112

Studio, D. (2015). *4.1 visualizer*. San Diego, USA: Accelrys Software Inc.

Tripathi, N., Danger, R., Chesneau, M., Brouard, S., and Laurent, A. D. (2022). Structural insights into the catalytic mechanism of granzyme B upon substrate and inhibitor binding. *J. Mol. Graph. Model.* 114, 108167. doi:10.1016/j.jmgm.2022.108167

Trott, O., and Olson, A. J. (2010). AutoDock Vina: Improving the speed and accuracy of docking with a new scoring function, efficient optimization, and multithreading. *J. Comput. Chem.* 31, 455–461. doi:10.1002/jcc.21334

Van Der Spoel, D., Lindahl, E., Hess, B., Groenhof, G., Mark, A. E., and Berendsen, H. J. (2005). Gromacs: Fast, flexible, and free. *J. Comput. Chem.* 26, 1701–1718. doi:10.1002/jcc.20291

Wang, X., Lu, D., and Tian, C. (2021). Analysis of melanin biosynthesis in the plant pathogenic fungus *Colletotrichum gloeosporioides*. *Fungal Biol.* 125, 679–692. doi:10.1016/j.funbio.2021.04.004

Wang, X., Xu, X., Liang, Y., Wang, Y., and Tian, C. (2018). A CDC42 homolog in *Colletotrichum gloeosporioides* regulates morphological development and is required for ROS-mediated plant infection. *Curr. Genet.* 64, 1153–1169. doi:10.1007/s00294-018-0833-9

Wiederstein, M., and Sippl, M. J. (2007). ProSA-web: Interactive web service for the recognition of errors in three-dimensional structures of proteins. *Nucleic Acids Res.* 35, W407–W410. doi:10.1093/nar/gkm290

Xie, Y., Peng, Q., Ji, Y., Xie, A., Yang, L., Mu, S., et al. (2021). Isolation and identification of antibacterial bioactive compounds from *Bacillus megaterium* L2. *Front. Microbiol.* 12, 645484. doi:10.3389/fmicb.2021.645484

Yousafi, Q., Amin, H., Bibi, S., Rafi, R., Khan, M. S., Ali, H., et al. (2021). Subtractive proteomics and immuno-informatics approaches for multi-peptide vaccine prediction against Klebsiella oxytoca and validation through in silico expression. *Int. J. Pept. Res. Ther.* 27, 4 2685–2701. doi:10.1007/s10989-021-10283-z

Zheng, W., Zhao, Z., Chen, J., Liu, W., Ke, H., Zhou, J., et al. (2009). A CDC42 ortholog is required for penetration and virulence of *Magnaporthe grisea*. *Fungal Genet. Biol.* 46, 450–460. doi:10.1016/j.fgb.2009.03.005

How to Cite:
Mendam, K., Naik, S. J. K., Sriram, K. B. H., Pawar, A. C., & Vamshi, S. (2022). Anticancer properties of nanoparticle synthesized from Cyphostemma auriculatum. Roxb on nude mice. *International Journal of Health Sciences*, *6*(S4), 1463–1474. https://doi.org/10.53730/ijhs.v6nS4.6232

Anticancer properties of nanoparticle synthesized from Cyphostemma auriculatum. Roxb on nude mice

Kishore Mendam
Occupational Health and Toxicology Lab, Department of Zoology, University College of Science, Osmania University, Hyderabad, Telangana -500007

S. Jithender Kumar Naik
Occupational Health and Toxicology Lab, Department of Zoology, University College of Science, Osmania University, Hyderabad, Telangana -500007

K. Bala Hanumath Sriram
Malla Reddy Pharmacy College, Dhulapally, Hyderabad, Telangana-500100

Anusha C Pawar
Occupational Health and Toxicology Lab, Department of Zoology, University College of Science, Osmania University, Hyderabad, Telangana -500007

S.Vamshi
Occupational Health and Toxicology Lab, Department of Zoology, University College of Science, Osmania University, Hyderabad, Telangana -500007

***Abstract*---**The present study was aimed to establish the pharmacological and therapeutic properties of a green synthesized silver nanoparticles (AgNPs) in breast cancer induced by 7,12-dimethylbenzanthracene (DMBA) in nude mice. In this study, AgNPs made from *Cyphostemma auriculatum* Roxb. leaf extract(CA-AgNPs) were tested in a nude mice model for anticancer activity. A significant elevate changes in blood chemistry like heamoglobin, RBC, WBC, platelets and also on blood biochemical parameters such as catalase and SOD with obtained after 28 days of treatment with carcinogen. However, these levels were restored to normal at the end of the study period treated with CA-AgNPs. The liver oxidative stress enzymes showed no significant alterations. With 15 and 30 mg/kg b.w of CA-AgNP, histopathological analysis revealed no significant abnormalities in the kidney, spleen, lungs, heart, testis, or brain. However, 30 mg/kg b.w. of CA-AgNPs caused considerable cell edema and vacuolar degeneration in the liver, which returned to normal at the conclusion

International Journal of Health Sciences ISSN 2550-6978 E-ISSN 2550-696X © 2022.
***Corresponding author**: Naik, S.J.K.; Email: drnaik8777@yahoo.com*
Manuscript submitted: 27 Feb 2022, Manuscript revised: 18 March 2022, Accepted for publication: 09 April 2022

of the washout period. The findings of this study suggest that green produced CA-AgNPs at low concentrations could be beneficial.

***Keywords*---**Anticancer, *Cyphostemma auriculatum* Roxb., DMBA, CA-AgNPs.

Introduction

Nanotechnology has experienced phenomenal growth in recent years as a result of its numerous applications in sectors such as material science, chemistry, medicine, nanobiotechnology, and others. Nanoparticles (NPs) have attracted a lot of attention because of their high surface-to-volume ratio and extremely small size, which leads to differences in physical and chemical properties when compared to bulk materials with the same composition [1]. Due to several improved approaches created by researchers for the synthesis of NPs with defined size and form to fulfill highly particular criteria, there has been significant progress in the nanotechnology research field in the recent times. New applications for NPs are fast emerging, and numerous patents and research papers describing new nanoparticle synthesis techniques are published each year. The weight unit of a specific material in the Nano size scale has a much higher surface area than the same weight unit for the same material in the macro scale size due to its incredibly small size. Particle composition, morphology, crystallinity, size, and shape all influence the intrinsic properties of metal nanoparticles.

Silver NPs (AgNPs) have piqued researchers' interest among the NPs due to their wide variety of applications in antibacterial, catalysis, medicinal, optical, and energy (2-14). Intensive study has been done based on these findings to investigate their qualities and possible applications for a variety of objectives, including antimicrobial agents in wound dressings, anticancer agents, electronic devices, and water purification. *In-vivo* investigations of AgNPs made using diverse chemical methods revealed toxicity. The size, concentration, coating, and distribution level of AgNPs have an impact on their behaviour. Alternatively, to synthesis NPs without using harsh and expensive toxic chemicals, microbial and biological system (green chemistry) techniques are being developed. Because of their environmentally favourable creation of NPs, microorganism-based NPs synthesis is quickly developing. However, the microbial technique has drawbacks because it takes more effort to maintain colonies. Because of their natural availability, quick creation, and environmentally beneficial character, NPs are being produced using various plant sources.

Cancer is a category of diseases that cause a variety of pathogenic and metabolic alterations in cells. Cell proliferation, angiogenesis, and metastasis are all examples of signaling processes that contribute to its development (15-18). Aerobic glycolysis, mitochondrial DNA depletion, and changes in respiratory chains and genetic expressions are all aberrant metabolic processes in cancer cells. The second biggest cause of death in women is breast cancer. The high prevalence of breast cancer has had a significant influence on society. The majority of breast cancers are estrogen-dependent, and 30-40% of patients who

receive adjuvant tamoxifen medication experience a relapse (19). As a result, endocrine treatment resistance appears to be a clinical issue. Cancer treatments, both physical and pharmacological, are limited at various stages. Currently existing medicines, on the other hand, have a negative impact on normal cell functioning while exposing patients to excessive drug and radiation exposures.

In earlier reports AgNPs were synthesized using *Cyphostemma auriculatum* Roxb., leaf extract. *Cyphostemma auriculatum* Roxb., is used as a folklore medicine and blood purifier in cardiac disorders, intestinal worm diseases, earache, wound abscess, dog bite, rheumatism, purulent wounds, wound healing, tumors, cough, colds, and hydrocele, but also as a tonic and an astringent, according to an ethnomedicinal survey (20). This herb has also been used to treat animal bloody dysentery and diarrhea in veterinary medicine. Alkaloids, flavonoids, saponins, steroids, terpenoids, stilbenoids, and tannins have been found in Vitaceae family plants, according to phytochemical investigations. In a previous paper, described the synthesis and characterization of silver nanoparticles (21). The AgNPs were tested *invivo* in this study to see how effective they are against breast cancer. DMBA (7,12-dimethylbenz(a)anthracene), a prototype of polyaromatic hydrocarbons (PAH), induced breast cancer model on nude mice for *invivo* evaluations among the different preclinical rodent models investigated for breast cancer studies.

Materials and Methods

Sigma-Aldrich, Merck, and Himedia provided all organic compounds and solvents required for all assays and biological studies. The rest of the compounds were of analytical grade.

In-vivo studies

Acclimatization of animals

Thirty six female nude mice (20 ± 2 g) were purchased from National institute of nutrition (Hyderabad, India). All animals were kept in clean, sanitized PVC coated stainless steel cages in an air-conditioned animal house with typical climatic conditions such as a constant temperature of 20–25°C, relative humidity of 45–55%, and a 12 hour light–dark cycle. Animals were provided a regular pellet meal and free access to water before and throughout the experiment. Animals were fasted for 12 hours before administering experimental treatments, but were allowed proper access to water. All of the trials were carried out during the day. Before the experiment, the animals were given a 7-day acclimatization period.

Preparation of DMBA and experimental design for treatment-oriented study

Sigma Chemicals in Mumbai, India, provided the DMBA, which was stored at 20°C to avoid decomposition and dissolved in olive oil carrier. The typical medication, tamoxifen citrate, was dissolved in ethanol (100 mg/mL) and dilute it hundred fold in distilled water to get a final concentration of 1mg/mL. The plant crude and CA-AgNPs also dissolved in ethanol and dilute in distilled water. The mice were placed into six groups, each with six rodents. Animals with tumors were chosen to receive therapy for 28 days. Except for the control group, all 30

animals were given a single gastric intubation in 1 ml olive oil to induce mammary carcinogen (25 mg/kg b.w), during which the Latency period (the number of days between the DMBA injection and the emergence of the first tumor in each mice) was recorded. Palpation revealed the presence of a tumor. Animals with tumors were chosen for treatment for 28 days.

Experimental design

The mice were split into six groups, each with six mice (n = six). The trial lasted a total of 28 days. All of the mice in the study were fed a standard pellet diet. The experiment was conducted in six groups of six mice each as mentioned below.
Group-1: Normal saline treated mice (Normal control-NC)
Group-2: Cancer induced Nude mice (given DMBA (25 mg/kg) by single gastric intubation in 1 mL olive oil.
Group-3: Cancer induced Nude mice (given DMBA (25 mg/kg) by single gastric intubation in 1 mL olive oil + crude plant extract 120 mg/kg body weight
Group-4: Cancer induced Nude mice (given DMBA (25 mg/kg) by single gastric intubation in 1 mL olive oil + AgNPs 15 mg/kg body weight
Group-5: Cancer induced Nude mice (given DMBA (25 mg/kg) by single gastric intubation in 1 mL olive oil + AgNPs 30 mg/kg body weight.
Group-6: Cancer induced Nude mice (given DMBA (25 mg/kg) by single gastric intubation in 1 mL olive oil + tamoxifen citrate 10 mg/kg body weight

Blood samples were collected on Day-01, Day-07, Day-14, Day-21, and Day-28. The animals were sedated on the 28th day, blood was obtained through the retro-orbital sinus and utilized to study hematological parameters, and the blood was centrifuged and the serum was collected. Biochemical parameters were investigated using the serum obtained. After the blood was collected, the animals were decapitated and the entire liver and kidney were perfused with ice-cold 0.9 percent sodium chloride. The organs were then carefully removed, trimmed free of superfluous tissue, and the mammary tumors were excised and histological effects evaluated.

Histopathology

Tissues having gross pathological alterations, as well as normal tissue, were cut into thin slices of 3 to 5 mm thickness. Keep the tissue in a 10% formalin fixative at room temperature for 24-48 hours. Xylol was used to deparaffinize the portion for 5 to 10 minutes before pure alcohol was used to remove the xylol. After cleaning the segment, it was stained with hematoxylin for 3-4 minutes before being counterstained with 0.5 percent eosin for 15 to 30 seconds until the section became bright pink. Blotted and dehydrated in alcohol for 15 to 30 seconds before clearing with xylol. Keep the slide dry and free of air bubbles by mounting it on a Canada balsam or DPX mutant.

Determination of serum biochemical parameters

Hemoglobin content, WBC, RBC, and platelet counts were all measured in the blood samples. Various biochemical parameters such as SOD and catalase were measured in the serum collected after centrifugation of the collected blood. The

activity of superoxide dismutase (SOD) was determined by adding 0.5 mL of serum sample to 1.5 mL of carbonate buffer pH10.2, 0.5 mL of 0.1 Mm EDTA, and 0.4 mL of epinephrine to 1.5 mL of carbonate buffer pH10.2, and reading the OD at 480 nm. SOD activity was measured in units/min/mg protein. The amount of enzyme that decreases the rate of adrenaline autoxidation by 50% is defined as one unit of the enzyme. Catalase activity was determined spectrophotometrically by the method of Koroliuk et.al (22). Briefly 0.1mL of sample was incubated with 100 µmol/mL of H_2O_2 in 0.05 mmol/L Tris-HCl buffer (pH-7) for 10 minutes. The reaction was terminated by rapidly adding 0.5 mL of 4% ammonium molybdate. Yellow complex of ammonium molybdate and H_2O_2 was measured at 410nm. One unit of catalase activity was defined as the amount of enzyme required to decompose 1µmol H_2O_2/minute.

Results and Discussion

The presence of a miniscule amount of silver is usually non-hazardous (23). However, the toxicity of AgNPs has remained a source of debate due to the potential for harm when utilised in biological systems. For further successful use in future applications in biology and medicine, it is required to examine the *in vivo* effect of green synthesized AgNPs in animal models.

Histopathology of breast tissue

The segment of breast derived from normal mice showed no signs of cancer in the histology reports (Fig. 1a). Infiltrating neoplasm constituted of cells grouped in glands was found in tumor-induced mice with only DMBA treatment, as seen in the image. Individual cells were round to oval in shape, with somewhat eosinophilic cytoplasm and round oval vesicular nuclei, with nucleoli visible in some (Fig.1b). Neoplastic cell mass slightly replaced in plant crude treated mice (Fig.1c). AgNP-treated, DMBA-induced mice tissue slices from the breast exhibited a confined lesion with diffused hyperplasia of ducts (adenosis) separated by fibro collagenous stroma at low doses (15 mg/kg body weight). A cystic lesion constituted of disseminated neutrophil infiltration was discovered in DMBA mice sections treated with a high dose of CA-AgNPs (30 mg/kg body weight). Neoplastic cell mass replaced more than plant crude treated mice in CA-AgNPs treated mice (Fig.1d & Fig.1e). Tamoxifen-treated DMBA-induced mice breast tissue revealed a circumscribed lesion with areas of adenosis and fibrosis and mostly neoplastic mass are replaced with fibrous tissues. There was no evidence of malignancy (Fig. 1f). Congested arteries and fibro-collagenous tissue were visible in the stroma. There was no evidence of malignancy. The mice given 15 mg/kg b.w of CA-AgNPs had normal hepatic parenchyma, but the mice given 30 mg/kg b.w of CA-AgNPs had histological changes such as significant cell swelling and vacuolar degeneration. These histological changes, however, were not seen in mice following the washout period. The kidney, spleen, lungs, heart, testis, and brain did not show any histopathological changes after being treated with 15 and 30 mg/kg b.w of CA-AgNPs.

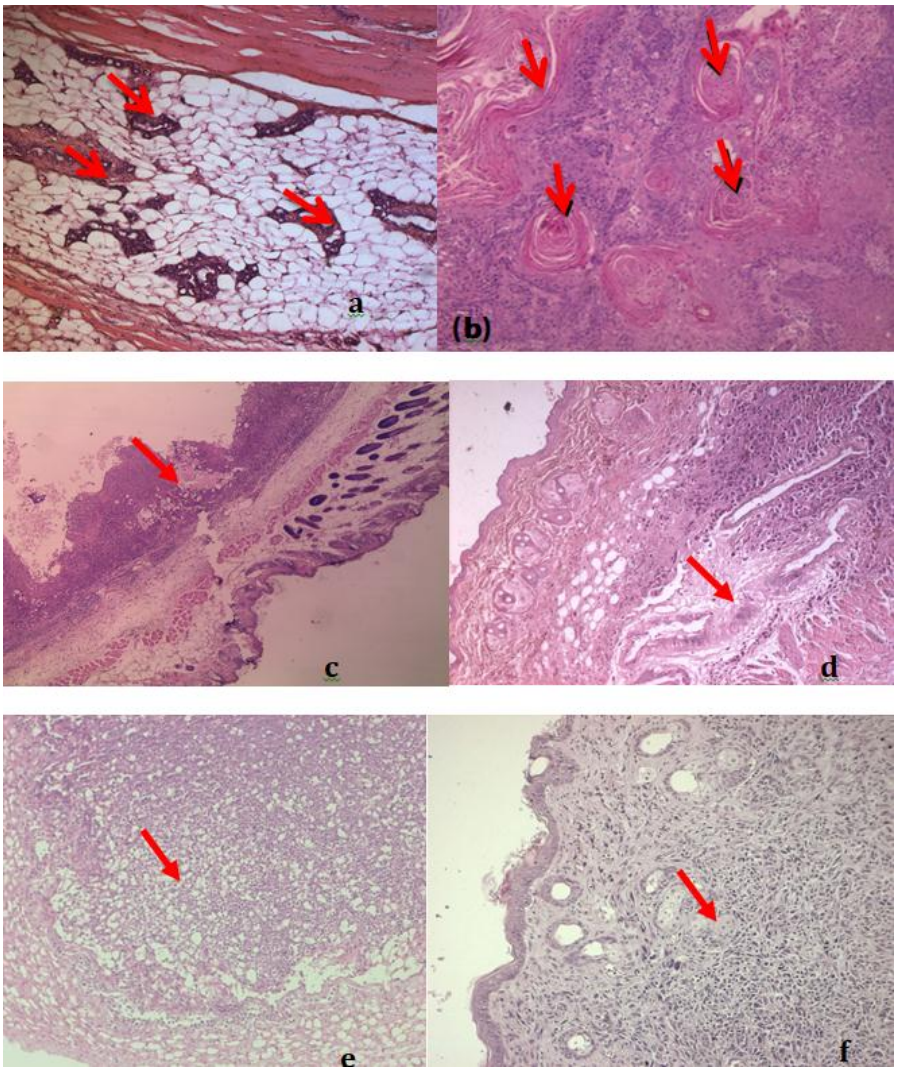

Figure 1: Morphology of mammary gland in sub-cutaneous region of skin
(1a) Morphology of mammary gland in normal control mice (Group-I) (x100). (1b) Large area of squamous metaplasia noticed in between tumor mass (Group-II) (x200). (1c) Neoplastic cell mass slightly replaced with fibrous tissue (Group-III) (x400). (1d & 1e) Neoplastic cell mass replaced with fibrous tissues in CA-AgNPs treated mice (Group- IV & V)(x 400 and x500), (1f) Neoplastic mass mostly replaced with fibrous tissues in tamoxifen treated mice (Group- VI)(x500).

Biochemical markers

Because oxidative stress is linked to cancer, antioxidant experiments were conducted *in vivo* on DMBA-induced mammary carcinoma in mice models. The enzymes listed below were investigated. In the event of cancer, the transport function of cell organelles, particularly hepatocytes, is disrupted, resulting in the release of enzymes and increased plasma membrane permeability. In tumor-induced mice, recent studies have found an increase in tumor volume. At various

time intervals and washout periods, anti-oxidant enzymes such as SOD and CAT were examined. In CA-AgNPs treated mice, serum antioxidant levels increased significantly in a time-dependent manner as compared to control group mice, but there was significant difference between the 15 and 30 mg/kg b.w treated group mice. In comparison to control mice, CA-AgNPs treated mice showed less significant changes in other biochemical parameters such as haemoglobin, RBC, WBC, and platelets, as well as anti-oxidant enzymes like SOD and catalase.

Effect of AgNPs on Catalase

When DMBA-induced mice were compared to normal mice, the catalase level was found to be 51.6 unit/mg lower. It appears that the decline is statistically significant. Catalase levels rose when DMBA-induced mice were given *Cyphostemma auriculatum* Roxb.,leaf extract (120 mg/kg b.w) and low and high dose of (15 and 30 mg/kg b.w) CA-AgNPs. When low and high dose (15 and 30 mg/kg b.w) CA-AgNPs were given, catalase levels increased in a concentration and time dependent manner and nearly equal to the results observed for standard drug Tamoxifen-treated DMBA mice. (Figure-2).

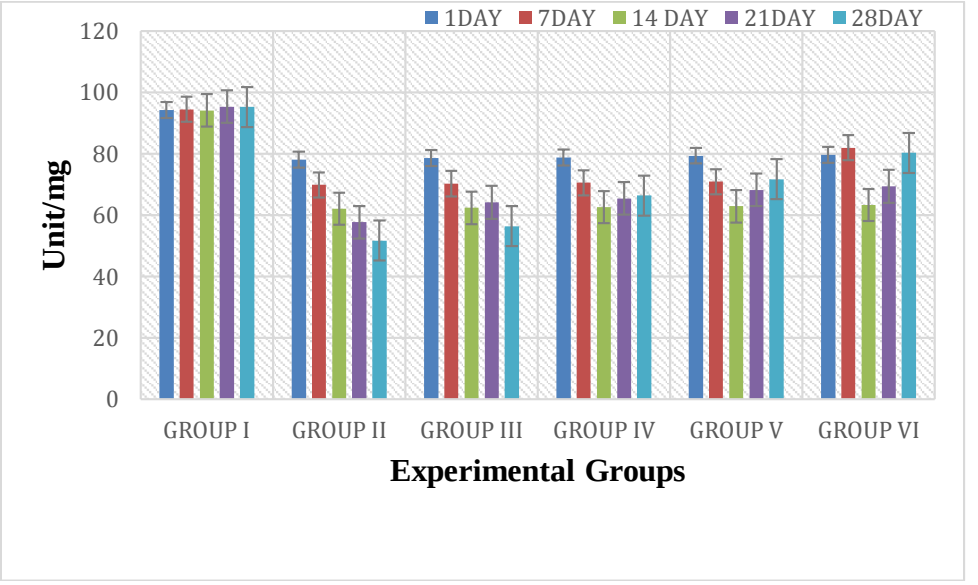

Figure 2: Effect of silver nanoparticles synthesized from *Cyphostemma auriculatum* Roxb. on Catalase

Effect of AgNPs on Superoxide dismutase

DMBA-induced mice had a 3.25 unit/mg lower SOD level than normal mice. It appears that the drop is statistically significant. SOD levels rose in DMBA-induced mice treated with *Cyphostemma auriculatum* leaf extract (120 mg/kg) and low and high dose of (15 and 30 mg/kg b.w) CA-AgNPs. When AgNPs of low and high doses (15 and 30 mg/kg b.w) were given, SOD levels increased in a concentration and time dependent manner, as seen in Fig.3 and nearly equal to the results observed for standard drug Tamoxifen-treated DMBA mice.

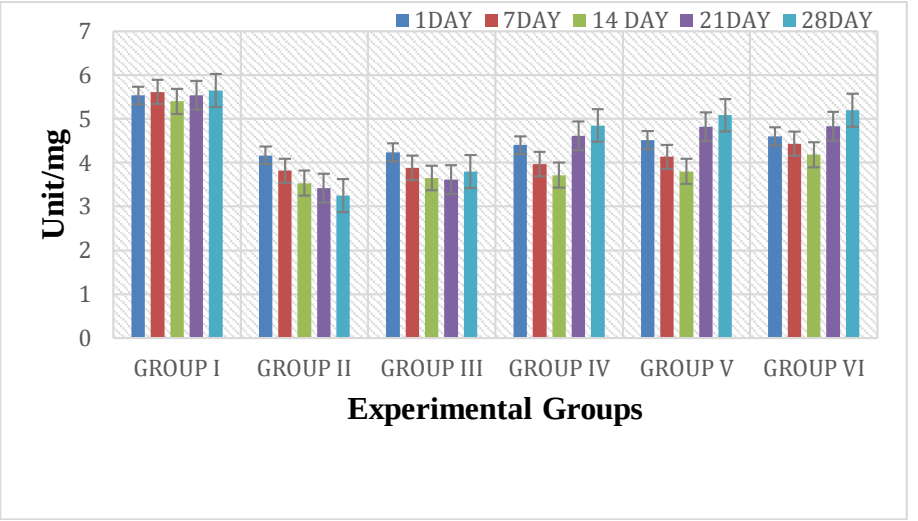

Figure 3: Effect of silver nanoparticles synthesized from *Cyphostemma auriculatum* Roxb. on SOD

In our study, group II (DMBA-induced mice) showed a significant decrease in antioxidant enzyme levels compared to group I (normal). Conversely, group III (plant extract 120 mg/kg treated mice), group IV (CA-AgNPs 15 mg/kg treated mice) and group V (CA-AgNPs 30 mg/kg), group VI (tamoxifen-treated DMBA-induced mice), showed a significant increase in the level of antioxidant enzymes levels compared to group II.

Hematological parameters

Glycation of proteins such as haemoglobin occurs when blood glucose levels are high (Gupta et al., 1997), resulting in the generation of reactive oxygen species (ROS), which leads to increased lipid peroxidation and cytotoxicity (Anwer et al., 2007). Hematological parameters of cancer patients are often substantially lower than usual. In the current investigation, a significant decrease in the Hemoglobin, RBC, and platelets level and a significant increase WBC level was observed in DMBA-induced mice, compared to normal mice. In CA-AgNPs treated DMBA-induced mice, an increase in Hemoglobin, RBC, and platelets levels were observed compared to DMBA-induced mice (Group-II). Significantly in CA-AgNPs treated DMBA-induced mice, a decrease in WBC levels compared to DMBA-induced mice (Group-II) were observed. The protective effect of CA-AgNPs is supported by these findings. By measuring blood Hemoglobin, RBC, WBC and platelets level, the impact of CA-AgNPs was determined. The results seem to be statistically significant. When DMBA-induced mice were treated with *Cyphostemma auriculatum* Roxb. leaf extract (120 mg/kg), the hemoglobin, RBC, and platelets levels increased and WBC levels decreased. When CA-AgNPs of low and high dose (15 and 30 mg/kg b.w) were administered a concentration and time dependent increase in Hemoglobin, RBC, and platelets levels and a decrease in WBC levels were observed as seen in Fig. 4,5,6 and 7.

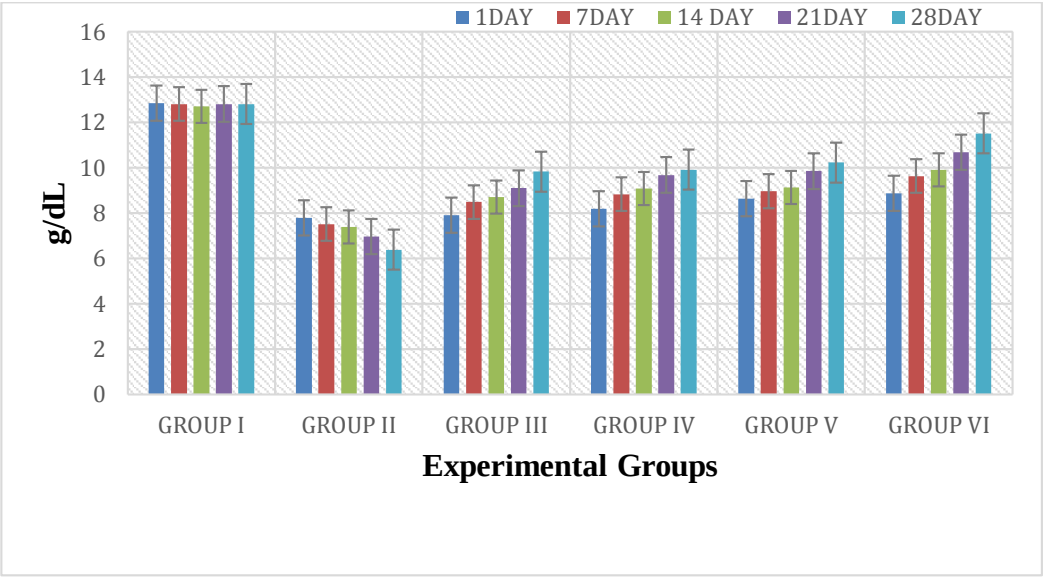

Figure 4: Effect of silver nanoparticles synthesized from *Cyphostemma auriculatum* Roxb. on Hemoglobin

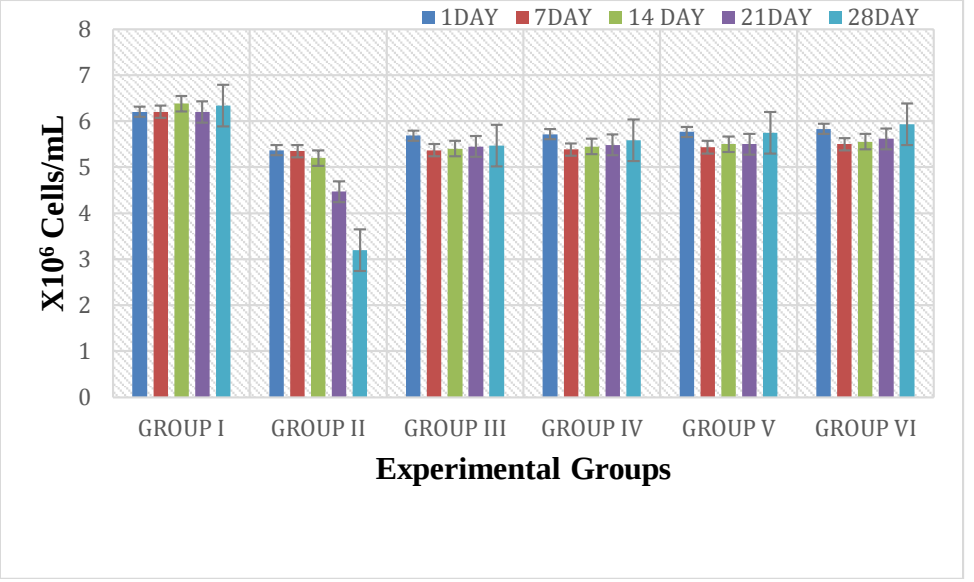

Figure 5: Effect of silver nanoparticles synthesized from *Cyphostemma auriculatum* Roxb. on RBC

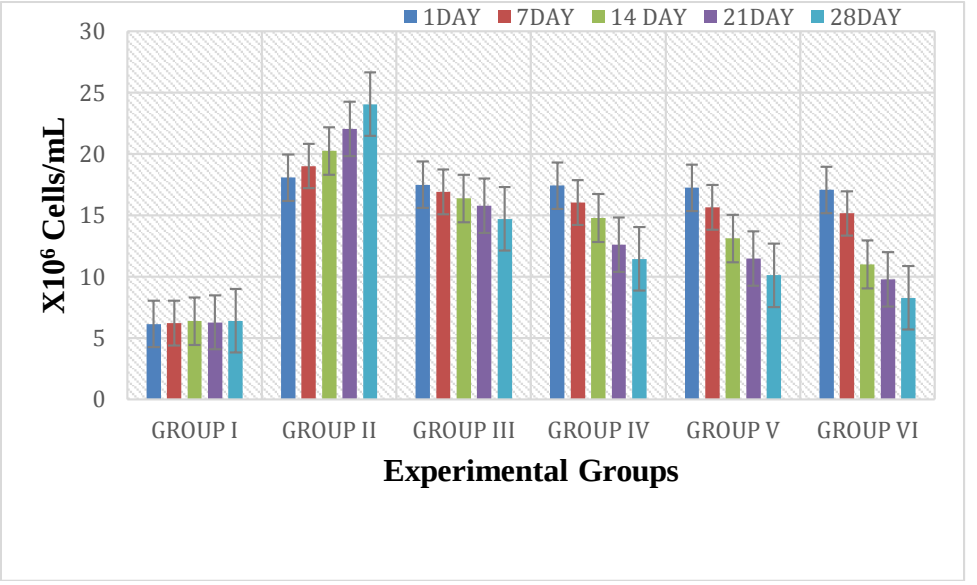

Figure 6: Effect of silver nanoparticles synthesized from *Cyphostemma auriculatum* Roxb. on WBC

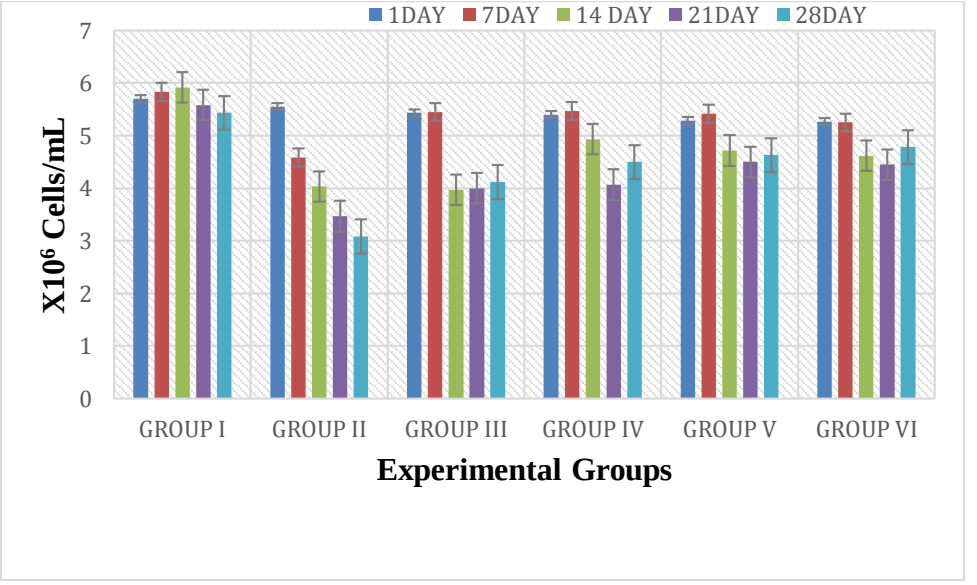

Figure 7: Effect of silver nanoparticles synthesized from *Cyphostemma auriculatum* Roxb. on Platelets

Conclusion

Finally, we were able to gain a better knowledge of the possible anticancer properties of green produced CA-AgNPs. The findings of our *in vivo* investigation confirm our belief that, if further investigated, this could lead to the development

of a novel therapeutic agent with medically and economically significant implications for saving the lives of troubled and oppressed people.

Acknowledgments

Authors are thankful to the central facility for research and development, Osmania University, Hyd and central analytical facility, University College of Technology, Osmania University, Hyd and Department of Zoology, Osmania University, Hyd and Department of Physics, Osmania university, Hyd and Department of Biochemistry, Osmania university, Hyd for providing facilities to carry out the research work.

Conflict of Interest

The authors declare no conflict of interest.

References

1. Labhasetwar, V., Leslie-Pelecky, D.L. 2007. *Biomedical applications of nanotechnology*. John Wiley & Sons.
2. Ibrahim Khan, Khalid Saeed, Idrees Khan, Nanoparticles: Properties, applications and toxicities, Arabian Journal of Chemistry, Volume 12, Issue 7, 2019, Pages 908-931, ISSN 1878-5352.
3. Loureiro, A., Azoia, N.G., Gomes, A.C., Cavaco-Paulo, A., 2016. Albumin-based nanodevices as drug carriers. Curr. Pharm. Des. 22, 1371–1390.
4. Martis, E., Badve, R., Degwekar, M., 2012. Nanotechnology based devices and applications in medicine: an overview. Chron. Young Sci. 3, 68.
5. Nikalje, A.P., 2015. Nanotechnology and its applications in medicine. Med Chem 5.
6. Zhuang, J., Gentry, R.W., 2011. Environmental application and risks of nanotechnology: a balanced view. pp. 41–67.
7. AshaRani, P.V., Low Kah Mun, G., Hande, M.P., Valiyaveettil, S., 2009. Cytotoxicity and genotoxicity of silver nanoparticles in human cells. ACS Nano 3, 279–290.
8. Ma, E., 2003. Nanocrystalline materials: controlling plastic instability. Nat. Mater. 2, 7–8.
9. Dong, H., Wen, B., Melnik, R., 2014. Relative importance of grain boundaries and size effects in thermal conductivity of nanocrystalline materials. Sci. Rep. 4, 7037.
10. Todescato, F., Fortunati, I., Minotto, A., Signorini, R., Jasieniak, J., Bozio, R., 2016. Engineering of semiconductor nanocrystals for light emitting applications. Materials 9, 672.
11. Weiss, J., Takhistov, P., McClements, D.J., 2006. Functional materials in food nanotechnology. J. Food Sci. 71, R107–R116.
12. Ripp, S., Henry, T.B. (Eds.), 2011. Biotechnology and Nanotechnology Risk Assessment: Minding and Managing the Potential Threats around Us, ACS Symposium Series. American Chemical Society, Washington, DC, DC.
13. Zhuang, J., Gentry, R.W., 2011. Environmental application and risks of nanotechnology: a balanced view. pp. 41–67.

14. Kosmala, A., Wright, R., Zhang, Q., Kirby, P., 2011. Synthesis of silver nano particles and fabrication of aqueous Ag inks for inkjet printing. Mater. Chem. Phys. 129, 1075–1080.
15. Alés-Martínez JE, Ruiz A, Chacón JI, Lluch HA, Ramos M, Córdoba O, Aguirre E et al (2015) Preventive treatments for breast cancer: recent developments. Clin Transl Oncol 17:257.
16. Benoni G, Cuzzolin L (2009) Safety and efficacy of phytomedicines in cancer prevention and treatment. In: Ramawat K (ed) Herbal Drugs: Ethnomedicine to Modern Medicine. Springer, Berlin, Heidelberg, pp 207–220.
17. Gandhi AK, Kumar P, Bhandari M, Devnani B, Rath GK (2017) The burden of preventable cancers in India: time to strike the cancer epidemic. J Egypt Natl Canc Inst. 29:11–18.
18. Schneider AP, Zainer CM, Kubat CK, Mullen NK, Windisch AK (2014) The breast cancer epidemic: 10 facts. The Linacre Quarterly. 81(3):244–277.
19. Haldosén L, Zhao C, Dahlman-Wright K (2014) Estrogen receptor beta in breast cancer. Molecular and Cellular Endocrinology. 382:665–672.
20. Trias Blasi, Anna & Chayamarit, Kongkanda & Parnell, J.. (2015). Cyphostemma auriculatum (Roxb.) P. Singh & B. V. Shetty (Vitaceae): typification and a new generic record confirmed for Thailand. Kew Bulletin. 70. 1-7.
21. Kishore Mendam, S.Jithender Kumar Naik, Anusha C Pawar, S.Vamshi, V.Mangesh,P.Sonu. Synthesis and Characterization of Silver Nanoparticle from *Cyphostemma auriculatum* Roxb.: Its application as antibacterial activity and mode of action. Nat.volatiles & Essent.Oils, 2021; 8(6): 3369-3383.
22. M.A. Koroliuk, L. I. Ivanova, I.G. Maiorova et al., “A method of determining catalase activity”, Laboratornoe Delo, vol.1988, no.1, pp.16-19, 1988.
23. M.A.M. Khan, S. Kumar, M. Ahamed, S.A. Alrokayan, M.S. AlSalhi, Structural and thermal studies of silver nanoparticles and electrical transport study of their thin films, Nanoscale Res. Lett. 6 (2011) 434.

(12) PATENT APPLICATION PUBLICATION
(19) INDIA
(22) Date of filing of Application :09/03/2022

(21) Application No.202241012796 A
(43) Publication Date : 25/03/2022

(54) Title of the invention : A processing herbal medicine and composition from medicinal plants for external skin applications and preparation method thereof

(51) International classification :A61K0036185000, A61K0008970000, A61K0009000000, A61K0036610000, A61Q0019000000
(86) International Application No :PCT//
Filing Date :01/01/1900
(87) International Publication No : NA
(61) Patent of Addition to Application Number :NA
Filing Date :NA
(62) Divisional to Application Number :NA
Filing Date :NA

(71)**Name of Applicant :**
1)Mr. Kishore Mendam
Address of Applicant :Assistant Professor (C), Department of Zoology, Dr. B.R. Ambedkar Open University, Jubilee hills, Hyderabad, Telangana, India, Pincode: 500033 ---------- ----------
2)Dr. Gajula Prabhakar
3)Mr. Yerkala Kumar
4)Dr. S. Jithender Kumar Naik
Name of Applicant : NA
Address of Applicant : NA
(72)**Name of Inventor :**
1)Mr. Kishore Mendam
Address of Applicant :Assistant Professor (C), Department of Zoology, Dr. B.R. Ambedkar Open University, Jubilee hills, Hyderabad, Telangana, India, Pincode: 500033 ---------- ----------
2)Dr. Gajula Prabhakar
Address of Applicant :Assistant professor (P), Department of Botany, University College for Women, Koti, Hyderabad, Telangana, India, Pincode:500 095 ---------- ----------
3)Mr. Yerkala Kumar
Address of Applicant :Assistant Professor (C), Department of Botany, Dr. B.R. Ambedkar Open University, Jubilee hills, Hyderabad, Telangana, India, Pincode: 500033 ---------- ----------
4)Dr. S. Jithender Kumar Naik
Address of Applicant :Professor, Toxicology Lab, Department of Zoology, Osmania University, Hyderabad, Telangana, India, Pincode: 500007 ---------- ----------

(57) Abstract :
[27] The present invention discloses a processing herbal medicine and 5 composition from medicinal plant for external skin applications and preparation method thereof. The method for preparing the composition includes, but is not limited to, a combination of a water extract of an aerial part of Rhodomyrtus tomentosa; a water extract of an aerial part of Cipadessa baccifera; a methanol extract of a fruit of Woodfordia fruticose;.(10 Leaves of Cyphostemma auriculatum and Capparis divarcata) a water extract of a tender shoot of Camellia sinensis as an antioxidant; and cosmeceutically acceptable carriers. Further, the composition further comprising beeswax, stearic acid, glycerol monostearate, olive oil, Aloe vera gel, rose water, glycerine, triethanolamine, propylene glycol, geranium oil, 15 sandalwood oil, vetiver oil, methyl paraben and propyl paraben in amounts of 4.4-5%; 3.5-4%; 6.5-7%; 20-25%; 11-12%; 20-25% 14-18% 1.5-2%; 6-8%; 0.5-1%; 0.5-1%; 0.5-1%; 0.15-0.2% and 0.15-0.2% respectively, wherein the said constituents are expressed in terms of weight %.

No. of Pages : 20 No. of Claims : 8

Biomass Conversion and Biorefinery
https://doi.org/10.1007/s13399-022-02868-5

ORIGINAL ARTICLE

Bioethanol production from alkali-pretreated cassava stem waste via consolidated bioprocessing by ethanol-tolerant *Clostridium thermocellum* ATCC 31,924

Narendra Kumar Papathoti[1] · Kishore Mendam[2] · Wannaporn Thepbandit[1] · Niharika Burgula[3] · Rungthip Sangpueak[1] · Chanon Saengchan[1] · Nguyen Huy Hoang[1] · Praveen Kumar Keshav[3] · Toan Le Thanh[4] · Natthiya Buensanteai[1]

Received: 26 February 2022 / Revised: 7 May 2022 / Accepted: 24 May 2022

Abstract

Clostridium thermocellum is a thermophilic, obligately anaerobic bacterium and an ideal candidate for bioconversion of cellulosic biomass into ethanol through consolidated bioprocessing. Ethanol tolerance is one of the important parameters concerning process economics. Consolidated bioprocessing (CBP) using *C. thermocellum* provides single-step direct microbial conversion for large-scale bioethanol production. In this study, CBP of cassava stem waste was explored for bioethanol production using *C. thermocellum* ATCC 31,924. Initially, cassava stem waste was pretreated with dilute alkali (1–3% w/v NaOH; 120 °C; 30–60 min), which led to a maximum of 71.50 ± 1.04% lignin removal with 67.22 ± 0.80% holocellulose recovery. Furthermore, to improve the ethanol tolerance of *C. thermocellum*, chemical mutagenesis followed by adaptive laboratory evolution (ALE) was carried out for 120 days. After the ALE period, ethanol tolerance of *C. thermocellum* (ALE mutant) was improved from 3% (v/v) to a maximum of 5%. Finally, ALE mutant *C. thermocellum* was investigated for bioethanol production via CBP using a mixture of cellobioses, xylose sugars, and alkali-treated cassava stem residue. It was found that fermentation of 6.12 ± 0.18 g/L sugars by ALE mutant of *C. thermocellum* produced 1.35 ± 0.02 g/L bioethanol with 49.30% fermentation efficiency. Meanwhile, CBP fermentation of cassava stem hydrolysate with ALE mutant of *C. thermocellum* produced 7.84 ± 0.31 g/L bioethanol with 62.37 ± 0.25% cellulose conversion efficiency.

Keywords Adaptive laboratory evolution · Bioethanol · Cassava stem waste · *Clostridium thermocellum* · Consolidated bioprocessing · Fermentation

1 Introduction

The increased usage of non-renewable energy sources such as fossil fuels along with climate change caused by increased levels of greenhouse gasses in the atmosphere has drawn the attention of the scientific community to developing alternative, eco-friendly, sustainable, and renewable energy sources [1, 2]. Lignocelluloses from plant biomass are widely accessible, which is an inexpensive, renewable carbon source. Lignocellulosic feedstocks such as agricultural residues (rice straw, wheat straw, corn straw, sugarcane bagasse), forest residues, and dedicated energy crops are mainly composed of carbohydrate polymers (cellulose and hemicellulose), and lignin [2, 3]. These lignocellulosic feedstocks are considered potential energy sources and play an important role in shifting from a petroleum-based economy to a biobased economy [4].

The polysaccharide fraction of plant biomass is the most widely considered substrate for biochemical conversion to organic acids and biofuels such as bioethanol [2]. Generally, biofuels produced from microbes using renewable biomass not only decrease the dependence on fossil fuels but also mitigate climate change by reducing harmful emissions

✉ Natthiya Buensanteai
natthiya@sut.ac.th

[1] School of Crop Production Technology, Institute of Agricultural Technology, Suranaree University of Technology, Nakhon Ratchasima 30000, Thailand

[2] Department of Zoology, Dr. B.R. Ambedkar, Open University, Hyderabad, Telangana, India

[3] R&D Division, Sri Yuva Biotech Pvt Ltd, Hyderabad, Telangana, India

[4] Department of Plant Protection, Can Tho University, Can Tho City 900000, Vietnam

Published online: 31 May 2022

released by motor vehicles [5]. Bioethanol produced from lignocelluloses can potentially replace petrol-based fuels. The advantages of using bioethanol as renewable biofuel include its flexibility for existing engines, higher octane number, and higher heat of vaporization as compared to gasoline. Finally, bioethanol-blended gasoline in motor vehicles can considerably reduce greenhouse gas emissions [2, 6]. Moreover, bioethanol can be a potential alternative to phasing-out MTBE (methyl tert-butyl ether) by mixing ethanol with gasoline E5 or E10 blends [7].

Cassava (*Manihot esculenta*) crop is a perennial shrub, most widely cultivated in Asian countries especially South and Southeast Asian countries such as India and Thailand, respectively [8]. Worldwide cassava production accounts for 268.28 MT (million tonnes), grown with an area of 23.867 million ha. While India produces 8.14 MT of cassava with an area of 0.228 million ha [9]. During the farming and processing of the cassava crop, a large number of waste residues such as cassava stem and peels are generated which hardly find any alternative applications [8, 10]. The cassava stem is mainly composed of lignocellulose, which could act as a low-cost feedstock for biochemical conversion to value-added bioproducts [9].

The conventional biochemical platform for bioethanol production involves four different steps such as pretreatment of biomass, saccharification, fermentation, product recovery, and purification [11, 12]. During bioethanol production, pretreatment plays an essential and most expensive processing step that facilitates the release of fermentable sugars from biomass. An effective pretreatment method should (i) act on all lignocellulosic feedstocks, (ii) improve sugar yields for the fermentation process, (iii) release the minimum amount of inhibitors, (iv) reduce energy and operation costs, and (v) regenerate value-added lignin co-products [13]. Among various chemical pretreatment methods, dilute alkaline pretreatment (DAP) is the most extensively studied method for various agricultural residues. The dilute alkali pretreatment method is known to eliminate the maximum amount of lignin from biomass and also reduces the crystallinity of cellulose with enhanced biomass porosity [2].

One potential approach to minimize the number of processing steps and improve productivity is consolidated bioprocessing (CBP), which integrates all biochemical steps into a single bioconversion stage [14, 15]. CBP integrates on-site saccharification of holocellulose and subsequent fermentation of the hexose and pentose sugars into a single step process carried out either by a single microbial strain or consortia without the usage of commercial cellulolytic enzymes [16]. The major applications of CBP include reducing the feedback inhibition of cellulases by sugars, decreasing the number of unit operations, and the overall process economics [14, 17]. Generally, thermophilic, obligate anaerobic microbial strains are potential candidates for CBP bioethanol production from lignocellulose owing to their higher rate of hydrolysis of sugar polymers [14, 16]. Microbial contamination is a major issue in industrial fermentation processes, and the usage of high temperatures can solve this problem. Furthermore, compared to mesophilic temperatures, the higher temperature conditions facilitate lower solubility of gas, which further maintains the anaerobic environment [14, 18]. Among the thermophilic anaerobes, *C. thermocellum* is the most widely studied ethanologenic, which efficiently depolymerizes lignocellulosic biomass as compared to other microbial strains. *C. thermocellum* efficiently depolymerizes lignocelluloses by the synergistic action of the multienzyme complex known as cellulosome, which is attached to the external cell wall of the bacteria [16, 19]. *C. thermocellum* has considerable biotechnological interest due to its innate ability to saccharify celluloses and produce cellodextrins into various organic products such as ethanol, acetate, lactic acid, formic acid, and CO_2 [14]. Furthermore, *C. thermocellum* is a potential candidate for CBP, but its application has been restricted by lower ethanol tolerance and lower bioethanol yields, which are potential targets for strain improvement strategies [17, 20].

Adaptive laboratory evolution (ALE) is a powerful microbial technique, where a specific microbial strain is cultivated under predefined conditions for a particular time ranging from weeks to months, which permits the selection of an improved phenotype [21]. Therefore, ALE could be an invaluable tool for strain improvement in the metabolic engineering field. The major applications of ALE include optimization of microbial growth rate, increasing tolerance to toxic metabolites, improving the substrate uptake rate, and improving titer and yield [22]. Wild-type *C. thermocellum* is unable to grow when inoculated into a medium containing 20 g/L ethanol concentration. However, improved strains of *C. thermocellum* can grow up to a medium containing ≥ 50 g/L ethanol, which can be obtained by repeated serial transfer in the medium containing increasing concentrations of ethanol. The highest reported ethanol concentration produced by *C. thermocellum* is 27 g/L, which is lower as compared to desired levels of 40 g/L for commercial application [14, 23]. In *C. thermocellum*, the mechanism of ethanol tolerance has been ascribed to both modifications in properties of the membrane, and metabolic enzymes, specifically, the bifunctional alcohol dehydrogenase/acetaldehyde-CoA gene (*adhE*) [23].

The major objective of the present study was to evaluate bioethanol production from cassava stem waste via consolidated bioprocessing using *C. thermocellum* ATCC 31,924. In this study, the diluted NaOH pretreatment method was developed to enrich the holocellulose fraction of biomass for the subsequent fermentation process. Furthermore, the ALE technique was implemented to generate ethanol-tolerant *C. thermocellum* strain to improve its fitness as ethanologenic.

After ALE experiments, growth behavior patterns were studied under different ethanol concentrations, and, subsequently, the efficiency of bioethanol fermentation was compared between wild-type and ALE mutant. To the best of our knowledge, this is the first study on bioethanol production via CBP from alkali-treated cassava stem residue using ethanol-tolerant *C. thermocellum*.

2 Material and methods

2.1 Feedstock collection and processing

The feedstock material cassava stem waste was uniformly collected from the agricultural fields of Namakkal district of Tamil Nadu State, India (11°15′46.8″ N, 78°14′36.9″ E). Before processing, the substrate was chopped into medium pieces, water-washed, and subsequently dried at room temperature. After drying (moisture content < 10%), the cassava stem pieces were pulverized into fine particles in a laboratory grinder (Cello Mixer Grinder 1100 W, India), sieved through 250 µm mesh size, and then used for subsequent pretreatment studies. The raw and pretreated biomass samples were analyzed for cellulose, hemicellulose, and lignin by using standard laboratory methods [24]. All the media components and chemicals were purchased from Sigma Aldrich, Hi Media, and Merck (Mumbai, India).

2.2 Dilute alkaline pretreatment of cassava stem waste

The pulverized cassava stem waste (10 g dry weight) was subjected to dilute alkaline pretreatment (1%, 2%, and 3% (w/v) NaOH) using an initial 10% (w/v) solid loading and incubated in the water bath at 120 °C for 30–60 min under agitation. The pretreated biomass residue was washed with distilled water until neutral pH and dried in a hot air oven until constant weight is gained. Subsequently, alkali delignified biomass was used to estimate the dry weight percentages of cellulose, hemicellulose, and lignin.

2.3 Microorganism and growth medium

Clostridium thermocellum strain ATCC 31,924 was obtained from the American Type Culture Collection (Manassas, Virginia, USA). The bacterial strain was cultured and maintained in an anaerobic chamber (10% CO_2, 5%H_2, and 85% N_2) using a modified CTFuD medium as described by Lin et al. [25], in sealed serum bottles at 60 °C of incubation. The CTFuD medium contains (g/L) cellobiose 5, yeast extract 4.5, sodium citrate tribasic dehydrate 3, $(NH_4)_2SO_4$ 1.3, KH_2PO_4 1.43, K_2HPO_4 1.37, cysteine- HCl 0.5, MOPS (morpholinopropane sulfonic acid) 20, glycerol-2-phosphate disodium 6, $CaCl_2$ 0.01, $MgCl_2$ 0.011, $FeSO_{4\cdot 7}H_2O$ 0.0006, thiamine 0.01, and resazurin 0.001. Pure cultures were stored as glycerol stocks (30% v/v glycerol) at − 80 °C and revived before each experiment. For the preparation of seed culture, *C. thermocellum* was successively cultured over 4 generations with shaking at 150 rpm at 60 °C for 48 h incubation time and subsequently used as the inoculum for fermentation experiments with 5% v/v (OD_{600} ~0.7–1.00) inoculum size.

2.4 Determination of optimum temperature and ethanol tolerance of *C. thermocellum*

Optimum cell growth and bioethanol fermentation efficiency of *C. thermocellum* were determined at different growth temperatures (50, 55, 60, 65, and 70 °C) using a CTFuD medium containing 5 g/L cellobiose and xylose as carbon source with 5% (v/v) inoculum and incubated for 72 h time. Meanwhile, ethanol tolerance of *C. thermocellum* was also studied at different ethanol concentrations ranging from 1 to 6% (v/v). The inoculated serum bottles were incubated at the optimized growth conditions for 72 h time. Samples were withdrawn at regular intervals, centrifuged at 10,000 *g* for 10 min, and subsequently analyzed for cell growth (OD_{600}). For determination of optimum temperature, ethanol, acetate, and residual sugars were analyzed.

2.5 Chemical mutagenesis

To improve the genetic diversity of starting population of *C. thermocellum* and its subsequent application in ALE experiments, the chemical mutagen ethyl methanesulfonate (EMS) was employed. Chemical mutagenesis was conducted as previously described by Chen and Xu [26]. Initially, the wild-type strain of *C. thermocellum* ATCC 31,924 was grown in a CTFuD medium at 60 °C for 24 h; the pellet was harvested by centrifugation at 5000 × g and then washed with buffer (0.1 M sodium phosphate; pH 7.0). Furthermore, 75 µL of EMS was added to 5 mL of the bacterial suspension (OD_{600} ~ 0.8) and incubated at 60 °C for 60 min. Subsequently, the mutagenesis reaction was hindered by adding 15 mL of 5% (w/v) $Na_2S_2O_3.5H_2O$ (sodium thiosulphate). The mutagenized bacterial cells were recovered by centrifugation and washed again with 5% sodium thiosulphate and then resuspended in sterile saline solution. The mutagenized bacterial suspension was again cultured in a CTFuD medium for 24 h at 60 °C and then subsequently used as the starter culture for the ALE experiments.

2.6 Adaptive laboratory of evolution

The ALE experiments involve serial batch culture propagation of chemically mutagenized *C. thermocellum* strain. ALE experiments were carried out in anaerobic serum bottles (125 mL) with a working volume of 50 mL CTFuD medium containing 3 g/L cellobiose at 120 rpm and 60 °C. For ALE, a total of 120 serial subcultures were performed using a CTFuD medium with a gap of every 24 h. Initially, the CTFuD medium was diluted after achieving the stationary phase, and then 3 g/L cellobiose, 1 g/L yeast extract, and 3% (v/v) ethanol were supplied to the CTFuD medium. For every 30 serial subcultures, the amount of yeast extract was progressively reduced with a gradual increase of 0.5% (v/v) up to 5% (v/v) final ethanol concentration in the culture medium. For every 30th serial subculture, the selection of ethanol tolerant strain was performed on a CTFuD medium containing a high concentration of ethanol (3 to 5% ethanol), and the bacterial strains that formed large-sized colonies are assumed as ethanol-tolerant strains. Later, the ethanol-tolerant strains were stored at a culture medium containing 50% (v/v) glycerol at − 80 °C. In this study, during the entire progress of adaptive evolution, OD_{600} was assessed to record the status of cell growth. The wild-type *C. thermocellum* strain before the ALE period is termed CT0d, and the 120th-day evolved *C. thermocellum* population is called CT120d.

2.7 Bioethanol production via consolidated bioprocessing

Bioethanol production via CBP was compared between wild-type and laboratory evolved ethanol-tolerant strains of *C. thermocellum*. Initially, small-scale fermentation was conducted in 125 mL anaerobic serum bottles containing 70 mL CTFuD medium supplemented with 5.50 ± 0.50 g/L of cellobiose and xylose as carbon source. Fermentation bottles were filled with CTFuD medium without temperature-sensitive growth supplements and autoclaved at 121 °C for 20 min. After autoclaving and cooling the media, sterile growth supplements were added to the CTFuD medium. Subsequently, 5% (v/v) inoculum of wild-type and ALE mutants of *C. thermocellum* was anaerobically transferred to fermentation bottles. Fermentation was carried out at 60 °C at 125 rpm orbital shaking condition for 84 h. Samples were anaerobically withdrawn at regular intervals from the fermentation medium and centrifuged at 10,000 *g*. Subsequently, cell-free supernatant was analyzed for cell growth (OD_{600}), residual sugars, ethanol, and acetic acid metabolites.

To study bioethanol production via CBP from alkali-treated cassava stem residue, a bioreactor with a 2-L working volume was employed using ALE mutant (CT120d) of *C. thermocellum* strain. The alkali-treated cassava stem waste used as carbon is composed of 52.17% cellulose, 15.05% hemicellulose, and 6.05% lignin fractions. One hundred grams of the alkali-treated residue of cassava stem was used as the carbon source in 2 L of CTFuD medium at pH 7.0. The fermentation was carried out in a 3-L anaerobic, sterile, and controlled bioreactor at 60 °C and 150 rpm for 84 h time. Before fermentation, the bioreactor was autoclaved at 121 °C for 20 min to retain a sterile environment. After 12 h time, 10% (v/v) inoculum of ethanol-tolerant *C. thermocellum* was anaerobically transferred into a medium containing bioreactor. Furthermore, nitrogen was continuously fed into the bioreactor for 5 min at the beginning of the fermentation to deplete other gasses. The pH value was regularly examined by an online monitoring system. Samples were anaerobically collected at regular interval times from the bioreactor, and cell-free supernatant was separated by centrifugation and subsequently analyzed for cell growth (OD_{600}), ethanol, and acetate levels.

Fermentation efficiency (%) was calculated using the following equation:

$$Fermentation\ efficiency(\%) = \frac{Actual\ ethanol\ yield\ (g/L)}{Theoretical\ ethanol\ yield(g/L} \times 100\%$$

For fermentation via CBP, the bioconversion of celluloses to bioethanol was evaluated using equation:

$$Cellulose\ conversion\ to\ ethanol\ (\%) = \frac{[EtOH]}{Biomass\ x\ f\ x1.11\ x\ 0.51} \times\ 100$$

where *[EtOH]* is the concentration of ethanol concentration at the end of the fermentation (g/L); *Biomass* represents a concentration of dry pretreated biomass at the starting of the fermentation (g/L); *f* is the cellulose content of pretreated biomass (g/g); *0.51* indicates conversion factor for glucose to ethanol based on yeast stoichiometric biochemistry; and *1.11* represents the conversion of cellulose to equivalent glucose.

2.8 Analytical methods

2.8.1 Chemical compositional analysis of cassava stem waste

The content of structural carbohydrates (cellulose, hemicellulose) and lignin of cassava stem waste before and after pretreatment was analyzed by using National Renewable Energy Laboratory (NREL) procedures [24]. According to protocol, for lignin determination, 0.3 g of extractive free raw samples or pretreated samples was hydrolyzed with

3 mL of 72% H_2SO_4 in a water bath (30 °C) and incubated for 1 h. During incubation, the samples were stirred every 5 min without removing the sample from the bath. After hydrolysis, the concentration of the acid solution was diluted to 4% by adding 84 mL of deionized water and subsequently autoclaved at 121 °C for 50 min. Later, acid-insoluble lignin (AIL) was estimated by weighting the collected fraction after vacuum filtration of autoclaved hydrolysis solution. Meanwhile, acid-soluble lignin (ASL) was determined using UV-spectrophotometer (Systronics, India) at 205 nm by using diluted aliquots of the hydrolysis liquor. The monomeric and oligosaccharide fractions of carbohydrates (cellulose, hemicellulose) were estimated through HPLC (Shimadzu, Japan). The concentration of oligosaccharides in the liquid fractions obtained after pretreatment was analyzed after hydrolysis with H_2SO_4 (4% v/v) at 121 °C for 1 h. The oligosaccharide concentration was estimated based on the content of monosaccharides in a liquid fraction before and post-hydrolysis process using the HPLC method. While total reducing sugars in fermentation media were measured by the protocol as described by Miller [27].

2.8.2 Determination of cellobiose, glucose, xylose sugars, and acetate

The amount of soluble sugars such as cellobiose, glucose, xyloses, and acetate was estimated by using HPLC (Shimadzu, Japan), equipped with an Aminex HPX-87H column (Bio-Rad, USA) containing RID (refractive index detector) and a UV detector, according to the protocol as previously described by Singh et al. [28].

2.8.3 Estimation of ethanol by gas chromatography

The concentration of bioethanol in fermentation media was determined by gas chromatography (Shimadzu, Japan) with a ZB-Wax column containing a flame ionization detector (FID) at 250 °C. The temperature of the column was maintained at 150 °C (isothermal) with an injector temperature of 175 °C and nitrogen was used as a carrier gas (16 kPa), while the flow rate was set at 40 mL/min with the spilt ratio of 1/50, and the velocity of H_2 flow was set at 60 mL/min.

2.8.4 Determination of bacterial growth

The cell growth was evaluated by measuring optical density at 600 nm (OD_{600}) using a UV–visible spectrophotometer (Systronics, India). Meanwhile, the specific growth rate was determined by the protocol as previously described by da Silveira et al. [29].

2.8.5 Data analysis

All the experiments were carried out in triplicate, and mean and standard deviation (SD) values were calculated. The standard error values have been indicated as Y-error bars in graphical figures, and the probability values ($p \leq 0.05$) were observed as a statistically significant difference. Statistical analysis was performed by *t*-test, while posthoc comparisons were carried out by Tukey's multiple comparison method using the statistical software Sigma Plot version 12.5 (USA).

3 Results and discussion

3.1 Chemical composition of raw and pretreated cassava stem waste

The selection of a feedstock and its effective utilization are the crucial steps in developing cost-effective bioconversion processes. In the present study, an inexpensive raw material, cassava stem waste, rich in lignocellulose was evaluated. The raw substrate cassava stem used in the present study contains a high fraction of polysaccharides in the cell wall (52.50% by dry weight), suggesting an ideal raw material for bioethanol production. The raw material (cassava stem waste) used in the present study contained 32.40 ± 0.65% cellulose, 20.10 ± 0.40% hemicellulose, 14.56 ± 0.20% lignin, 7.15 ± 0.10% ash, and 1.05 ± 0.05% extractives. The total holocellulose content (52.50%) of cassava stem obtained in the present study varies from the previous study conducted by Kamalini et al. [30], who reported 68.57% of holocellulose in cassava stem with 36.27% cellulose, 32.30% hemicellulose, and 19.33% lignin contents. Meanwhile, the chemical composition of cassava stem reported by Kouteu et al. [31] showed cellulose (28.86%), hemicellulose (21.12%), and lignin (30.62%). The changes in the lignocellulose composition of cassava stem from different studies could be due to the geographical location of feedstock, season, feedstock heterogeneity, harvesting, processing methods, and the analytical procedures employed for the chemical composition of biomass [9, 32]. The holocellulose content of cassava stem can be compared with other widely studied lignocellulosic feedstocks such as wheat straw (54%), switchgrass (52.9%), corn stover (58.29%), sorghum straw (61%), and sugarcane bagasse (67.15%) [33].

Dilute NaOH pretreatment is the most frequently employed method for delignification of any lignocellulosic material. In the present study, dilute NaOH pretreatment of milled cassava stem was carried out to remove maximum lignin from biomass. The lignin-removed biomass was subsequently used as the carbon source for CBP bioethanol production. The pretreatment was also aimed to improve the holocellulosic fraction (celluloses and hemicelluloses)

of biomass to attain maximum sugars for subsequent fermentation steps. Dilute NaOH pretreatment of cassava stem was carried out at different NaOH concentrations ranging from 1 to 3% (w/v) at 120 °C for 30–60 min residence time. Table 1 shows various solid recoveries (solids remained after pretreatment divided by the original oven-dried weight of biomass) and the chemical composition of alkali-treated cassava stem residues under different pretreatment conditions. The percentages of biomass recovery after different alkaline pretreatments were ranged between 68.42 ± 2.42% (3% NaOH; 120 °C for 60 min) and 81.23 ± 2.05% (1% NaOH; 120 °C for 30 min) (Table 1). A similar observation of the reduction in biomass solid recoveries after pretreatment was also observed by Keshav et al. [32], who carried out the steam explosion of cotton under different pretreatment conditions and reported a decrease in solid recoveries from 76.80% to 58.14%.

In the current study, as compared to raw cassava stem waste composition, a significant increase (*t*-test, $n = 3$, $p \leq 0.05$) in cellulose content was observed under all pretreatment conditions. The cellulose fraction of pretreated residue was ranged between 38.84 ± 1.05% (1% NaOH; 120 °C for 30 min) and 55.40 ± 0.50% (3% NaOH; 120 °C for 60 min). The increase in cellulose content under all pretreatment conditions was attributed to the significant ($p < 0.05$) removal of lignin and hemicellulosic fractions from pretreated cassava residue. Furthermore, it was also observed that the hemicellulosic fraction of biomass was significantly ($p \leq 0.05$) reduced between 12.84 ± 0.70% (3% NaOH; 120 °C for 60 min) and 18.32 ± 0.85% (1% NaOH; 120 °C for 30 min). Finally, regarding the lignin content of biomass, a significant decrease ($p \leq 0.05$; $n = 3$; *t*-test) in lignin fraction was observed at all tested pretreatment conditions. The lignin content of pretreated cassava stem residue ranged from 4.15 ± 0.58 to 11.05 ± 0.45%. It was also found that a maximum of 71.50 ± 1.04% lignin removal was achieved at 3% NaOH at 120 °C for 60 min. Finally, as a result of higher lignin removal and hemicellulose solubilization, the holocellulose fraction of alkali-pretreated cassava stem residue was significantly ($p \leq 0.01$) increased from 52.45 ± 0.65% (raw material) to 67.22 ± 0.80% (2% NaOH; 120 °C for 60 min).

Kamalini et al. [30] conducted microwave-assisted alkaline pretreatment of cassava stem waste at different NaOH concentrations (2–4% w/v) and reaction times (60, 90, 120 s). They reported similar compositional changes in cassava stem waste before and after pretreatment as follows: celluloses (36.27 to 52.34%), hemicelluloses (32.30 to 27.15%), and lignin (19.33 to 14.59%). Papathoti et al. [9] carried out alkali-assisted hydrothermal pretreatment of cassava peel waste at different temperatures (110–130 °C) and reaction times (15–30 min) using different concentrations of NaOH (0.25–1.0% w/v). They reported decreased hemicelluloses (5.70%) and lignin (2.45%) contents as compared to raw biomass material. Table 2 compares the percentage of lignin removal obtained after dilute alkaline pretreatment in the present study with that of previously studied pretreatment of lignocellulosic substrates.

Table 1 Solid recoveries and chemical composition of alkali-treated cassava stem waste at various pretreatment conditions

Time (min)	NaOH (%w/v)		Celluloses (%)	Hemicelluloses (%)	Lignins (%)
30	1	81.23 ± 2.05	38.84 ± 1.05*	18.32 ± 0.85*	11.05 ± 0.45***
	2	78.65 ± 3.42	45.40 ± 0.86***	16.90 ± 0.42***	08.70 ± 1.02***
	3	74.18 ± 1.80	52.36 ± 0.11***	14.58 ± 1.20*	06.64 ± 0.70***
60	1	77.60 ± 3.15	45.20 ± 1.15***	17.60 ± 0.74**	08.34 ± 0.85***
	2	73.36 ± 2.20	52.17 ± 0.90***	15.05 ± 0.25***	06.50 ± 0.18***
	3	68.42 ± 2.42	55.40 ± 0.50***	12.84 ± 0.70***	04.15 ± 0.58***

* specifies ($p < 0.05$), ** specifies ($p < 0.01$), and.*** specifies ($p < 0.001$) significant differences between raw cassava stem waste and alkali-pretreated cassava stem waste performed by *t*-test ($n = 3$)

Table 2 Comparison of dilute alkaline pretreatment from previously explored lignocellulosic substrates

Feedstock name	Pretreatment	Lignin removal (%)	Reference
Sugarcane bagasse	Sequential 1% HNO3-NaOH pretreatment at 121 °C for 30 min	70.63	[42]
Prosopis juliflora	2% (w/v) Na2S2O4 at 30 °C for 18 h	79.23	[43]
Cotton stalk	3% w/v NaOH at room temperature for 24 h	52.48	[33]
Corn stover	Sequential dilute acid and alkali pretreatment	85.9–89.4	[44]
Cassava stem waste	3% NaOH at 120 °C for 60 min	71.50	This study

3.2 The effect of cell growth and fermentation performance of *C. thermocellum* at different temperatures

The effect of different temperatures on the growth of *C. thermocellum* and the fermentation efficiency of bioethanol and by-product acetate production were investigated using cellobiose and xylose as carbon sources during fermentation. As shown in Fig. 1a, an increase in incubation temperature from 50 °C to 60 °C had significantly improved bioethanol production. The maximum bioethanol production (1.02 ± 0.04 g/L) with 1.10 ± 0.1 g/L residual sugars was observed at 60 °C for 72 h time. When the temperature was increased to 65 °C, a significant decrease in bioethanol production was detected. Further rise in temperature above 65 °C improved neither bioethanol production nor cell growth (OD_{600}) and rather observed increased acetate production at the end of the fermentation period. It was found that a significant increase in acetate production was also observed from 50 °C to 65 °C, with a maximum of 1.58 ± 0.05 g/L acetate observed at 65 °C incubation temperature (Fig. 1a). It was found that *C. thermocellum* was able to grow at 70 °C with decreased cell growth. These observations are in agreement with previous studies [16, 28], which reported lower bioethanol production with bacterial growth at 65–70 °C, suggesting that 60 °C incubation temperature could be an optimum temperature for thermophilic bioethanol production.

3.3 The effect of cell growth and ethanol tolerance of C. thermocellum at different ethanol concentrations

In order to study maximum ethanol tolerance levels of *C. thermocellum* ATCC 31,924, different concentrations of ethanol were supplemented with a growth medium containing cellobiose as a carbon source, and the effect of cell growth (OD_{600}) was determined. During growth on a CTFuD medium containing sugars and added ethanol, the wild-type strain of *C. thermocellum* tolerated a maximum of 3.0% (v/v) ethanol concentration with OD_{600} of 0.44 ± 0.03, which was significantly lower (OD_{600} 0.78 ± 0.02) as compared to wild-type strain grown on the same medium without ethanol (Fig. 1b). Furthermore, severe growth inhibition was detected when the culture was grown on a medium containing ≥ 4% (v/v) ethanol concentration, indicating that 3% (v/v) ethanol concentration is the maximum tolerance level of wild-type *C. thermocellum* strain. Similar outcomes were observed with Singh et al. [34], who reported maximum ethanol tolerance of *C. thermocellum* at 3.5% (v/v) or higher ethanol concentration levels.

3.4 Improvement of ethanol tolerance of *C. thermocellum* by ALE

To improve ethanol tolerance levels of the wild-type strain of *C. thermocellum*, ALE was carried out until the desired phenotype is achieved. In the present study, the bacterial population obtained after chemical mutagenesis was used as parent culture for ALE experiments. ALE was performed for 120 days corresponding to 120 serial subcultures, and bacterial strains with maximum growth rate were chosen

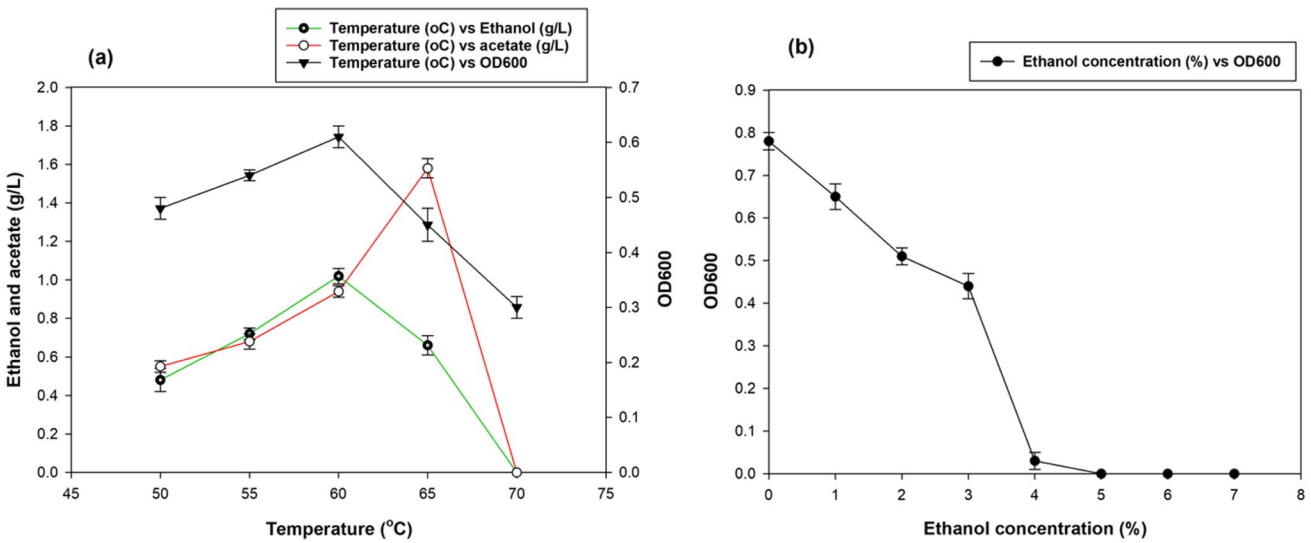

Fig. 1 **a** Ethanol and acetic acid production (g/L) and **b** the effect of growth (OD_{600}) of *C. thermocellum* at different temperatures

at every 30th subculture. Furthermore, the concentration of 0.5% (v/v) ethanol was progressively increased in the ALE medium for every 30th subculture and the growth rate (OD_{600}) was assessed. Figure 2a shows the specific growth rates of adapted strains as evaluated for every 30th subculture. It was found that a significant ($p < 0.05$) increase in specific growth rate was observed at 30th, 60th, 90th, and 120th serial subcultures as compared to wild-type strain (CT0d), indicating improvement in ethanol tolerance from 3 to 5% (v/v) ethanol concentration. Figure 2b shows the ALE mutant developmental process for 120 days. At the end of the ALE process, a population of an improved ethanol tolerance to 5% (v/v) ethanol concentration was obtained (Fig. 2b). A growth comparison study was carried out between wild-type strain (CT0d) and ALE mutant strain (CT120d) at different concentrations of ethanol (0%, 3%, 5% v/v) and is shown in Fig. 3a–c. As shown in Fig. 3a, in the absence of ethanol, no significant growth difference (OD_{600}) was observed between the strains. However, the difference in growth rate was significantly observed at 3% ethanol concentration, where CT0d showed retarded growth, while CT120d showed a higher growth rate (Fig. 3b). Furthermore, CT120d strain showed significantly ($p < 0.05$) higher growth rate at 5% (v/v) ethanol concentration whereas CT0d failed to grow at this ethanol concentration (Fig. 3c).

Tian et al. [35] studied two rounds of adaptive evolution of *C. thermocellum* using CTFuD growth media. The first round of ALE experiments involved 150 serial transfers, while the second round contained 13 serial transfers, which ultimately improved ethanol titer and yield during bioethanol fermentation via consolidated bioprocessing. In another study, Holwerda et al. [36] carried out ALE in *C. thermocellum* to improve the growth rate and bioethanol yield. They reported the significant role of ALE in improving the growth rate by channeling the elevated levels of pyruvate and amino acid towards bioethanol production. In addition, ALE also induced mutations in the *adhE* gene which increased the production of bioethanol. Zhu et al. [37] studied the mechanism of ethanol tolerance in *C. thermocellum* using a systematic metabolomics approach. They analyzed metabolic phenotypes of wild-type *C. thermocellum* and ethanol tolerant (3% v/v) strains and concluded that the ethanol-tolerant strain showed an improved adaption under ethanol stress conditions as compared to the wild-type strain. These authors also observed an accumulation of cellodextrins inside the cell in response to ethanol stress conditions. Shao et al. [38] developed ethanol-tolerant mutants of *C. thermocellum* ATCC 27,405 using adaptive evolution and reported ALE strains with a higher growth rate in 50 g/L bioethanol concentration.

3.5 Bioethanol production from wild-type and mutant strains of *C. thermocellum* via consolidated bioprocessing

Based on improved ethanol tolerance studies of *C. thermocellum*, bioethanol production via consolidated bioprocessing was carried out using alkali-treated cassava stem waste. Initially, small-scale anaerobic bioethanol fermentation was carried out to evaluate the concentration of important end products of fermentation (ethanol and acetate), including bioethanol fermentation efficiency of *C. thermocellum*.

As shown in Fig. 4a, the wild-type strain of *C. thermocellum* produced a maximum of 1.26 ± 0.06 g/L bioethanol at 72 h time with 47.43% fermentation efficiency. As expected, the lower bioethanol fermentation efficiency was attributed

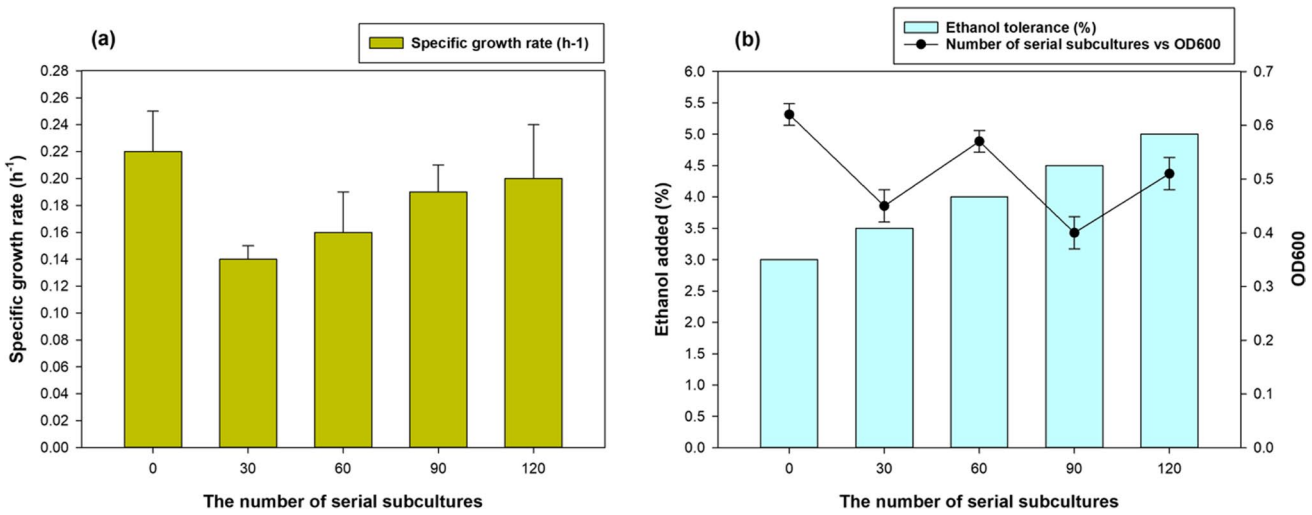

Fig. 2 **a** Specific growth rate ($h.^{-1}$) and **b** ethanol tolerance vs. bacterial growth (OD_{600}) of *C. thermocellum* at different sub-cultures of the adaptive laboratory evolution process

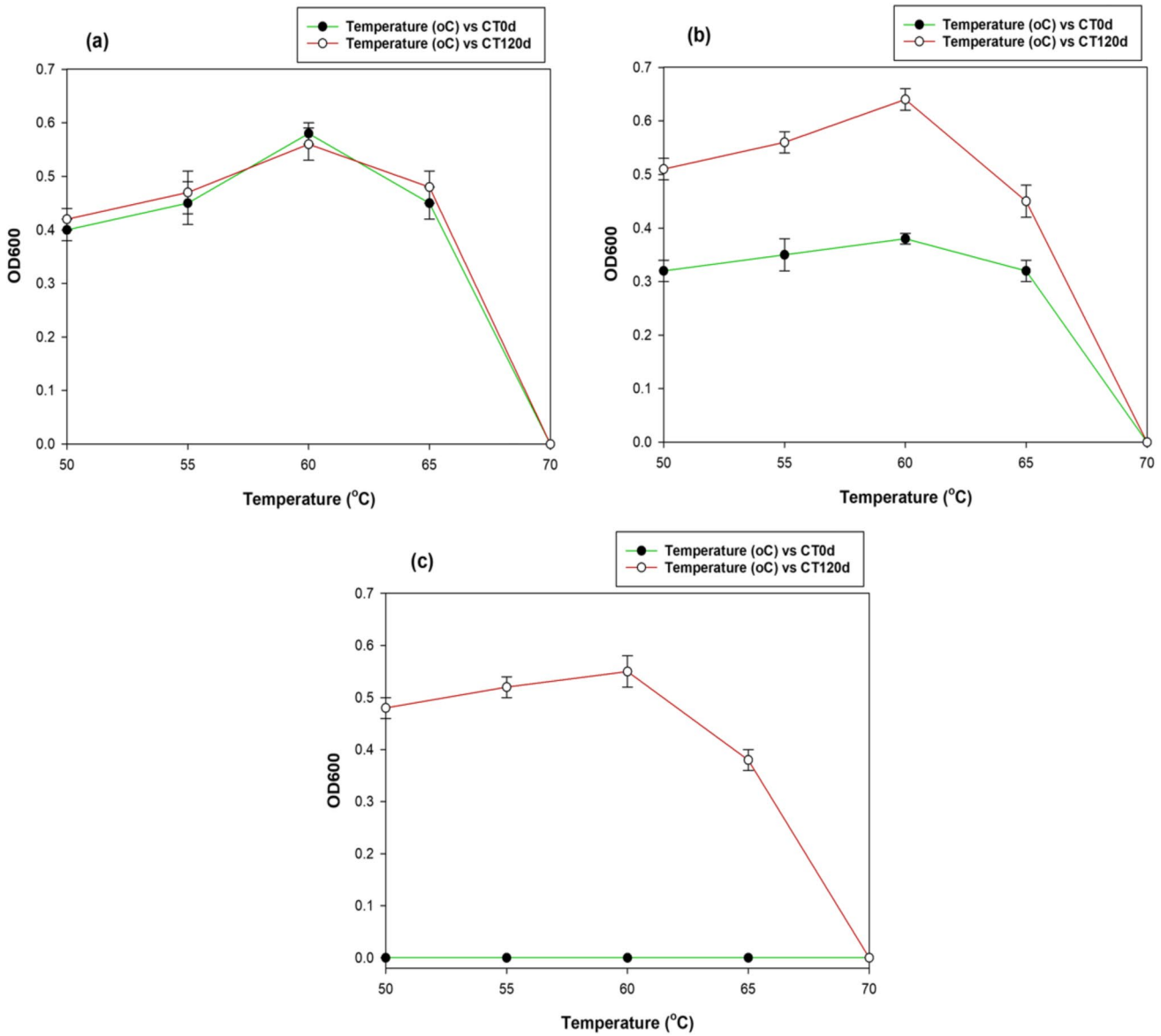

Fig. 3 Comparison of bacterial growth (OD_{600}) of wild-type and ALE mutant of *C. thermocellum* at different ethanol concentrations. **a** No ethanol, **b** 3% (v/v), **c** 5% (v/v), and temperatures (50–70 °C)

to increased levels of acetate production (1.23 ± 0.03 g/L) at the end of fermentation time (84 h). Acetate is one of the key metabolites produced along with bioethanol during cellulosic fermentation by *C. thermocellum*. Previous studies also reported a similar observation of increased acetate production during the bioethanol fermentation process [16, 34]. Meanwhile, ALE mutant of *C. thermocellum* (CT120d) produced 1.35 ± 0.02 g/L bioethanol at 72 h incubation period (Fig. 4b). A slightly higher 49.30% bioethanol fermentation efficiency was observed as compared to the wild-type strain. It was found that cell growth of ALE mutant strain CT120d was comparatively higher (OD_{600} 0.65 ± 0.04) as compared to parent strain CT0d (OD_{600} 0.45 ± 0.01), indicating considerable tolerance towards ethanol and acetate present in fermentation media.

Furthermore, bioethanol production via CBP was also carried out using alkali-treated cassava stem residue using ALE mutant of *C. thermocellum* strain. It was found that a maximum of 7.84 ± 0.31 g/L bioethanol was produced with 62.37 ± 0.25% cellulose conversion efficiency (Fig. 5). However, during the fermentation process, acetate concentration was significantly increased and ranged between 0.92 ± 0.25 and 5.71 ± 0.50 g/L. The decrease in bioethanol concentration at 84 h time might be due to the inhibitory effect of acetate on bioethanol production. A similar report of an inhibitory effect of acetate on ethanol production was also

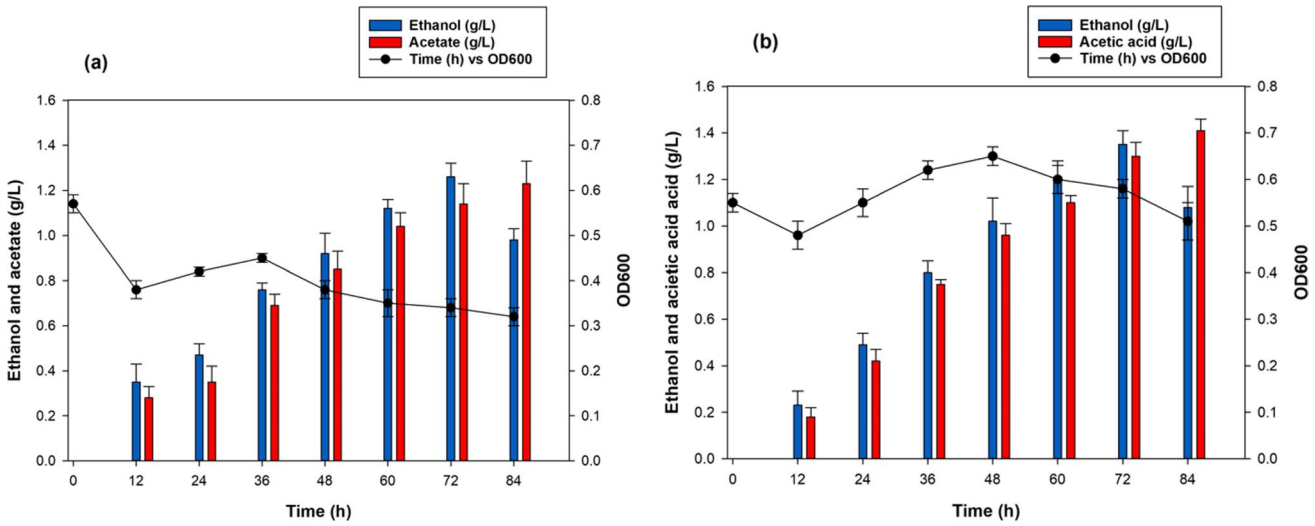

Fig. 4 Ethanol, acetic acid production (g/L), and growth (OD_{600}) assessment of **A** wild-type and **B** ALE mutant of *C. thermocellum* at batch culture conditions. Fermentation was carried out using 5.50 ± 0.50 g/L cellobioses and xyloses at 150 rpm orbital shaking and incubated at 60 °C for 84 h

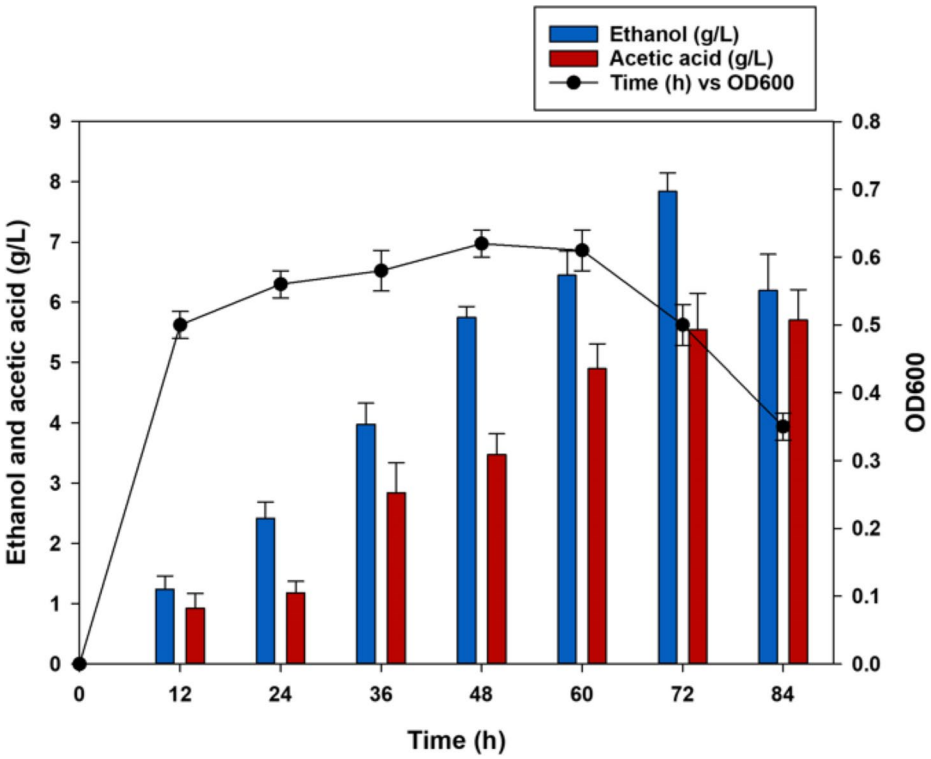

Fig. 5 Ethanol and acetic production from alkali-treated cassava stem residue via consolidated bioprocessing using ALE mutant of *C. thermocellum*. Fermentation was carried out at 150 rpm orbital shaking and incubated at 60 °C for 84 h

observed by Liu et al. [16] and Singh et al. [34]. In a recent study, Kavitha et al. [39] studied CBP bioethanol production with *Hangateiclostridium thermocellum* KSMK1203 using pretreated *Nannochloropsis gaditana* microalga and reported 12.90 g/L bioethanol production. In another study, Selvakumar et al. [40] studied bioethanol production from pretreated *Manihot esculenta* Crantz stem via consolidated bioprocessing (CBP) using *Cellulomonas fimi* MTCC 24 and *Zymomonas mobilis* MTCC 92 and reported the maximum 9.39 g/L bioethanol from 20.7 g/L cellulose consumption.

Li and Zhu [41] carried out ethanol production via CBP from cassava pulp using a coculture of *C. thermocellum* and *Thermoanaerobacterium aotearoense*, which generated 13.65 g/L glucose sugars. Subsequent fermentation

Table 3 Comparison of various process parameters of ethanol production via consolidated bioprocessing (CBP) from different feedstocks

Feedstock	Type of pretreatment	CBP strain	Fermentation parameters	Reference
Cassava stem waste	Dilute NaOH (2% NaOH 120 °C for 60 min)	*C. thermocellum* ATCC 27,405	CBP; 7.84 g/L ethanol; 62.37% cellulose conversion	Present study
Cellobiose and xylose	–	*C. thermocellum* ATCC 27,405	CBP; 1.35 g/L ethanol; 49.30% ethanol conversion efficiency	Present study
Sugarcane bagasse	Dilute NaOH pretreatment	C. *thermocellum* DSM 1237	CBP; 83.30% theoretical yield	[16]
Crystalline celluloses	–	C. *thermocellum* ATCC 31,924	CBP; Ethanol yield 0.30 g/g celluloses; 95.32% cellulose conversion	[34]
Parthenium hysterophorus	Ionic liquid pretreatment	Enzyme saccharification: *Aspergillus aculeatus* PN14 Fermentation: *S. cerevisiae* NCIM 3078 and *Pichia stipitis* NCIM 3497	CBP; 0.078 g/g ethanol yield. 36.27% fermentation efficiency	[45]

with *Saccharomyces cerevisiae* produced 8.83 g/L bioethanol with 64.95 ± 2.71% fermentation efficiency. Liu et al. [16] studied bioethanol production from sugarcane bagasse through CBP using *C. thermocellum* DSM 1237. They reported a 0.68-g/L ethanol yield, which was a 65.8% theoretical yield from alkali-treated sugarcane bagasse. They also reported 0.86 g/L bioethanol with 83.3% of theoretical yield from sugarcane bagasse using a 3-L fermenter scale. In another study, cellulosic ethanol production was studied via CBP using crystalline celluloses as the sole carbon source with *C. thermocellum* ATCC 31,924. Under optimum fermentation conditions, they reported a maximum of 0.30 g ethanol yield with 95.32% cellulose conversion [34]. Table 3 summarizes bioethanol production and cellulose conversion efficiency obtained in the present study with previous CBP studies conducted on other feedstocks.

4 Conclusions and future perspectives

In the present study, cassava stem waste was evaluated as an ideal lignocellulosic substrate for the production of bioethanol via CBP. Dilute NaOH pretreatment could be an efficient pretreatment method to improve the holocellulose fraction of cassava stem waste and generate maximum sugar yield for subsequent fermentation studies. The present study suggests the application of chemical mutagenesis followed by ALE could be an ideal strategy to improve ethanol tolerance in *C. thermocellum*. However, the accumulation of acetate production in fermentation media showed decreased ethanol titer. For an ideal cassava waste-to-ethanol technology, there will be a need for effective pretreatment methods to retain maximum holocellulosic fraction of biomass, while effectively fractionating other biomass components, which is vital for the realization of the lignocellulosic biorefinery process. It is also a prerequisite to develop an effective microbial biocatalyst, which effectively saccharifies and ferments all the sugars in the hydrolysate. Further research is required to improve ethanol tolerance and pentose sugar utilization in *C. thermocellum* through the CBP approach. It is also mandatory to eliminate native metabolic pathways for acetate and formate production, which ultimately improves bioethanol titers in *C. thermocellum* strain. This can be achieved by conventional strain improvement methods such as improved ALE methods as well as advanced systems metabolic engineering techniques.

Acknowledgements The authors are thankful to Suranaree University of Technology, Thailand, for providing financial support. Authors would also like to express sincere thanks to the Thailand Science Research and Innovation (TSRI), and National Science Research and Innovation Fund (NSRF). The authors are also thankful to Sri Yuva Biotech Pvt. Ltd, Hyderabad, India for their help and support in this work.

Declarations

Competing interests The authors declare no competing interests.

References

1. Leitão VO, Noronha EF, Camargo BR, Hamann PRV, Steindorff AS, Quirino BF, de Sousa MV, Ulhoa CJ, Felix CR (2017) Growth and expression of relevant metabolic genes of *Clostridium thermocellum* cultured on lignocellulosic residues. J Ind Microbiol Biotechnol 44(6):825–834. https://doi.org/10.1007/s10295-017-1915-2
2. Keshav PK, Banoth C, Kethavath SN, Bhukya B (2021) Lignocellulosic ethanol production from cotton stalk: an overview on pretreatment, saccharification and fermentation methods for improved bioconversion process. Biomass Conv Bioref. https://doi.org/10.1007/s13399-021-01468-z
3. Tursi A (2019) A review on biomass: importance, chemistry, classification, and conversion. Biofuel Res J 6(2):962–979. https://doi.org/10.18331/brj2019.6.2.3
4. González-Chavez JdJ, Arenas-Grimaldo C, Amaya-Delgado L, Vázquez-Núñez E, Suarez-Vázquez S, Cruz-López A,

Segovia-Hernández JG, Pérez-Vega S, Salmerón I, Molina-Guerrero CE (2022) Sotol bagasse (Dasylirion sp.) as a novel feedstock to produce bioethanol 2G: bioprocess design and biomass characterization. Ind Crop Prod 178:114571. https://doi.org/10.1016/j.indcrop.2022.114571
5. Panahi HKS, Dehhaghi M, Kinder JE, Ezeji TC (2019) A review on green liquid fuels for the transportation sector: a prospect of microbial solutions to climate change. Biofuel Res J 6(3):995–1024. https://doi.org/10.18331/brj2019.6.3.2
6. Wirawan F, Cheng C-L, Lo Y-C, Chen C-Y, Chang J-S, Leu S-Y, Lee D-J (2020) Continuous cellulosic bioethanol co-fermentation by immobilized *Zymomonas mobilis* and suspended *Pichia stipitis* in a two-stage process. Appl Energy 266:114871. https://doi.org/10.1016/j.apenergy.2020.114871
7. Panahi HKS, Dehhaghi M, Aghbashlo M, Karimi K, Tabatabaei M (2020) Conversion of residues from agro-food industry into bioethanol in Iran: an under-valued biofuel additive to phase out MTBE in gasoline. Renew Energ 145:699–710. https://doi.org/10.1016/j.renene.2019.06.081
8. Zhang M, Xie L, Yin Z, Khanal SK, Zhou Q (2016) Biorefinery approach for cassava-based industrial wastes: current status and opportunities. Bioresour Technol 215:50–62. https://doi.org/10.1016/j.biortech.2016.04.026
9. Papathoti NK, Laemchiab K, Megavath VS, Keshav PK, Numparditsub P, Le Thanh T, Buensanteai N (2021) Augmented ethanol production from alkali-assisted hydrothermal pretreated cassava peel waste. Energy Sources, Part A: Recovery, Utilization, and Environmental Effects:1–11. https://doi.org/10.1080/15567036.2021.1928338
10. Pooja NS, Sajeev MS, Jeeva ML, Padmaja G (2018) Bioethanol production from microwave-assisted acid or alkali-pretreated agricultural residues of cassava using separate hydrolysis and fermentation (SHF). 3 Biotech 8(1):69. https://doi.org/10.1007/s13205-018-1095-4
11. Liu Y, Zhang Y, Xu J, Sun Y, Yuan Z, Xie J (2015) Consolidated bioprocess for bioethanol production with alkali-pretreated sugarcane bagasse. Appl Energy 157:517–522. https://doi.org/10.1016/j.apenergy.2015.05.004
12. Sanchez A, Sevilla-Güitrón V, Magaña G, Gutierrez L (2013) Parametric analysis of total costs and energy efficiency of 2G enzymatic ethanol production. Fuel 113:165–179. https://doi.org/10.1016/j.fuel.2013.05.034
13. Cheah WY, Sankaran R, Show PL, Tg Ibrahim TNB, Chew KW, Culaba A, Chang J-S (2020) Pretreatment methods for lignocellulosic biofuels production: current advances, challenges and future prospects. Biofuel Res J 7(1):1115–1127. https://doi.org/10.18331/brj2020.7.1.4
14. Lynd LR, Guss AM, Himmel ME, Beri D, Herring C, Holwerda EK, Murphy SJ, Olson DG, Paye J, Rydzak T, Shao X, Tian L, Worthen R (2017a) Advances in consolidated bioprocessing using *Clostridium thermocellum* and *Thermoanaerobacter saccharolyticum* industrial biotechnology. pp 365–394. https://doi.org/10.1002/9783527807796.ch10
15 Akinosho H, Yee K, Close D, Ragauskas A (2014) The emergence of *Clostridium thermocellum* as a high utility candidate for consolidated bioprocessing applications. Front Chem 2(66):1–18. https://doi.org/10.3389/fchem.2014.00066
16. Liu Y, Xie X, Liu W, Xu H, Cao Y (2020) Consolidated bioprocess for bioethanol production from lignocellulosic biomass using *Clostridium thermocellum* DSM 1237. BioRes 15:8355–8368. https://doi.org/10.15376/biores.15.4.8355-8368
17. Liu Y-J, Li B, Feng Y, Cui Q (2020) Consolidated bio-saccharification: leading lignocellulose bioconversion into the real world. Biotechnol Adv 40:107535. https://doi.org/10.1016/j.biotechadv.2020.107535
18. Jiang Y, Xin F, Lu J, Dong W, Zhang W, Zhang M, Wu H, Ma J, Jiang M (2017) State of the art review of biofuels production from lignocellulose by thermophilic bacteria. Bioresour Technol 245:1498–1506. https://doi.org/10.1016/j.biortech.2017.05.142
19. Olson DG, Sparling R, Lynd LR (2015) Ethanol production by engineered thermophiles. Curr Opin Biotechnol 33:130–141. https://doi.org/10.1016/j.copbio.2015.02.006
20. Brown SD, Sander KB, Wu C-W, Guss AM (2015) Chapter 16 - *Clostridium thermocellum*: engineered for the production of bioethanol. In: Himmel ME (ed) Direct microbial conversion of biomass to advanced biofuels Amsterdam: Elsevier 321–33. https://doi.org/10.1016/B978-0-444-59592-8.00016-6
21. Dragosits M, Mattanovich D (2013) Adaptive laboratory evolution – principles and applications for biotechnology. Microb Cell Fact 12(1):64. https://doi.org/10.1186/1475-2859-12-64
22. Sandberg TE, Salazar MJ, Weng LL, Palsson BO, Feist AM (2019) The emergence of adaptive laboratory evolution as an efficient tool for biological discovery and industrial biotechnology. Metab Eng 56:1–16. https://doi.org/10.1016/j.ymben.2019.08.004
23. Tian L, Perot SJ, Stevenson D, Jacobson T, Lanahan AA, Amador-Noguez D, Olson DG, Lynd LR (2017) Metabolome analysis reveals a role for glyceraldehyde 3-phosphate dehydrogenase in the inhibition of C. thermocellum by ethanol. Biotechnol Biofuels 10(1):276. https://doi.org/10.1186/s13068-017-0961-3
24. Sluiter A, Hames B, Ruiz R, Scarlata C, Sluiter J, Templeton D, Crocker DJL (2008) Determination of structural carbohydrates and lignin in biomass. Nat Renew Energy 1617(1):1–16
25. Lin PP, Mi L, Morioka AH, Yoshino KM, Konishi S, Xu SC, Papanek BA, Riley LA, Guss AM, Liao JC (2015) Consolidated bioprocessing of cellulose to isobutanol using *Clostridium thermocellum*. Metab Eng 31:44–52. https://doi.org/10.1016/j.ymben.2015.07.001
26. Chen S, Xu Y (2014) Adaptive evolution of *Saccharomyces cerevisiae* with enhanced ethanol tolerance for Chinese rice wine fermentation. Appl Biochem Biotechnol 173(7):1940–1954. https://doi.org/10.1007/s12010-014-0978-z
27. Miller GL (1959) Use of dinitrosalicylic acid reagent for determination of reducing sugar. Anal Chem 31(3):426–428. https://doi.org/10.1021/ac60147a030
28. Singh N, Mathur AS, Tuli DK, Gupta RP, Barrow CJ, Puri M (2017) Cellulosic ethanol production *via* consolidated bioprocessing by a novel thermophilic anaerobic bacterium isolated from a Himalayan hot spring. Biotechnol Biofuels 10(1):73. https://doi.org/10.1186/s13068-017-0756-6
29. da Silveira FA, de Oliveira Soares DL, Bang KW, Balbino TR, de Moura Ferreira MA, Diniz RHS, de Lima LA, Brandão MM, Villas-Bôas SG, da Silveira WB (2020) Assessment of ethanol tolerance of *Kluyveromyces marxianus* CCT 7735 selected by adaptive laboratory evolution. Appl Microbiol Biotechnol 104(17):7483–7494. https://doi.org/10.1007/s00253-020-10768-9
30. Kamalini A, Muthusamy S, Ramapriya R, Muthusamy B, Pugazhendhi A (2018) Optimization of sugar recovery efficiency using microwave assisted alkaline pretreatment of cassava stem using response surface methodology and its structural characterization. J Mol Liq 254:55–63. https://doi.org/10.1016/j.molliq.2018.01.091
31. Kouteu Nanssou PA, Jiokap Nono Y, Kapseu C (2016) Pretreatment of cassava stems and peelings by thermohydrolysis to enhance hydrolysis yield of cellulose in bioethanol production process. Renew Energy 97:252–265. https://doi.org/10.1016/j.renene.2016.05.050
32. Keshav PK, Naseeruddin S, Rao LV (2016) Improved enzymatic saccharification of steam exploded cotton stalk using alkaline extraction and fermentation of cellulosic sugars into ethanol. Bioresour Technol 214:363–370. https://doi.org/10.1016/j.biortech.2016.04.108

33. Keshav PK, Shaik N, Koti S, Linga VR (2016) Bioconversion of alkali delignified cotton stalk using two-stage dilute acid hydrolysis and fermentation of detoxified hydrolysate into ethanol. Ind Crops Prod 91:323–331. https://doi.org/10.1016/j.indcrop.2016.07.031
34. Singh N, Mathur AS, Gupta RP, Barrow CJ, Tuli D, Puri M (2018) Enhanced cellulosic ethanol production *via* consolidated bioprocessing by *Clostridium thermocellum* ATCC 31924. Bioresour Technol 250:860–867. https://doi.org/10.1016/j.biortech.2017.11.048
35. Tian L, Perot SJ, Hon S, Zhou J, Liang X, Bouvier JT, Guss AM, Olson DG, Lynd LR (2017) Enhanced ethanol formation by *Clostridium thermocellum* via pyruvate decarboxylase. Microb Cell Fact 16(1):171. https://doi.org/10.1186/s12934-017-0783-9
36. Holwerda EK, Olson DG, Ruppertsberger NM, Stevenson DM, Murphy SJL, Maloney MI, Lanahan AA, Amador-Noguez D, Lynd LR (2020) Metabolic and evolutionary responses of *Clostridium thermocellum* to genetic interventions aimed at improving ethanol production. Biotechnol Biofuels 13(1):40. https://doi.org/10.1186/s13068-020-01680-5
37. Zhu X, Cui J, Feng Y, Fa Y, Zhang J, Cui Q (2013) Metabolic adaption of ethanol-tolerant *Clostridium thermocellum*. PLoS ONE 8(7):e70631. https://doi.org/10.1371/journal.pone.0070631
38. Shao X, Raman B, Zhu M, Mielenz JR, Brown SD, Guss AM, Lynd LR (2011) Mutant selection and phenotypic and genetic characterization of ethanol-tolerant strains of *Clostridium thermocellum*. Appl Microbiol Biotechnol 92(3):641–652. https://doi.org/10.1007/s00253-011-3492-z
39. Kavitha S, Gajendran T, Saranya K, Selvakumar P, Manivasagan V (2021) Study on consolidated bioprocessing of pre-treated *Nannochloropsis gaditana* biomass into ethanol under optimal strategy. Renew Energy 172:440–452. https://doi.org/10.1016/j.renene.2021.03.015
40. Selvakumar P, Kavitha S, Sivashanmugam P (2019) Optimization of process parameters for efficient bioconversion of thermo-chemo pretreated *Manihot esculenta* Crantz YTP1 stem to ethanol. Waste Biomass Valor 10(8):2177–2191. https://doi.org/10.1007/s12649-018-0244-7
41. Li P, Zhu M (2011) A consolidated bio-processing of ethanol from cassava pulp accompanied by hydrogen production. Bioresour Technol 102(22):10471–10479. https://doi.org/10.1016/j.biortech.2011.08.134
42. Ascencio JJ, Chandel AK, Philippini RR, da Silva SS (2020) Comparative study of cellulosic sugars production from sugarcane bagasse after dilute nitric acid, dilute sodium hydroxide and sequential nitric acid-sodium hydroxide pretreatment. Biomass Conv Bioref 10(4):813–822. https://doi.org/10.1007/s13399-019-00547-6
43. Naseeruddin S, Desai S, Venkateswar Rao L (2017) Ethanol production from lignocellulosic substrate *Prosopis juliflora*. Renew Energy 103:701–707. https://doi.org/10.1016/j.renene.2016.10.085
44. Lee JW, Kim JY, Jang HM, Lee MW, Park JM (2015) Sequential dilute acid and alkali pretreatment of corn stover: sugar recovery efficiency and structural characterization. Bioresour Technol 182:296–301. https://doi.org/10.1016/j.biortech.2015.01.116
45. Nargotra P, Sharma V, Bajaj BK (2019) Consolidated bioprocessing of surfactant-assisted ionic liquid-pretreated *Partheniumhysterophorus* L. biomass for bioethanol production. Bioresour Technol 289:121611. https://doi.org/10.1016/j.biortech.2019.121611